SPECTROSCOPIC AND THEORETICAL INVESTIGATIONS OF HALOPYRIDINES, HALOBISMUTHATES AND A SPIRO KETAL

A Dissertation

by

HONG-LI SHEU

Submitted to the Office of Graduate and Professional Studies of
Texas A&M University
in partial fulfillment of the requirements for the degree of

DOCTOR OF PHILOSOPHY

Chair of Committee,	Jaan Laane
Committee Members,	Christian Hilty
	Steven E. Wheeler
	Goong Chen
Head of Department,	David Russell

December 2014

Major Subject: Chemistry

ABSTRACT

Infrared and Raman spectra of 2,6-difluoropyridine (26DFPy) and 2,3,5,6-tetrafluoropyridine were recorded and vibrational assignments made for their electronic ground states. Theoretical *ab initio* and density functional theory (DFT) calculations were used to complement the experimental work. The electronic excited states of these molecules were investigated with ultraviolet absorption spectroscopy and theoretical CASSCF calculations. For 2,6-difluoropyridine the structure is planar in its $S_1(\pi,\pi^*)$ electronic excited state, but a barrier to planarity of 256 cm^{-1} was predicted for its $S_2(n,\pi^*)$ electronic excited state which has its band origin at 37820.2 cm^{-1}. For 2,3,5,6-tetrafluoropyridine a barrier of 124 cm^{-1} was predicted for the $S_1(\pi,\pi^*)$ state which has its band origin at 35704.6 cm^{-1}. Lower frequencies for the out-of-plane ring bending vibrations for the electronic excited states result from the weaker π bonding within the pyridine ring in these states.

The infrared and Raman spectra of 2-chloro-, 3-chloro-, 2-bromo-, and 3-bromopyridine have been measured and assigned for the electronic ground state. Density functional theory (DFT) calculations at the B3LYP level of theory with the 6-311++G(d,p) basis set for vibrational frequencies produced excellent agreement with the experimental values. MP2 calculation methods with cc-pVTZ basis set were utilized to compute the molecular structures. A shortening of the N-C(2) bond resulting from halogen substitution on the C(2) carbon atom was shown for all 2-halopyridines.

Theoretical calculations including *ab initio* and density functional theory (DFT) methods were carried out to study the bond lengths and vibrational frequencies of halobismuthates and haloantimonates. The results were also compared to experimental crystal structures, and to the infrared and Raman spectra of these species. Although the presence of cations was neglected in the calculations, the observed trends in the bond distances and bond stretching vibrational frequencies were verified. External bonds across from bridging bonds are the shortest and have the highest stretching frequencies for all of the ions investigated. This supports the previously postulated *trans* effect.

The infrared and Raman spectra of the spiro molecule 2-cyclopenten-1-one ethylene ketal (CEK) have been recorded and compared to calculated spectra with good agreement. The structures and conformational energies for the two pairs of conformational minima, which can be defined in terms of ring-bending (x) and ring-twisting (τ) vibrational coordinates, have also been calculated. Utilizing the results from *ab initio* MP2/cc-PVTZ calculations, a two-dimensional potential energy surface (PES) was generated. The energy levels and wavefunctions for the PES were calculated and the characteristics of these were analyzed.

DEDICATION

Wish to dedicate to my beloved families and friends.

ACKNOWLEDGEMENTS

It is a rare opportunity to express my gratitude to all the people who made this dissertation possible. I would like to thank my research advisor, Dr. Jaan Laane, for his inspiration, patience and the knowledge he taught me on my research. I especially thank him for his support and the opportunity he gave me during my most difficult period of time. I would also like to thank my committee members, Dr. Steven Wheeler, Dr. Christian Hilty and Dr. Goong Chen for their advice and helpful suggestions. I deeply appreciate Dr. Kim for his help on excited state calculations, Dr. Meinander for the calculation of wavefunctions and Dr. Lisa Perez for her suggestions on my theoretical calculations. I also thank Bill for his nice suggestions on my Raman and UV cells. The dissertation cannot be completed without their effort. I would like to show appreciation to my research group members including Hye Jin and Esther for their advice. I am also grateful to our secretary, Linda Redd, for her friendship and help on my papers and dissertation. I truly appreciate Sandy Manning for her advice during my Ph.D. study. Finally, I am indebted to my families for their encouragement and their support is always beyond word description.

TABLE OF CONTENTS

LIST OF FIGURES

Page

LIST OF TABLES

Page

CHAPTER I

INTRODUCTION

Conformational changes in molecules often follow specific vibrational pathways which can be represented by a potential energy surface (PES). These molecular vibrations are often in the low frequency range with large amplitudes since the forces governing these motions are typically not large. These low frequency and large amplitude vibrations have characteristic frequencies below 400 cm^{-1} that rarely interact with high frequency modes.

Vibrational spectroscopy including infrared, Raman and UV spectroscopy serve as useful tools for studying these molecular motions. Infrared and Raman spectroscopy have been utilized to study electronic ground states for many decades. With the development of improved instrument and computer technology, the electronic excited state can now also be readily studied by ultraviolet absorption spectroscopy. These techniques provide valuable information for the low frequency vibrations including bending and twisting motions, especially for the excited states. Since a vast number of photochemical reactions are determined by the properties of the excited state, it is crucial to understand the molecular structure in these states. In addition, theoretical computations including *ab initio* and DFT calculations are also invaluable methods for the analysis of molecular motions and structures.

Several computational and spectroscopic studies have been carried out. First, the spectra and structure of 2,6-difluoropyridine and 2,3,5,6-tetrafluoropyridine were studied

in their electronic ground and excited states. The vibrational energy levels and assignments were also investigated in their electronic excited states. Computational methods including *ab initio* and DFT calculations were used to provide support for the molecular structures and assignments of 2,6-difluoropyridine and 2,3,5,6-tetrafluoropyridine in both states. Second, vibrational data were also collected for 2-chloropyridine (2ClPy), 3-chloropyridine (3ClPy), 2-bromopyridine (2BrPy), and 3-bromopyridine (3BrPy) molecules. Third, *ab initio* and DFT methods were utilized to calculate the bond lengths and vibrational frequencies of halobismuthates and haloantimonates. The results were also compared to experimental crystal structures and vibrational spectra. Fourth, the two dimensional potential energy surface (PES) was calculated for 2-cyclopenten-1-one ethylene ketal, a spiro compound. The calculated and observed spectra were also compared.

2,6-Difluoropyridine and 2,3,5,6-Tetrafluoropyridine

Several studies for the 2,6-difluoropyridine molecule have been carried out in the past decades.[1-14] Rotational spectra reported by C. W. Dijk, M. Sun and J. V. Wijagaarden[1] using microwave spectroscopy indicated that there is an obvious change in the structure of the pyridine backbone (C-N bond length) when a fluorine atom is substituted in the ortho- rather than meta position. The microwave spectrum reported by O. L. Stiefvater[2] also showed a shortening of C-N bond length compared to pyridine due to the influx of fluorine atom electrons into the π bonding system. In addition, the infrared and Raman spectra were reported for its electronic ground state and the

fundamental frequencies were analyzed. Later, the ultraviolet absorption spectrum was reported by K.C. Medhi[3] in the electronic excited states and vibrational modes were also assigned. The results indicated that the $\pi - \pi^*$ transition was observed with a band of origin at 37840 cm^{-1}. For 2,3,5,6-tetrafluoropyridine, only few crystal structures have been reported with focus on the crystal formation.[15-17]

Despite the studies on 2,6-difluoropyridine and 2,3,5,6-tetrafluoropyridine molecules in the past several decades, no results were reported on the differences in the out-of-plane ring bending frequencies and the geometry between electronic ground and excited states. The structures and vibrational assignments were recently reported in their electronic ground and excited states for pyridine (Py), 2-fluoropyridine (2FPy), and 3-fluoropyridine (3FPy) molecules in Laane's research group.[18-20] These results indicated that fluoropyridine molecules become more floppy in the electronic excited states compared to ground states. To further study the effect of additional fluorine atoms on the bending frequencies and the geometry of pyridine and fluoropyridine molecules, the structures and spectra were analyzed for both 2,6-difluoropyridine and 2,3,5,6-tetrafluoropyridine molecules in the present work.

Chloro- and Bromopyridines

2-Chloropyridine (2ClPy), 3-chloropyridine (3ClPy), 2-bromopyridine (2BrPy), and 3-bromopyridine (3BrPy) molecules were studied to extend the research on halopyridines. Previously only partial Raman spectra and assignments for 2ClPy and 3ClPy were reported by Ranjan K. Singh and co-workers,[21] but no information on the

structure was provided. In the present work, these molecules were investigated in their electronic ground state using infrared and Raman spectroscopy. *Ab initio* and DFT calculations were also carried out to determine their structures.

Halobismuthates and Haloantimonates

Many investigations have been done in the past several decades on the crystal structures of halobismuthates and haloantimonates with both external and bridging M-X bonds including the MX_6^{-3}, $M_2X_9^{-3}$, $M_2X_{10}^{-4}$, $(MX_5^{-2})_n$, and $(MX_4^{-1})_n$ anions.[22-46] All of these results provided valuable information on the bond lengths and the formation of the crystal structures. However, very few studies recognized the relationship of bond lengths and stretching frequencies between external and bridging bonds. This relationship, or the *trans* effect, was first discovered when the force constants were compared among several bromo- and iodo-bismuthates with the analysis of far-infrared and low-frequency Raman spectra in Laane's laboratory in 1980.[47-48] Due to the lack of advanced computer technology, no computational studies were done at that time. To further investigate this *trans* effect, theoretical calculations have been carried out for bromo- and iodo-bismuthates which contain both external and bridging M-X bonds (X = I, Br, Cl) to calculate the bond distances and stretching frequencies for each of these molecules.

2-Cyclopenten-1-one Ethylene Ketal

The investigation of potential energy surfaces (PESs) has always been a crucial part in understanding chemical reaction pathways. Numerous results on vibrational potential

energy surface have been reported previously in Laane's research group including four, five and six membered ring and bicyclic molecules.[49-68] The four-membered ring and pseudo-four-membered ring molecules can often be described by a single vibrational coordinate (x) in the form of $V = ax^4+bx^2$. For five or six membered ring and bicyclic molecules, two dimensional vibrational coordinates (x) and (y) are required due to the interactions between two vibrational motions. The molecule investigate in the present work is the spiro molecule 2-cyclopenten-1-one ethylene ketal (CEK). This molecule has two five membered rings including a cyclopentene ring and an oxygen containing ring. The ring puckering of one ring and ring twisting of the other ring are coupled together and thus two vibrational coordinates are utilized to study the PES of this molecule.

CHAPTER II

EXPERIMENTAL METHODS

Introduction

Various spectroscopic techniques were utilized to investigate vibrational motions and potential energy surfaces (PES) of halopyridines including infrared, Raman and ultraviolet spectroscopy. The different types of transitions are shown in Figure 1. Infrared and Raman spectroscopy were used for the determination of vibrational energy levels in electronic ground states, and ultraviolet spectroscopy was used for electronic excited states.

Chemicals

2,6-Difluoropyridine (99% purity), 2,3,5,6-tetrafluoropyridine (95% purity), 2-chloropyridine (2ClPy) (99% purity), 3-chloropyridine (3ClPy) (99% purity), 2-bromopyridine (2BrPy) (99% purity), 3-bromopyridine (3BrPy) (99% purity) and 2-cyclopenten-1-one ethylene ketal were purchased from Sigma-Aldrich.

Infrared Spectra

The liquid and vapor-phase infrared spectra were obtained using a Bruker Vertex 70 Fourier-transform spectrometer equipped with a globar light source, a KBr beamsplitter and a deuterated lanthanum triglycine sulfate (DLaTGS) detector for mid-

infrared. For far-infrared, a Mylar beamsplitter and a mercury cadmium telluride (MCT) detector were used. Liquid sample measurements were done by placing a drop of sample between two well-polished KBr windows for mid-infrared and CsI windows for far-infrared. The windows were wrapped with parafilm to avoid sample evaporation. Vapor sample spectra were collected in a gas cell after sample transfer using trap to trap distillation. The single beam spectrum of the sample was subtracted from the background spectrum to obtain the transmittance spectrum in the 400-4000 cm^{-1} region. 512 scans at 1 cm^{-1} resolution were measured for liquid samples and 1024 scans at 0.5 cm^{-1} resolution for vapor samples.

Raman Spectra

The liquid and vapor-phase Raman spectra were collected using a Jobin-Yvon U-1000 spectrometer equipped with a frequency-doubled Nd:YAG Verdi-10 Coherent laser and a liquid nitrogen-cooled charge-coupled device (CCD) detector. The laser excitation at 532 nm provided a power of 1W for liquid samples and 6W for vapor samples with 0.7 cm^{-1} effective resolution. The liquid Raman spectra were obtained by placing a liquid sample into a quartz cuvette. These were measured in the 100-3400 cm^{-1} region at room temperature. The vapor sample was collected by using trap to trap distillation and sealed in a specially designed glass cell,[69] which is 80 mm in length and 15 mm in diameter. The vapor sample was heated to approximately 200°C and scanned in the 100-3400 cm^{-1} region. Parallel and perpendicular polarization measurements were made utilizing the standard accessory and scrambler.

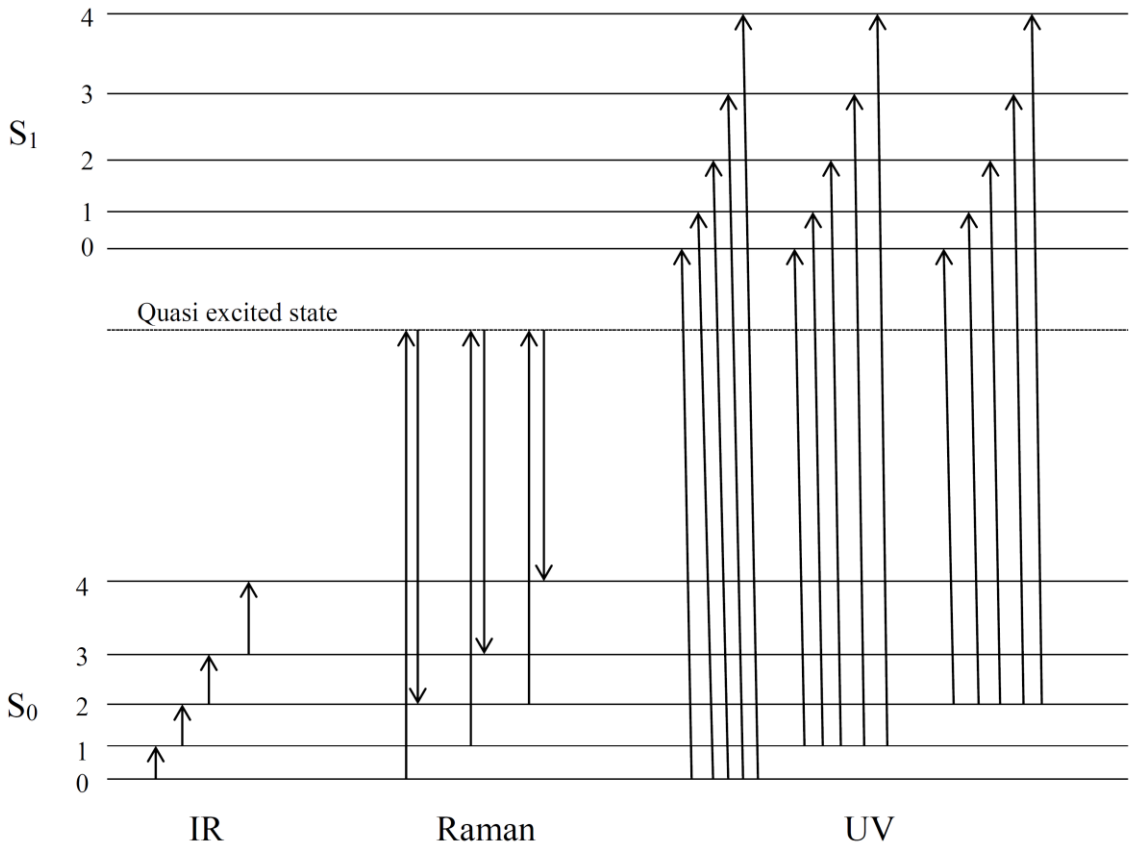

Figure 1 Transitions for different spectroscopic techniques

Ultraviolet Absorption Spectra

Ultraviolet absorption spectra of vapor samples were recorded at room temperature with a Bomem DA8.02 Fourier transform spectrometer including a deuterium lamp source, a quartz beam splitter and a silicon detector. The vapor sample was loaded into a 23.5 cm glass cell with quartz window by using trap to trap transfer and measurements were made by taking the average of 4000 scans at 1 cm^{-1} resolution in the 25000-40000 cm^{-1} region for 2,6-difluoropyridine sample.

CHAPTER III

THEORETICAL AND COMPUTATIONAL METHODS

Introduction

Theoretical calculations were used to support experimental observations and serve as a guide to predict the molecular structures, vibrational frequencies, and energy levels. The electronic ground state vibrational frequencies and structures were calculated using density functional theory (DFT) and ab initio methods using the Gaussian 09 program package.[70] The vibrational frequencies and structures of electronic excited states were calculated using the CASSCF method[71] with the GAMESS program package.[72] Fortran programs developed in Laane's research group were also used to determine the two dimensional potential energy functions.[73]

Density Functional Theory (DFT) Calculations

Density functional theory (DFT) is a quantum mechanical modelling method for the study of molecular structure and molecular properties mainly in the electronic ground state. The functional of electron density are utilized to reduce N electrons with 3N spatial coordinates to 3 spatial coordinates. The Becke and Lee-Yang-Parr (B3LYP) is one of these types of methods. The Becke and Lee-Yang-Parr (B3LYP) level of theory combined with the 6-311++G(d,p) basis set was utilized for the calculation of vibrational frequencies of 2,6-difluoropyridine and 2,3,5,6-tetrafluoropyridine in their electronic

ground state. A scaling factor of 0.964 was used for C-H stretching frequencies, and of 0.985 for frequencies below 1800 cm^{-1} based on previous work.[19,74-78] The Becke and Lee-Yang-Parr (B3LYP) method with cc-PVTZ basis set were also carried out for the calculations of vibrational frequencies in 2-cyclopenten-1-one ethylene ketal, halobismuthates and haloantimonates.

Ab Initio and CASSCF Calculations

The second order Moller-Plesset (MP2) level of theory with cc-PVTZ basis set were used for electronic ground state structure optimization in 2,6-difluoropyridine, 2,3,5,6-tetrafluoropyridine, 2-cyclopenten-1-one ethylene ketal, halobismuthates and haloantimonates. The electronic excited state calculations for structure optimization and vibrational frequencies were done in collaboration with Sunghwan Kim at the National Institute of Health (NIH). The CASSCF method with a 6-311++G(d,p) basis set was employed using the GAMESS program package. A scaling factor of 0.905 was used for all electronic excited state vibrational frequencies based on previous work.[20]

Energy Level Calculations

The Meinander-Laane DA2OPTN4 program[73] was used to calculate the ring-puckering energy levels and wavefunctions.

CHAPTER IV

INFRARED, RAMAN, AND ULTRAVIOLET ABSORPTION SPECTRA AND THEORETICAL CALCULATION AND STRUCTURE OF 2,6-DIFLUOROPYRIDINE IN ITS GROUND AND EXCITED ELECTRONIC STATES*

Introduction

The spectra, structures, and vibrational levels of pyridine (Py), 2-fluoropyridine (2FPy), and 3-fluoropyridine (3FPy) were reported in their ground and excited electronic states.[18-20] The results indicate that all of these molecules are planar in their S_0 electronic ground states and have nearly harmonic out-of-plane ring-bending vibrational frequencies near 410 cm^{-1}. In its $S_1(n,\pi^*)$ electronic excited state, pyridine becomes quasi-planar and very floppy with a barrier to planarity of 3 cm^{-1}. Its out-of-plane ring-bending vibration has a mostly quartic potential energy function and has a frequency of †59.5 cm^{-1}. The two fluoropyridines remain planar in their $S_1(n,\pi^*)$ states but become more floppy with the out-of-plane ring bending frequencies of 240 cm^{-1} (calculated) for 2FPy and 227 cm^{-1} for 3FPy. In their $S_2(\pi,\pi^*)$ states, the molecules are also planar and floppy with bending frequencies of 163 cm^{-1} for 2FPy and 272 cm^{-1} for 3FPy. As a

---

* Reprinted with permission from "Infrared, Raman, and Ultraviolet Absorption Spectra and Theoretical Calculations and Structure of 2,6-Difluoropyridine in Its Ground and Excited Electronic States" by Sheu, H.; Kim, S. and Laane, J. *J. Phys. Chem. A* **2013**, 117(50), 13596. Copyright [2013] by American Chemical Society.

continuation of the previous work, the 2,6-difluoropyridine (26DFPy) molecule was investigated to observe the effect of additional fluorine atoms on the structures and low-frequency vibrations in the electronic excited states. The ground state vibrational data is provided by infrared and Raman spectra and the data for the $S_1(\pi,\pi^*)$ state is provided by ultraviolet absorption spectra. Theoretical computations were carried out to assist in the assignment of the vibrational frequencies for both ground and excited states and also to calculate the structures for the S_0, $S_1(\pi,\pi^*)$ and $S_2(n,\pi^*)$ states.

Results and Discussion

At both B3LYP and CASSCF levels, 26DFPy in its ground state has a planar structure with the C_{2v} symmetry. For the $S_1(\pi,\pi^*)$ excited state, however, whereas a planar structure is predicted by the CASSCF method, the TD-B3LYP method resulted in a puckered structure with a barrier to planarity of 124 cm^{-1}. At the CASSCF level, the molecular structure of 26DFPy in its $S_2(n,\pi^*)$ state was predicted to be puckered with a barrier to planarity of 256 cm^{-1}. The calculated structures for 26DFPy in its S_0 state from B3LYP and CASSCF calculations is shown in Figure 2. The bond distances and angles can be seen to be very similar for the two different calculations. The molecular structures for 26DFPy in its $S_1(\pi,\pi^*)$ and $S_2(n,\pi^*)$ states, computed at the CASSCF/6-311++G(d,p) level is shown in Figure 3. The structure calculated by TD-B3LYP method for the $S_1(\pi,\pi^*)$ state is also shown in the same figure. The structure of 26DFPy in the $S_1(\pi,\pi^*)$ state, compared to its ground state, was characterized by increased bond lengths in the pyridine ring. The N-C, C(F)-C and C(3)-C(4) bond lengths were longer in the $S_1(\pi,\pi^*)$

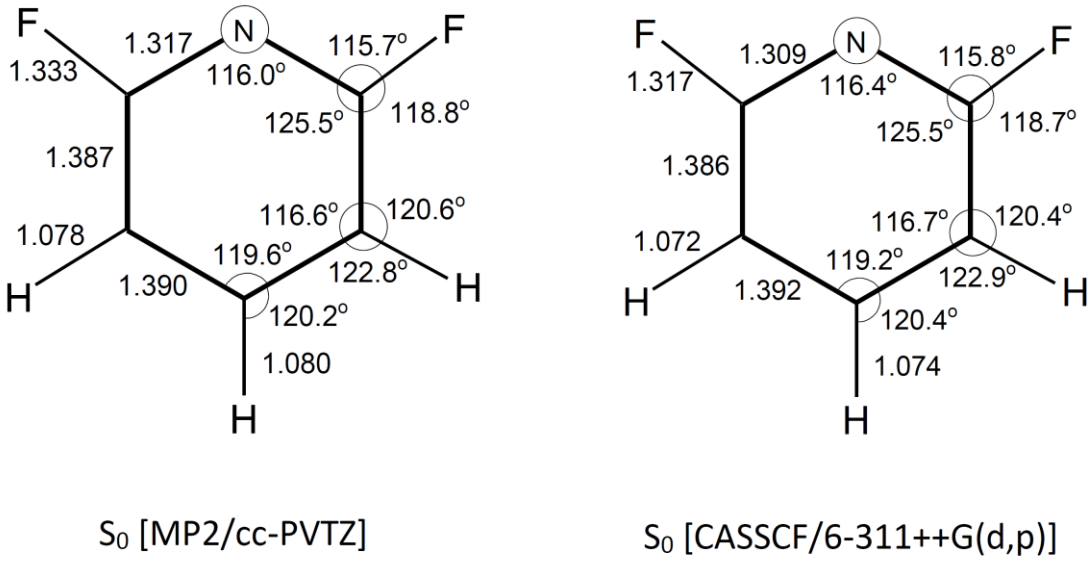

Figure 2 Calculated structures of 2,6-difluoropyridine (26DFPy) in its ground electronic state[79]

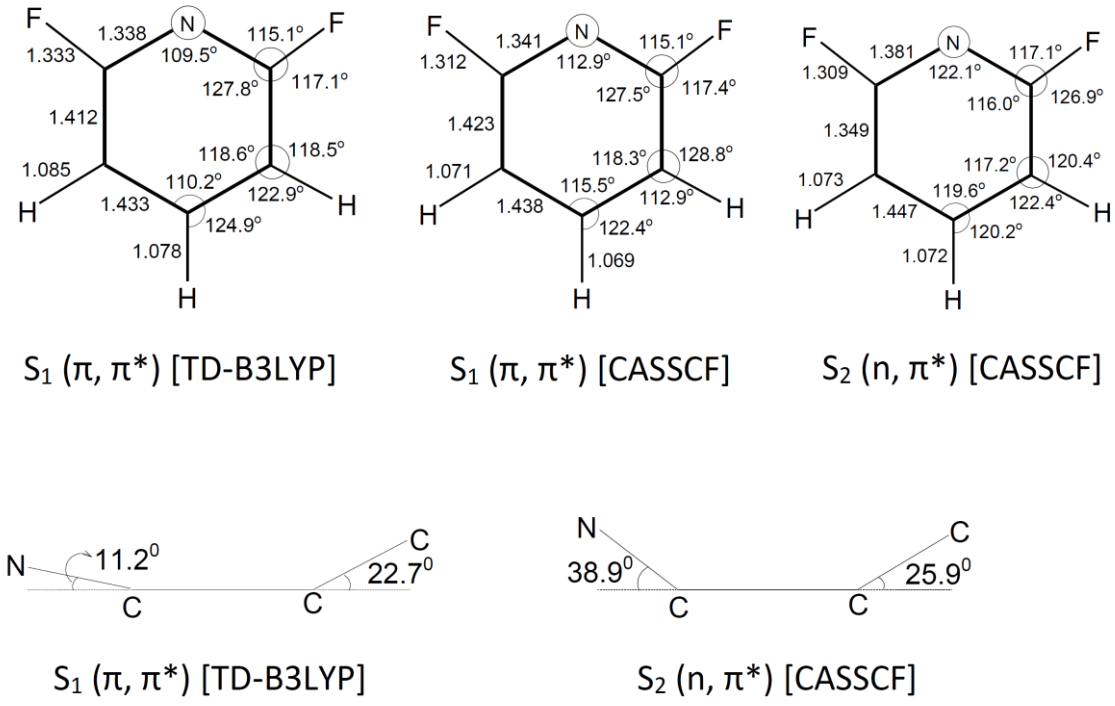

Figure 3 Calculated structures of 2,6-difluoropyridine (26DFPy) in its excited electronic state[79]

state than in the ground state, by 0.032 Å, 0.037 Å, and 0.046 Å, respectively, reflecting the excitation of an electron from a bonding π orbital to an antibonding π* orbital. The two determinants with the largest contribution to the CASSCF wave function for the $S_2(n,\pi^*)$ state of 26DFPy can be explained by the calculated n, π and π* molecular orbitals for 26DFPy shown in Figure 4. This corresponds to excitation from the nitrogen lone pair orbital to the π_4^* orbitals, which has a bonding character between the C(F) and C(H) atoms and an antibonding character between the N and C(F) atoms and between the C(H) and C(H) atoms. As a result, 26DFPy in the $S_2(n,\pi^*)$ state had a shorter C(F)-C bond length (by 0.037 Å) and longer N-C and C(H)-C(H) bond lengths (by 0.072 Å and 0.055 Å, respectively) than in its ground state. The selected geometrical parameters of 26DFPy in its ground and excited states with those of pyridine, 2FPy, and 3FPy are compared in Table 1.

The observed structural changes listed in Table 1 can be explained by Figure 4. For pyridine, 2FPy, 3FPy, and 26DFPy the bond length changes in the S(n,π*) and S(π,π*) states are similar. The N-C bonds increase in both excited states but the C(2)-C(3) and C(5)-C(6) bonds decrease in the S(n,π*) state and increase in the S(π,π*) state. The pyridine ring molecular orbitals are similar to those in benzene so the n→π* transition is to an antibonding orbital which has increased bonding character between the C(2)-C(3) and between the C(5)-C(6) bonds. The orbital nodes are at the N-C bonds and C(3)-C(4) and C(4)-C(5) bonds. For both the ground and excited states it is also evident that the fluorine substitution in the carbon(s) adjacent to the nitrogen atom decreases the N-C(F)

bond distances. This is due to both electrostatic effects as well as some bonding participation of the fluorine p orbitals with the ring π system.

The liquid and vapor infrared spectra are shown in Figure 5 and Raman spectra are shown in Figure 6. The calculated spectra from the B3LYP calculations are also shown in the same figure. The agreement between observed and calculated frequency values is excellent. The agreement for intensities is good for the most part although the ν_3 ring-stretching band at 1615 cm^{-1} in the observed Raman spectrum is much weaker than predicted. A few overtone bands, which are not in the calculated spectra for the fundamentals are also revealed in the same spectra. As can be seen in Figure 5, some distinct type A (ν_{22}, ν_{24}, ν_{26}, ν_{27}), type B (ν_5, ν_8), and type C (ν_{10}, ν_{15}) band contours which correspond for B_2, A_1 and B_1 symmetry species, respectively are clearly displayed in the infrared spectra of the vapor. Both the experimental and calculated data are summarized in table 2 and all vibrational assignments can be made unambiguously.

The ultraviolet absorption spectrum of 26DFPy vapor is shown in Figure 7. The band origin is at 37,820.2 cm^{-1} and corresponds to a transition to the $S_1(\pi,\pi^*)$ state. A value of 39,191 cm^{-1} for this transition and a value of 42,323 cm^{-1} for the transition to the $S_2(n,\pi^*)$ state are predicted by CASSCF calculations. The increasing absorption at higher frequencies results in part from the $S_2(n,\pi^*)$ absorption. The transition frequencies of 26DFPy to those of pyridine, 2FPy, and 3FPy are shown in Table 3. The UV spectrum in expanded form along with labels for the most significant transitions is shown in Figure 8. A summary of the observed UV bands is presented in Table 4. The

Table 1 Bond distances (Å) and bond angles (degrees) for pyridine and fluoropyridines[a, 79]

	S_0				$S(\pi, \pi^*)$					$S(n, \pi^*)$			
	Py	2FPy	3FPy	26DFPy	Py	2FPy	3FPy	26DFPy		Py	2FPy	3FPy	26DFPy
								TD-B3LYP	CASSCF				
N-C(H)	1.340	-	1.338, 1.340	-	1.375	1.386	1.363, 1.382	-	-	1.369	1.365	1.367, 1.370	-
N-C(F)	-	1.344	-	1.317	-	1.360	-	1.338	1.341	-	1.343	-	1.381
C-F	-	1.313	1.340	1.333	-	1.309	1.330	1.333	1.312	-	1.316	1.322	1.309
C(2)-C(3)	1.392	1.338	1.389	1.387	1.364	1.343	1.371	1.412	1.423	1.433	1.420	1.423	1.349
C(3)-C(4)	1.391	1.391	1.384	1.390	1.439	1.463	1.405	1.433	1.438	1.433	1.436	1.421	1.447
C(4)-C(5)	1.391	1.387	1.391	1.390	1.439	1.416	1.454	1.433	1.438	1.433	1.435	1.432	1.447
C(5)-C(6)	1.392	-	1.392	1.387	1.364	1.375	1.358	1.412	1.423	1.433	1.437	1.435	1.349
CNC angle	116.8	-	117.4	116.0	128.5	127.4	129.1	109.5	112.9	116.0	114.5	115.6	122.1

[a]Calculated using MP2/cc-PVTZ for the S0 states and CASSCF/6-311++G(d,p) for the electronic excited states unless otherwise indicated

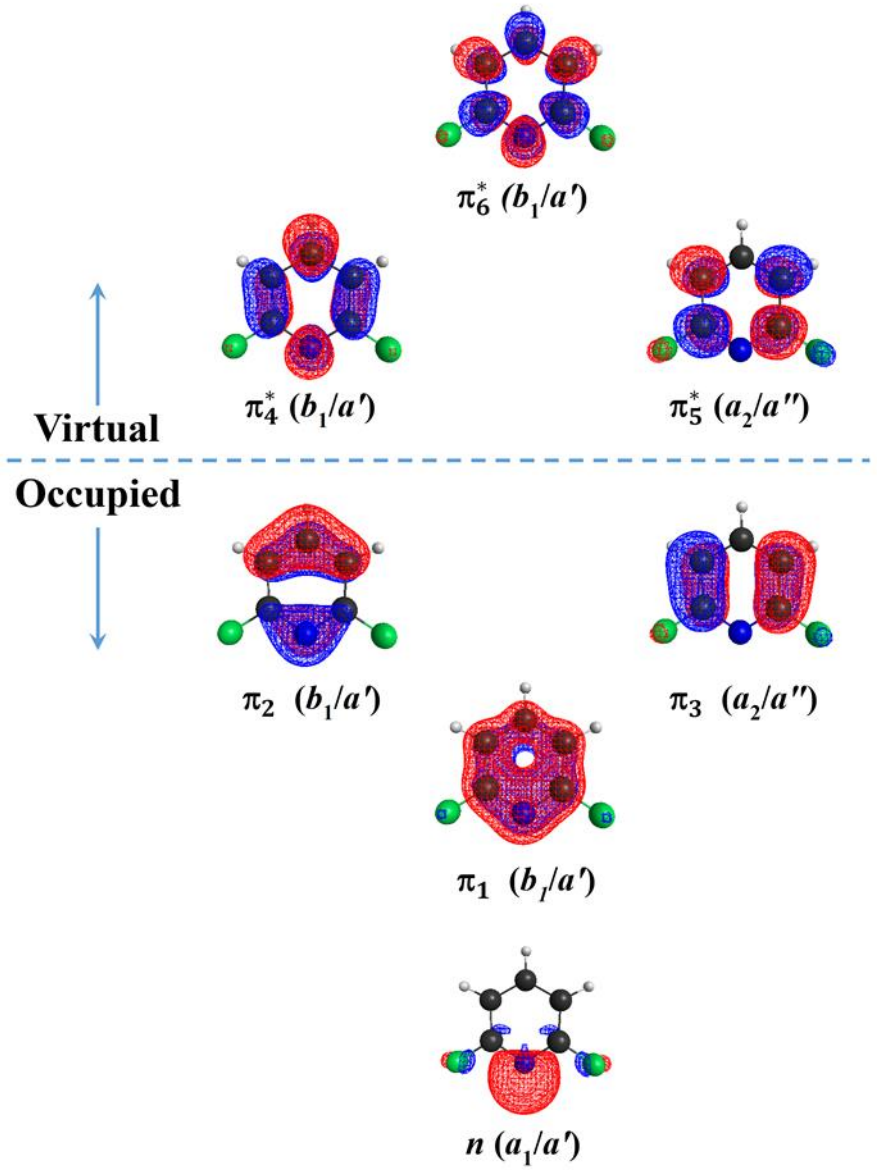

Figure 4 CASSCF-optimized molecular orbitals for 26DFPy in the ground state, computed at the CASSCF (8,7)/6-311++G(d,p) level. Orbital symmetries in the C2v/Cs point group are indicated in parentheses[79]

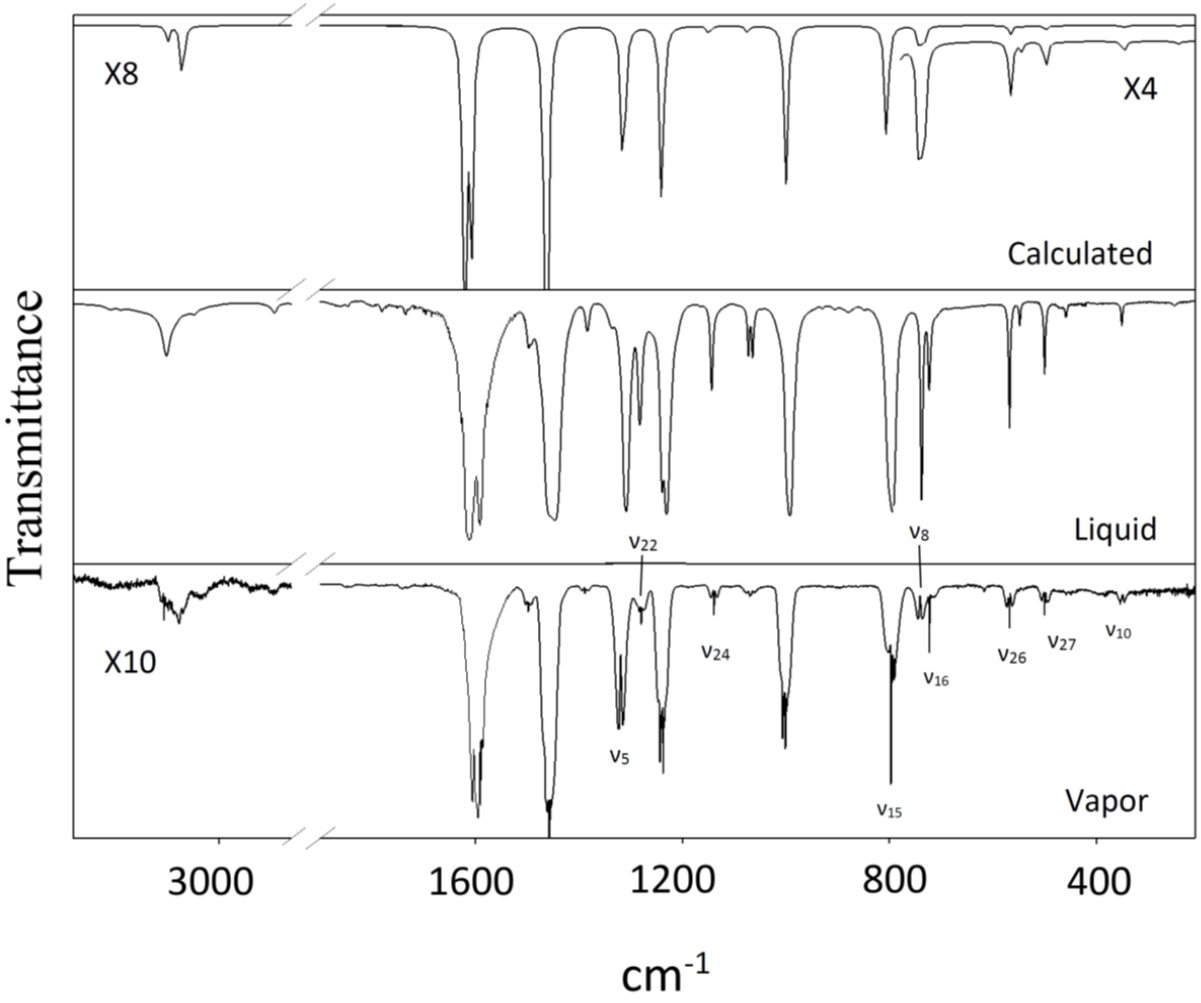

Figure 5 Calculated and observed infrared spectra of 26DFPy[79]

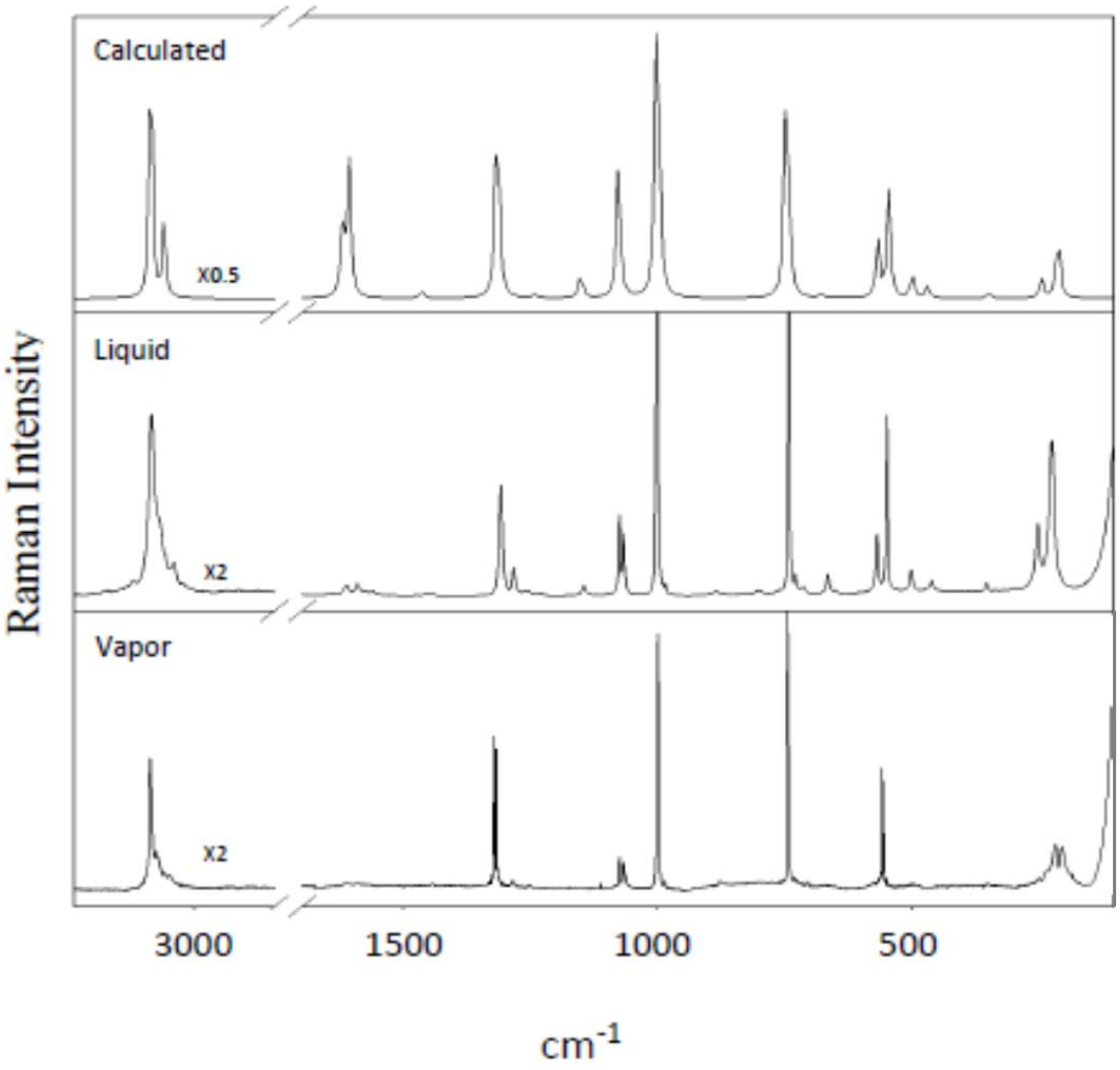

Figure 6 Calculated and observed Raman spectra of 26DFPy[79]

energy diagram for the low frequency vibrations for the S_0 and $S_1(\pi,\pi^*)$ states is shown in Figure 9. A comparison of observed and calculated frequency for the S_0, $S_1(\pi,\pi^*)$, an $S_2(n,\pi^*)$ states is presented in Table 5. Both excited states would have C_s symmetry if they are puckered with small barriers to planarity. However, the assignments were made according to C_{2v} symmetry which is applicable for planar structures. The data in Table 4 make it possible to assign most of the vibrational frequencies for the $S_1(\pi,\pi^*)$ state with considerable certainty.

The $S_1(\pi,\pi^*)$ state is calculated by TD-B3LYP to be floppy but slightly puckered as shown in Figure 3 and have a barrier to planarity of 124 cm^{-1}. This implies that this excited state should have a double-minimum potential function for the ring-puckering vibration. However, because the ring-puckering and C-F out-of-plane wagging motions of A_2 symmetry species are strongly coupled, a one-dimensional calculation of the puckering vibrational potential energy function cannot be readily applied. In fact, we have found no definitive evidence for inversion doubling in the $S_1(\pi,\pi^*)$ excited state which would have been reflected in the energy levels of ν_{17} and/or ν_{18}. Thus, the experimental results support the CASSCF calculation result that this excited state is planar. For pyridine[18] in its $S_1(n,\pi^*)$ state we did confirm with experimental data that the spectra for the ring-puckering vibration could be fit with a one-dimensional potential energy function with a tiny barrier to planarity of 3 cm^{-1}.

Although no experimental evidence for inversion doubling or a barrier to inversion for the $S_1(\pi,\pi^*)$ state was observed, it is instructive to present a picture of what would be expected if 26DFPy were in fact non-planar in this state as well as in its $S_2(n,\pi^*)$ state.

Table 2 Vibrational spectra (cm^{-1}) and assignments for the electronic ground state of 2,6- difluoropyridine[79]

C_{2v}	ν	Approximate description	Infrared		Raman		Calculated	
			Liquid	Vapor	Liquid	Vapor	υ	Intensity[a]
A_1	1	C-H stretch	-	-	3106 (10)	3109 (21)	3114	(0, 100)
	2	C-H stretch	-	3082 w	3086 (3)	3076 (3)	3083	(100, 4)
	3	Ring stretch	1613 s	1620 s	1612 (1)	1615 (0.8)	1617	(67,30)
	4	Ring stretch	1446 s	1458 s	1447 (0.3)	1443 (0.7)	1458	(3, 3)
	5	C-F sym. stretch	1309 s	1320 ms	1307 (12)	1318 (25)	1320	(36, 77)
	6	C-H in-plane wag	1069 m	1069 mw	1073 (8)	1072 (9)	1072	(1, 55)
	7	Ring breathing	992 s	1001 s	998 (71)	996 (82)	994	(1, 135)
	8	Ring bend	738 s	741 m	737 (100)	740 (100)	743	(5, 100)
	9	Ring bend	549 m	-	548 (19)	546 (22)	546	(0.3, 36)
	10	C-F in-plane wag	351 m	350 m	351 (1)	350 (0.9)	347	(0.4, 2)
A_2	11	C-H out-of-plane wag	-	-	881 (0.4)	874 (1)	875	(0, 0.02)
	12	Ring twisting	-	-	660 (2)	-	672	(0, 1)
	13	C-F out-of-plane wag	-	-	-	215 (13)	211	(0, 24)

Table 2 (Continued)[79]

C_{2v}	ν	Approximate description	Infrared		Raman		Calculated	
			Liquid	Vapor	Liquid	Vapor	υ	Intensity[a]
B_1	14	C-H out-of-plane wag	993 s	999 s	982 (1)	983 (2)	987	(0.05, 1)
	15	C-H out-of-plane wag	794 s	797 s	798 (0.4)	-	804	(24, 1)
	16	Ring twisting	723 s	723 m	725 (2)	727 (1)	733	(4, 3)
	17	Ring puckering[b]	460 m	-	460 (1)	-	470	(0.03, 4)
	18	C-F out-of-plane wag[b]	249 mw	-	250 (7)	247 (2)	242	(0.1, 7)
B_2	19	C-H antisym. stretch	3108 m	3113 w	3106 (10)	3097 (6)	3110	(29, 26)
	20	Ring stretch	1593 s	1606 s	1591 (1)	1593 (0.9)	1597	(47, 66)
	21	Ring stretch	1446 s	1461 s	1447 (0.3)	-	1461	(100, 0.2)
	22	Ring stretch	1282 s	1280 ms	1282 (3)	1285 (2)	1297	(1, 12)
	23	C-H in-plane wag	1239 s	1243 s	1231 (0.3)	1253 (0.8)	1242	(39, 2)
	24	C-H in-plane wag	1143 m	1139 m	1144 (0.9)	-	1146	(2, 11)
	25	C-F anti-sym. stretch	992 s	1007 s	-	1001 sh (9)	1003	(28, 0.8)
	26	Ring bend	568 m	568 m	568 (6)	-	565	(2, 20)
	27	C-F in-plane wag	501 m	501 m	500 (2)	-	498	(1, 9)

[a] Relative intensities for (IR, Raman); [b] Strongly coupled vibrations

Table 3 Observed and calculated electronic transition frequencies (cm^{-1})[79]

Transition	Pyridine		2-fluoropyridine		3-fluoropyridine		2,6-difluoropyridine	
	Obs.	Calc.[a]	Obs.	Calc.[a]	Obs.	Calc.[a]	Obs.	Calc.[a]
n → π*	34 767	36 296	-	39 199	35 051.7	36 617	-	42 323
π → π*	38 350[b]	38 312	38 030.4	38 796	37 339	38 311	37 820.2	39 191

[a] CASSCF/6-311++G(d,p) level of theory

[b] Ref 18

Table 4 Ultraviolet absorption spectra (cm^{-1}) and assignments for 2,6-difluoropyridine[79]

Observed	Peak intensity[a]	Assignment	Inferred
-547	s	9_1^0	0-546 = -546
-487	w	18_2^0	0-494 = -494
-383	s	10_2^1	318-700 = -382
-348	s	10_1^0	0-350 = -350
-331	w	16_1^1	395-723=-328
-302	w	12_1^1	372-668=-296
-245	w	$17_0^2 18_2^0$	254-494 = -240
-215	m	$10_1^0 17_1^3$	-350-247+381 = -216
-202	w	$13_2^2 17_1^1$	472-677=-205
		$9_1^0 13_0^2$	345-546=-201
-171	s	$13_2^0 17_0^2$	-430+254 = -176
-161	s	$13_1^1 17_1^1$	301-462=-161
-120	mw	$17_0^1 18_1^0$	127-247 = -120
-95	w	$10_1^0 17_0^2$	-350+254 = -96
-87	mw	13_2^2	345-430 = -85
-75	s	9_1^1	474-546 = -72
-49sh	m	27_1^1	455-501 = -46
-41	s	13_1^1	174-215 = -41
-31	s	10_1^1	318-350 = -32
-18	w	$18_2^0 9_0^1$	474-494=-20

Table 4 (Continued)[79]

Observed	Peak intensity	Assignment	Inferred
10	s	$13_1^2\,17_1^1$	472-462=10
46	w	$13_2^0\,9_0^1$	474-430=44
72	w	12_1^2	744-668=76
143	ms	$16_0^1\,18_1^0$	395-247=148
156	s	$12_0^1\,13_1^0$	372-215=157
254	m	17_0^2	127x2 = 254
300	s	$17_0^1\,18_0^1$	179+127 =306
		13_1^3	516-215=301
318	s	10_0^1	318-0 = 318
345	s	13_0^2	174x2 = 348
358	s	18_0^2	179x2 = 358
474	s	9_0^1	474-0 = 474
508	m	18_0^4	508-0=508
522	w	$16_0^1\,17_0^1$	127+395=522
549	mw	$12_0^1\,13_0^1$	372+174 = 546
572	w	$16_0^1\,18_0^1$	395+178 = 573
627	mw	$15_0^1\,17_0^1$	503+127 =630
637	w	10_0^2	318x2 = 636

Table 4 (Continued)[79]

Observed	Peak intensity	Assignment	Inferred
682	s	8_0^1	680-0 = 680
713	s	18_0^4 ?	358x2 = 716
745	m	12_0^2	372x2 = 744
782	w	$14_0^1 17_0^1$	653+127 = 780
791	w	16_0^2	395x2 = 790
		$9_0^1 10_0^1$	474+317 = 791
885	w	7_0^1	885-0 = 885
909	m	27_0^2	455x2 = 910
952	s	9_0^2	474x2 = 948
961	s	6_0^1	961-0 = 961
1000	s	$8_0^1 10_0^1$	680+318 = 998
		26_0^2	496x2 = 992
1006	m	15_0^2	503x2 = 1006
1058	m	$11_0^1 12_0^1$	680+372 = 1052
1091	w	$12_0^2 13_0^2$	744+345 = 1089
1148	w	5_0^1	1167 cal
		$8_0^1 9_0^1$	680+474 = 1154
1201	ms	$7_0^1 10_0^1$	885+318 = 1203

Table 4 (Continued)[79]

Observed	Peak intensity	Assignment	Inferred
1264	w	$15_0^2 17_0^2$	1006+254 = 1260
1282	mw	$6_0^1 10_0^1$	961+318 = 1279
1292	ms	4_0^1	1289-0 = 1289
1351	mw	11_0^2	680x2 = 1360
1395	m	$25_0^1 26_0^1$	877+496 = 1373
1428	m	3_0^1	1424-0 = 1424
1438	w	$6_0^1 9_0^1$	885+474 = 1435
1464	w	$5_0^1 10_0^1$	1147+318 = 1465
1671	w	$14_0^2 18_0^2$	1306+358 = 1664
1678	m	$22_0^1 26_0^1$	1191+496 = 1687
1715	mw	25_0^2	858x2=1716
1755	vw	25_0^2	877x2 = 1754
1768	w	7_0^2	885x2=1770
1902	w	$3_0^1 9_0^1$	1424+474 = 1898
1948	w	$23_0^1 25_0^1$	1071+877 = 1948
1963	w	$4_0^1 8_0^1$	1289+680 = 1969
2006	w	24_0^2	1003x2=2006
2060	w	$22_0^1 25_0^1$	1191+877 = 2068

Table 4 (Continued)[79]

Observed	Peak intensity	Assignment	Inferred
2104	w	$11_0^2 12_0^2$	1360+744 = 2104
2142	w	23_0^2	1071x2 = 2142
2243	w	$4_0^1 6_0^1$	1289+961 = 2250
2382	w	22_0^2	1191x2 = 2382

[a] s-strong, m-medium, w-weak, v-very

Table 5 Observed and calculated vibrational frequencies (cm^{-1}) for 2,6-difluoropyridine in its ground and excited electronic states[79]

C_{2v}	v	Approximate description	S_0		S_1 (π, π^*)			S_2 (n, π^*)
			Obs.	Calc.	Obs.	TD-B3LYP	CASSCF	CASSCF
A_1	1	C-H stretch	3109	3114	-	2954	3077	3049
	2	C-H stretch	3082	3083	-	2889	3055	3030
	3	Ring stretch	1620	1617	1424	1409	1525	1580
	4	Ring stretch	1458	1458	1289	1296	1364	1354
	5	C-F sym. stretch	1320	1320	1147	1167	1260	1270
	6	C-H in-plane wag	1069	1072	960	948	935	937
	7	Ring breathing	1001	994	885	877	923	899
	8	Ring bend	741	743	682	688	684	705
	9	Ring bend	546	546	474	476	466	542
	10	C-F in-plane wag	350	347	318	314	329	356
A_2	11	C-H out-of-plane wag	874	875	676	680	573	665
	12	C-F out-of-plane wag	660	672	372	377	380	378
	13	Ring twist	215	211	173	163	89	125

Table 5 (Continued)[79]

C_{2v}	ν	Approximate description	S_0		S_1 (π, π*)			S_2 (n, π*)
			Obs.	Calc.	Obs.	TD-B3LYP	CASSCF	CASSCF
B_1	14	C-H out-of-plane wag	999	987	653	653	547	737
	15	C-H out-of-plane wag	797	804	502	502	434	489
	16	Ring twist	723	733	395	405	349	454
	17	Ring pucker	460	470	127	112	158	69
	18	C-F out-of-plane wag	247	242	179	174	217	288
B_2	19	C-H anti-sym. stretch	3113	3110	-	2892	3059	3034
	20	Ring stretch	1606	1597	-	1328	1752	1515
	21	Ring stretch	1461	1461	-	1268	1481	1356
	22	Ring stretch	1280	1297	-	1205	1354	1292
	23	C-H in-plane wag	1243	1242	-	1080	1192	1200
	24	C-H in-plane wag	1139	1146	-	1001	1103	1023
	25	C-F antisym. stretch	1007	1003	858	877	895	950
	26	Ring bend	568	565	500	493	515	488
	27	C-F in-plane wag	501	498	455	450	458	464

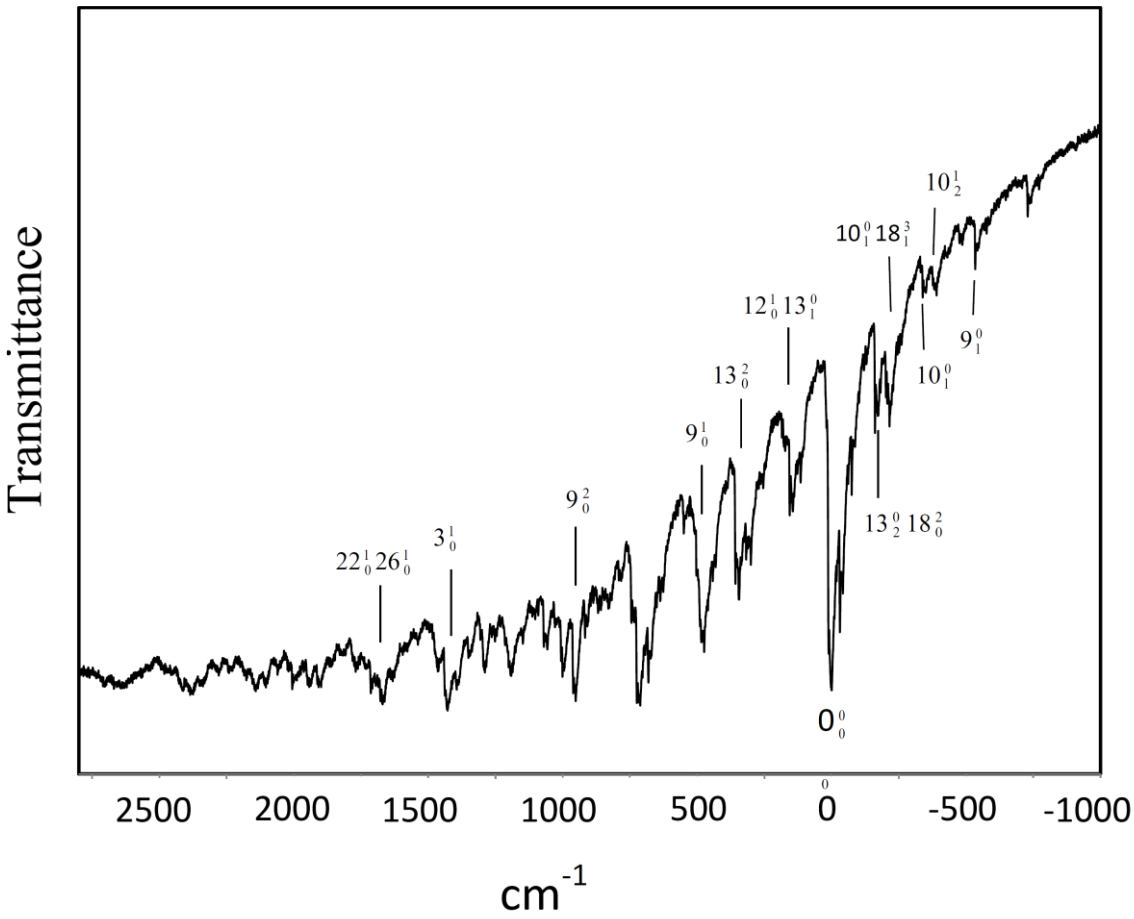

Figure 7 Ultraviolet absorption spectra of 26DFPy relative to the band origin[79]

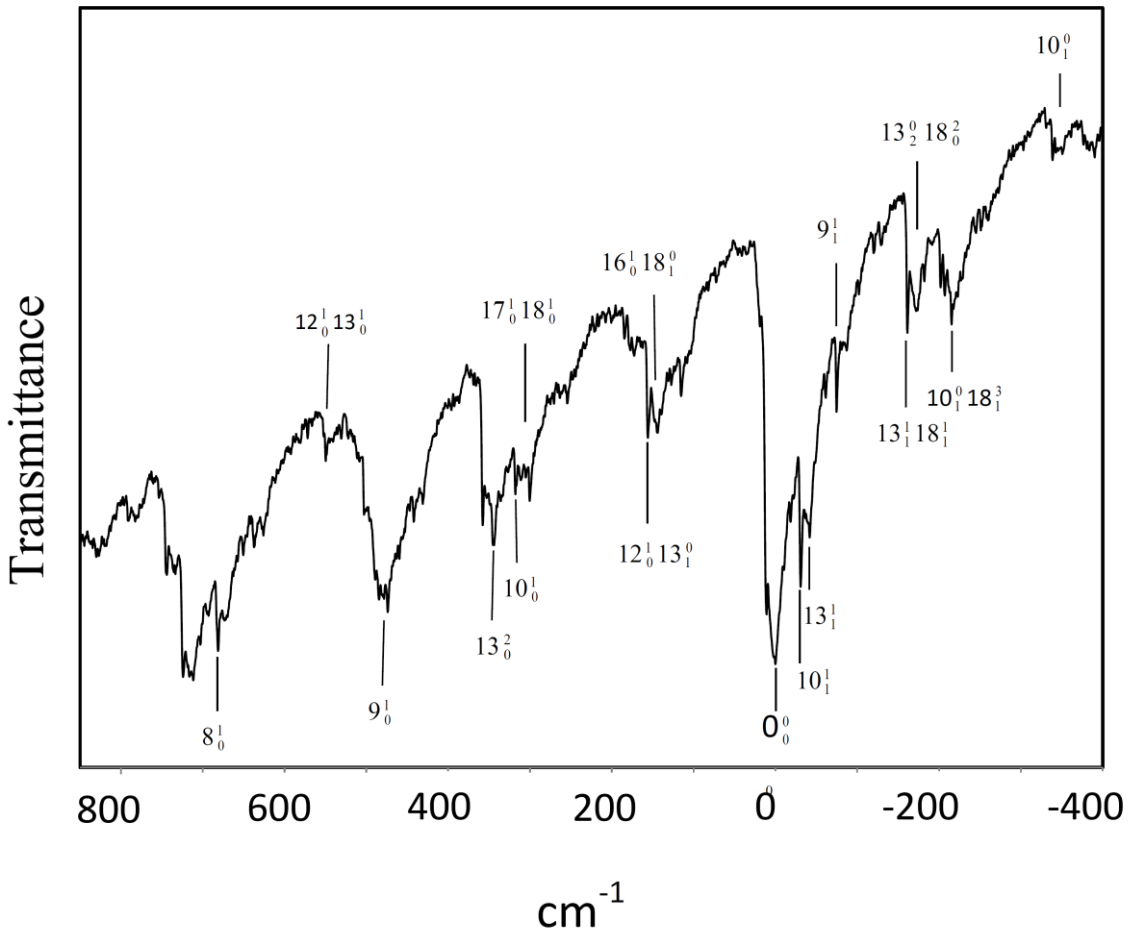

Figure 8 Ultraviolet absorption spectra of 26DFPy expanded near the band origin[79]

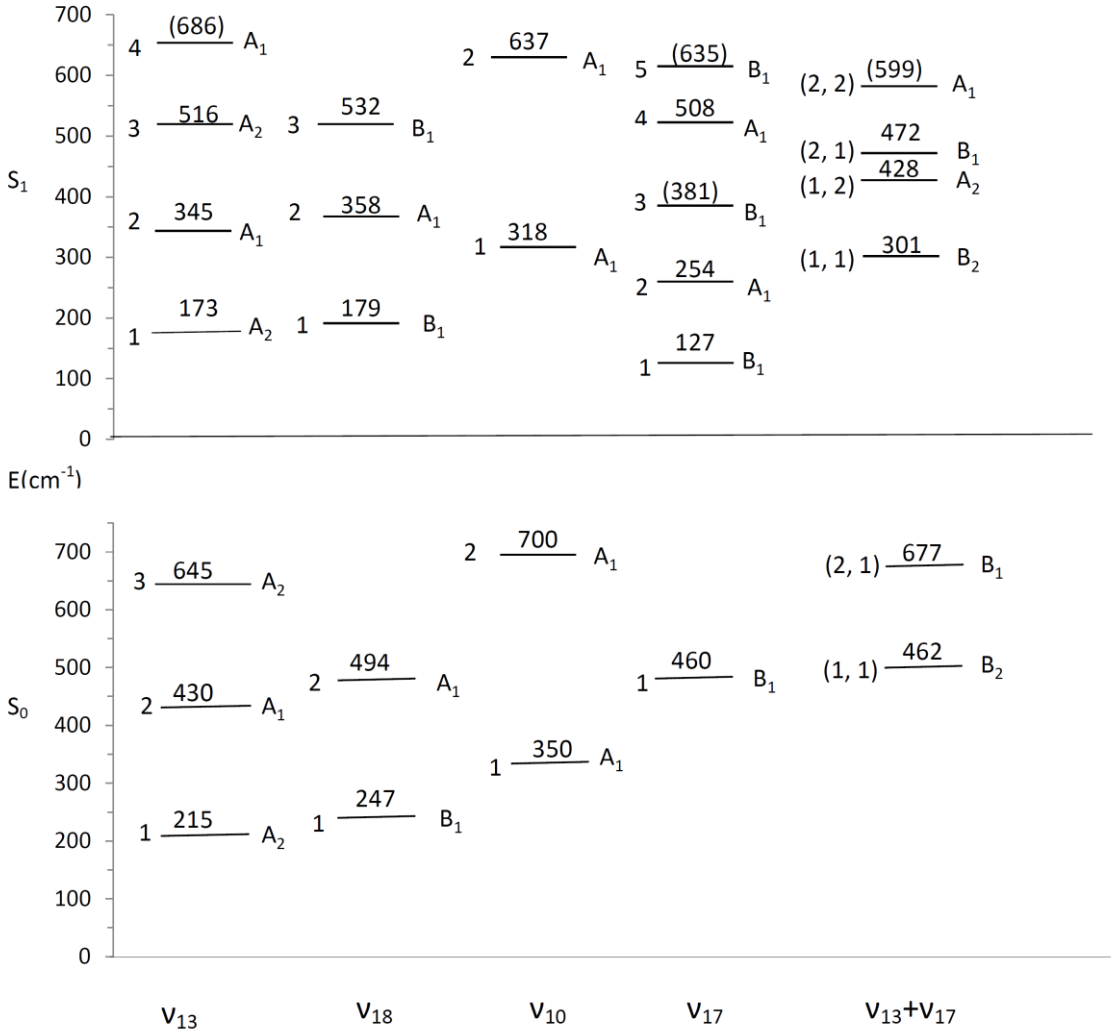

Figure 9 Energy diagram for the lower frequency vibrations of 26DFPy in its S_0 ground and $S_1(\pi,\pi^*)$ excited states[79]

As discussed, ν_{17}, the ring-puckering, and ν_{18}, the out-of-plane, in-phase C-F wagging motions are strongly coupled in both electronic excited states so it is not expected that one-dimensional calculations of the type that we successfully carried out for pyridine[1] are feasible here. Nonetheless, we believe that the calculation of one-dimensional functions based on the *ab initio* computations will provide insight into understanding the pattern of quantum states when energy barriers are present. The TD-B3LYP *ab initio* calculations predicted a barrier of 124 cm^{-1} for the $S_1(\pi,\pi^*)$ state and a predicted ring-puckering frequency (coupled to the C-F wagging mode) of 112 cm^{-1}. The CASSCF calculation predicted a barrier of 256 cm^{-1} and a ring-puckering frequency of 69 cm^{-1} for the $S_2(n,\pi^*)$ state.

As the Laane's group showed many years ago,[80] for double-minimum potential energy functions with high enough barriers the separations between lowest pairs of near-degenerate levels (caused by inversion doubling) become more and more harmonic. In other words, the separation between pairs of levels can be estimated quite well using a harmonic oscillator model to approximate the shape of each potential well. This means that the predicted harmonic frequency from the *ab initio* calculation is at least a fairly good estimate of the expected energy between the lowest pairs of levels. The Laane's group have demonstrated this in the past by observing experimental transitions for double-minimum potentials and finding them to be quite well estimated by DFT and *ab initio* calculations.[75,78,81-95] Applying this principle, we have calculated one-dimensional potential energy functions for the ring-puckering so that they match the computed barrier heights and the calculated *ab initio* frequencies. The latter were set to match the v = 0

$\rightarrow$ v = 3 puckering transitions. The calculations were done with reduced coordinates[80] since the reduced mass could not be reliably calculated due to the strong coupling with the C-F wagging motion. For the $S_1(\pi,\pi^*)$ the calculated function is

$$V(cm^{-1}) = 18.34\ (Z^4 - 5.20Z^2) \quad (1)$$

and for $S_2(n,\pi^*)$ it is

$$V(cm^{-1}) = 7.33(Z^4 - 12.6Z^2). \quad (2)$$

These functions are shown in Figures 10 and 11. The symmetry species for both sets of quantum states are A_1 for even v values and B_1 for odd values of v. Hence, electronic transitions to v = even levels should only arise from A_1 vibrational levels in the electronic ground state while transitions to v = odd should arise from B_1 vibrational excited state. In our experimental data for the $S_1(\pi,\pi^*)$ state, which only has a small calculated barrier to inversion of 124 cm^{-1}, we were not able to find transitions compatible with a function similar to Eq. (1). Thus, we conclude that 26DFPy is most likely planar in its $S_1(\pi,\pi^*)$ state although it is conceivable that the coupling with the C-F wagging sufficiently distorts the potential energy surface to invalidate the predicted picture. For the $S_2(n,\pi^*)$ state, however, the calculated barrier of 256 cm^{-1} is sufficiently higher that we feel it is very likely that the molecule is indeed non-planar and that the potential function shown in Figure 10 may present quite a reasonable picture of the puckering potential energy function.

Pyridine, 2FPy, 3FPy, and 26DFPy molecules all have planar and fairly rigid structures in their electronic ground states. Pyridine[18] in its $S_1(n,\pi^*)$ state becomes extremely floppy and its out-of-plane ring bending frequency drops to 57 cm^{-1}. In fact, it

even has a minute barrier to planarity of 3 cm^{-1}. 2FPy and 3FPy although remain planar also become floppier in their electronic excited states as reflected by their lower out-of-plane ring bending frequencies. 26DFPy becomes puckered according to TD-B3LYP calculations in its $S_1(\pi,\pi^*)$ state and according to CASSCF in its $S_2(n,\pi^*)$ excited state. The calculated barriers to planarity are quite small (124 cm^{-1} and 256 cm^{-1} for the $S_1(\pi,\pi^*)$ and $S_2(n,\pi^*)$ states, respectively). This implies that this excited state should have a double-minimum potential function for the ring-puckering vibration. However, because the ring-puckering and C-F out-of-plane wagging motions of A_2 symmetry species are strongly coupled, a one-dimensional calculation of the puckering vibrational potential energy function cannot be readily applied. In fact, we have found no definitive evidence for inversion doubling in the $S_1(\pi,\pi^*)$ excited state which would have been reflected in the energy levels of ν_{17} and/or ν_{18}. Thus, the planar structure revealed by the CASSCF excited state calculation is supported by experimental data.

The vibrational frequencies for pyridine, 2FPy, 3FPy, and 26DFPy molecules in their S_0, $S(\pi,\pi^*)$, and $S(n,\pi^*)$ states are summarized in Table 6. The C-F stretching and wagging frequencies are also listed in the same table. The symmetry species in the table apply to pyridine and 26DFPy both of which have C_{2v} symmetry point groups. For 2FPy and 3FPy, which have C_s symmetry, the vibrations listed under A_1 and B_2 in Table 6 correspond to the in-plane A' modes while A_2 and B_1 correspond to the out-of-plane A" modes. As expected, all of the ring stretching and bending vibrations for all four molecules drop in frequency as the bonds in the excited state become weaker and the

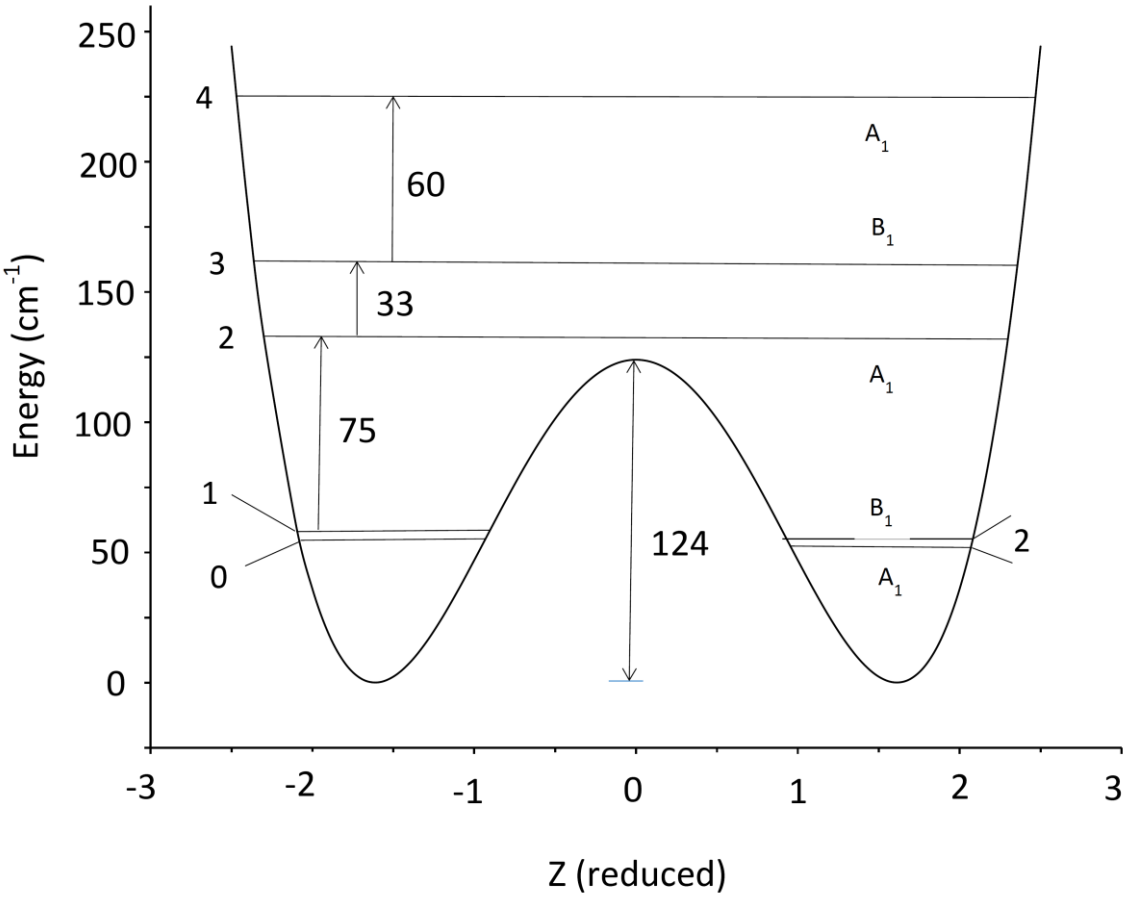

Figure 10 Hypothetical potential energy function for the ring puckering vibration of 26DFPy based on Eq. (1) for the $S_1(\pi, \pi^*)$ electronic excited state[79]

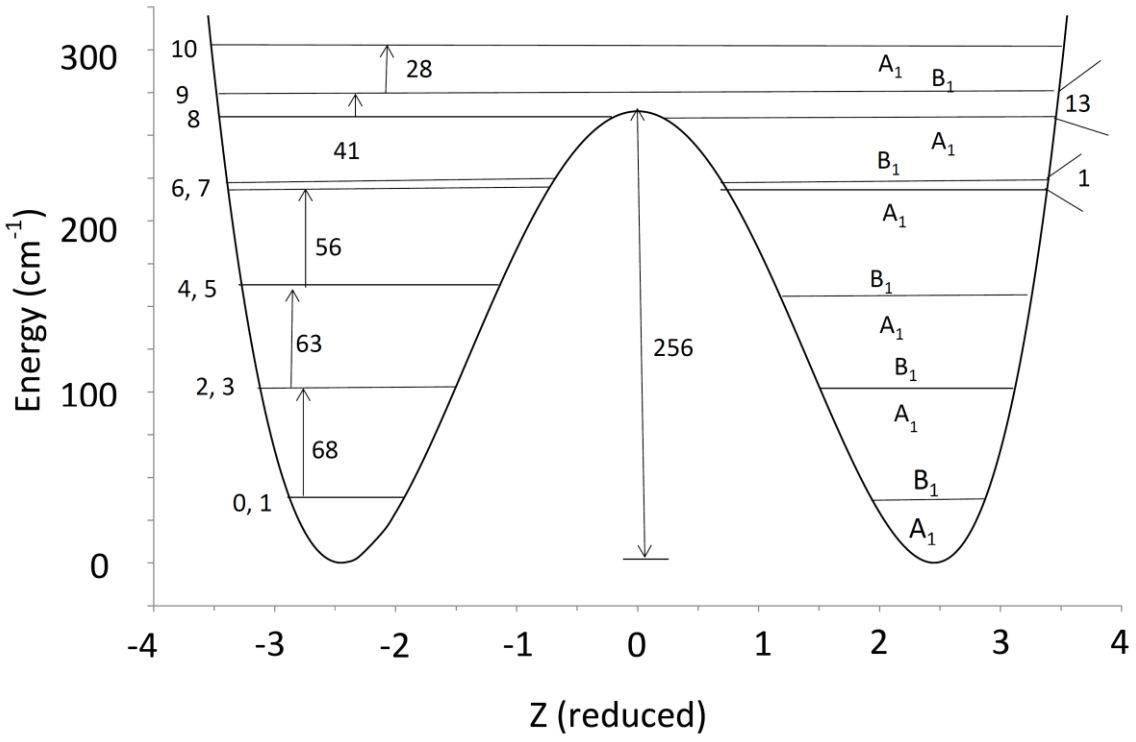

Figure 11 Hypothetical potential energy function for the ring puckering vibration of 26DFPy based on Eq. (2) for the $S_2(n, \pi^*)$ electronic excited state[79]

rings get floppier due to the decreased π bonding character. The C-F stretching frequency also drops in the excited state suggesting that the fluorine atoms do participate to some extent in the π bonding. By far the most significant changes in vibrational frequencies in the excited electronic states are for the A_2 and B_1 out-of-plane ring modes and the out-of-plane C-F wags. There is significant vibrational coupling between the ring-puckering and the out-of-plane C-F wagging modes so it is somewhat overly simplistic to look at the puckering frequencies separately. In the electronic ground state all four molecules have strong π bonding and are rigid with a puckering frequency over 400 cm^{-1}. Substitution of fluorine atoms increases this value and for 26DFPy it is 460 cm^{-1}. The in-phase out-of-plane C-F wagging is at 247 cm^{-1}. In both the $S_1(\pi,\pi^*)$ and $S_2(n,\pi^*)$ states, the puckering frequency is dropped below that of the C-F wagging due to increased anti-bonding character and the motions become even more highly mixed. For 26DFPy in the $S_1(\pi,\pi^*)$ state the puckering is at 127 cm^{-1} and the wagging at 179 cm^{-1}. For $S_2(n,\pi^*)$ the frequencies are calculated to be at 69 and 288 cm^{-1}, respectively.

Conclusions

The 2,6-difluoropyridine is rigidly planar in its ground state while the $S_2(n,\pi^*)$ state is predicted to be puckered with a barrier to planarity of 256 cm^{-1} with CASSCF calculation. The $S_1(\pi,\pi^*)$ state is predicted to be a planar molecule by CASSCF calculation while a puckered structure with a small barrier to planarity of 124 cm^{-1} is obtained by TD-B3LYP calculation method. The planar structure is more favored by the experimental data.

Table 6 Selected vibrational frequencies (cm^{-1}) of pyridine and fluoropyridines[79]

Sym.[a]	Description	S_0				S (π, π*)				S (n, π*)			
		Py	2FPy	3FPy	26DFPy	Py	2FPy	3FPy	26DFPy	Py	2FPy	3FPy	26DFPy
A_1	Ring stretch	1584	1605	1594	1620	(1499)[b]	1690	(1699)	1424	(1507)	(1586)	1532	(1580)
	Ring stretch	1483	1478	1480	1458	(1394)	1453	1488	1289	(1379)	(1381)	1320	(1354)
	Ring breathing	1031	997	1022	1001	(878)	946	(874)	885	(857)	(879)	790	(899)
	Ring bend	991	842	816	741	(883)	797	690	680	(885)	(789)	737	(705)
	Ring bend	654	620	613	546	(577)	532	500	474	636	(554)	540	(542)
	C-F stretch	-	1266	1227	1320	-	1243	1206	1147	-	(1168)	1132	(1270)
	C-F in-plane wag	-	433	398	350	-	396	316	317	-	(380)	383	(356)
A_2	Ring twisting	375	518	507	660	(434)	432	(387)	372	(476)	(454)	425	(378)
	C-F out-of-plane wag	-	226	231	215	-	163	272	173	-	(240)	227	(125)
B_1	Ring twisting	700	733	701	723	(260)	322	298	395	326	(380)	305	(454)
	Ring puckering	403	414	412	460[c]	(244)	96	118	127[c]	60	(40)	107	(69)[c]
	C-F out-of-plane wag	-	226	231	247[c]	-	163	272	179[c]	-	(240)	227	(288)[c]

Table 6 (Continued)[79]

Sym.[a]	Description	S_0				S (π, π*)				S (n, π*)			
		Py	2FPy	3FPy	26DFPy	Py	2FPy	3FPy	26DFPy	Py	2FPy	3FPy	26DFPy
B_2	Ring stretch	1576	1593	1588	1606	(1680)	1489	(1512)	-	(1453)	(1438)	1519	(1515)
	Ring stretch	1442	1439	1426	1461	(1476)	1353	(1385)	-	(1314)	(1327)	1309	(1356)
	Ring stretch	1227	1286	1249	1280	(1310)	1220	(1265)	-	(1185)	(1210)	1199	(1292)
	Ring bend	601	554	533	568	(509)	493	426	496	543	(494)	517	(488)
	C-F stretch	-	1266	1227	1007	-	1243	1206	877	-	(1168)	1132	(950)
	C-F in-plane wag	-	433	398	501	-	396	316	455	-	(380)	383	(464)

[a] Symmetry species apply to Py and 26DFPy. For 2FPy and 3FPy the C-F vibrations are listed twice and the A_1 and B_2 symmetry species correspond to A' for 2FPy and 3FPy while A_2 and B_1 correspond to A"

[b] Frequencies in parentheses are calculated values

[c] Strongly coupled vibrations

CHAPTER V

INFRARED, RAMAN, AND ULTRAVIOLET ABSORPTION SPECTRA AND THEORETICAL CALCULATION AND STRUCTURE OF 2,3,5,6-TETRAFLUOROPYRIDINE IN ITS GROUND AND EXCITED ELECTRONIC STATES

Introduction

As discussed in the previous chapter, the 2,6-difluoropyridine molecule has a barrier to planarity of 256 cm^{-1} in its $S_2(n,\pi^*)$ state predicted by CASSCF calculations, and it has a planar structure in its $S_1(\pi,\pi^*)$ excited state shown by CASSCF calculations and experimental data. The out-of-plane ring bending vibrational frequency is 460 cm^{-1} for the S_0 ground state and 127 cm^{-1} for the $S_1(\pi,\pi^*)$ excited state. This indicates that 2,6-difluoropyridine becomes more floppy in the excited state compared to the ground state due to the decreased π bonding character. As a continuing investigation of the fluoropyridine molecules, the spectra and structures of 2,3,5,6-tetrafluoropyridine (TFPy) in its ground and excites states are presented. The experimental data for the ground state were obtained using infrared and Raman spectra while the $S_1(\pi,\pi^*)$ excited state data were obtained by ultraviolet absorption spectra. Theoretical computations were carried out to calculate the structures for both ground and excited states and also to assist with vibrational analysis.

Results and Discussion

2,3,5,6-Tetrafluoropyridine has a planar structure in its S_0 ground state with C_{2v} symmetry. For the $S_1(\pi,\pi^*)$ excited state, a puckered structure with a barrier to planarity of 30 cm^{-1} was predicted by CASSCF calculations. The calculated structures for 2,3,5,6-tetrafluoropyridine in its S_0 ground state and $S_1(\pi,\pi^*)$ excited state are shown in Figure 12. The structure in the $S_1(\pi,\pi^*)$ excited state has increased bond lengths in the pyridine ring as compared to the ground state. The N-C, C(2)-C(3) and C(3)-C(4) bond lengths are longer in the $S_1(\pi,\pi^*)$ state than in the ground state, by 0.026 Å, 0.032 Å, and 0.043 Å, respectively, due to the excitation of an electron from a bonding π orbital to an antibonding π^* orbital.

The calculated, liquid and vapor phase infrared spectra of 2,3,5,6-tetrafluoropyridine are shown in Figure 13, and Raman spectra are shown in Figure 14. Good agreement between experimental and calculated frequency values was found. A few overtone bands were observed in the experimental liquid and vapor spectra, but the calculated spectrum provides only the fundamental vibrational frequencies. Both the experimental and calculated frequencies for infrared and Raman spectra are summarized in Table 7. The vibrational frequencies were readily assigned. As shown in Table 7, the ν_2 ring-stretching vibration is in Fermi resonance with a combination band of a C-H wag (ν_{14}) and ring twist (ν_{15}) which results in a band near 1611 cm^{-1} in the liquid and vapor infrared and Raman spectra. Three infrared band types (type A, type B and type C bands) were clearly observed in the infrared spectra and examples of these are shown in

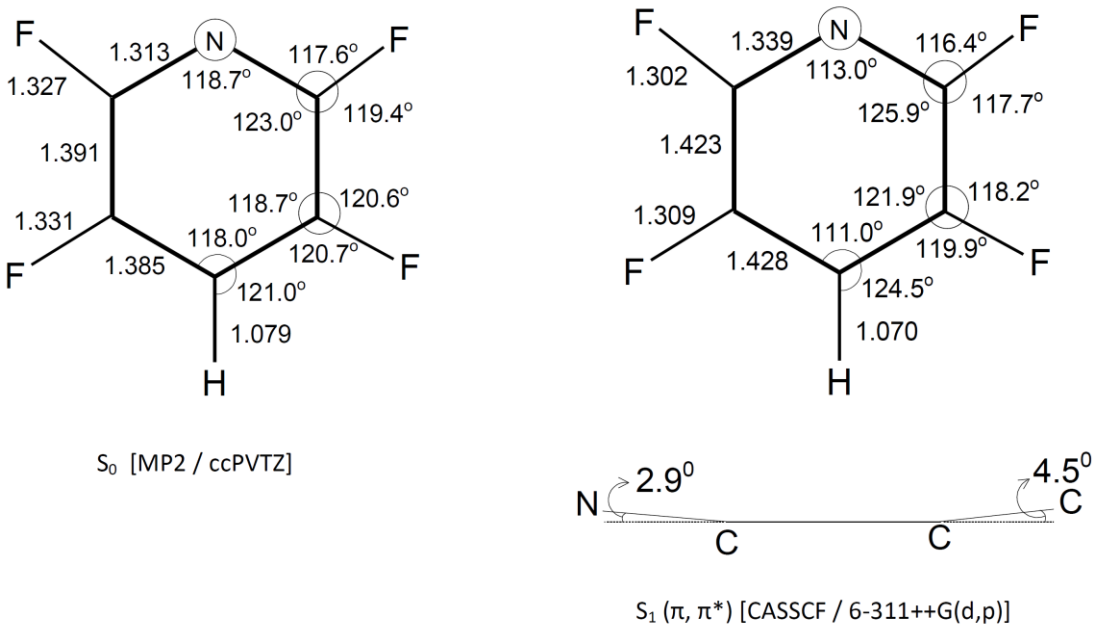

Figure 12 Calculated structures of 2,3,5,6-tetrafluoropyridine in its electronic ground and excited states

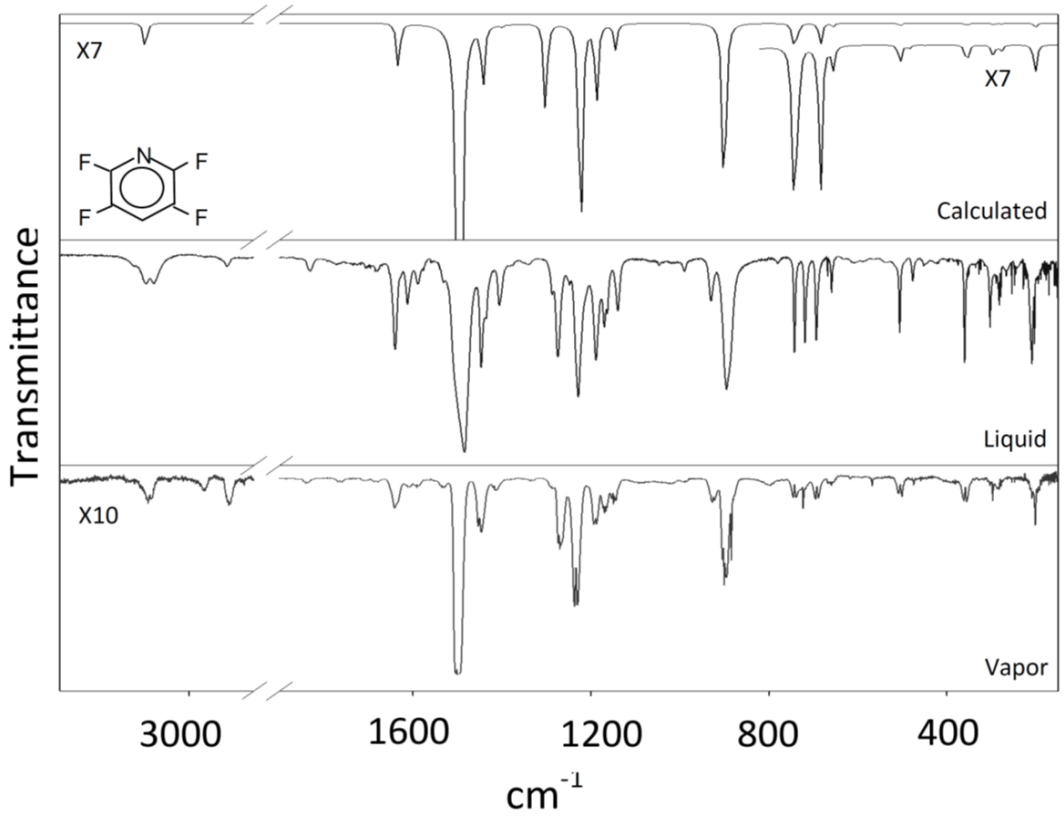

Figure 13 Calculated and observed infrared spectra of 2,3,5,6-tetrafluoropyridine

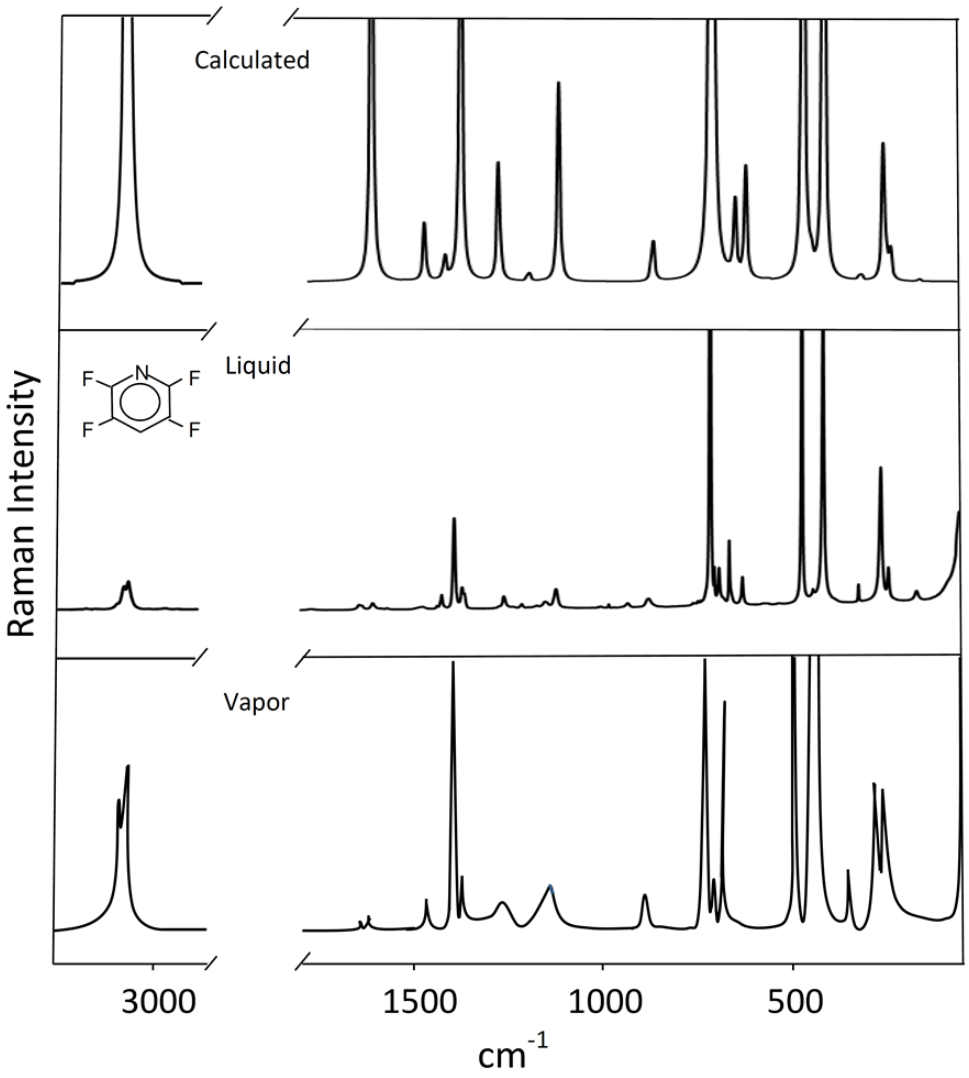

Figure 14 Calculated and observed Raman spectra of 2,3,5,6-tetrafluoropyridine

Figure 15. Type A and type C bands both have Q branches with a more obvious Q branch for type C, while type B bands have no Q branches.

The ultraviolet absorption spectrum of 2,3,5,6-tetrafluoropyridine vapor is shown in Figure 16. The band origin which corresponds to a transition to the $S_1(\pi,\pi^*)$ excited state is at 35,704.4 cm^{-1}. A comparison of observed and calculated vibrational frequencies for the $S_1(\pi,\pi^*)$ excited state is presented in Table 7. A strong coupling between the out-of-plane ring bending and out-of-plane C-F wag was observed. A summary of the excited states vibrational assignments is shown in Table 8.

Pyridine (Py),[18] 2-fluoropyridine (2FPy),[19-20] 3-fluoropyridine (3FPy),[19-20] 2,6-difluoropyridine (26DFPy) and 2,3,5,6-tetrafluoropyridine molecules all have planar and rigid structures in their electronic ground states. Pyridine is extremely floppy in its $S_1(n,\pi^*)$ excited state and its out-of-plane ring bending frequency drops from 403 cm^{-1} to 60 cm^{-1}. It has a tiny barrier to planarity of 3 cm^{-1}. Despite their planar structures, 2-fluoropyridine (2FPy), 3-fluoropyridine (3FPy) and 2,6-difluoropyridine (26DFPy) all become floppier in their excited states with significant drops in their ring puckering frequencies from 414 cm^{-1}, 412 cm^{-1} and 460 cm^{-1} to 96 cm^{-1}, 118 cm^{-1} and 127 cm^{-1}, respectively. A slightly puckered structure is predicted by CASSCF calculations for 2,3,5,6-tetrafluoropyridine with a barrier to planarity of only 30 cm^{-1}. This indicates that 2,3,5,6-tetrafluoropyridine also has a more floppy structure in the excited state and this is confirmed by the lowering of out-of-plane ring bending frequency from 475 cm^{-1} in the electronic ground state to 110 cm^{-1} in the $S_1(\pi,\pi^*)$ excited state. A strong coupling between the out-of-plane ring bending and the out-of-plane C-F wag motions was also

Table 7 Vibrational spectra (cm^{-1}) and assignments for the electronic ground and excited states of 2,3,5,6-tetrafluoropyridine

C_{2v}	ν	Approximate description	Calculated		Infrared		Raman		S_1	
			ν	Intensity[d]	Liquid[e]	Vapor	Liquid	Vapor	Cal.	Obs.
A_1	1	C-H stretch	3101	(0.4, 100)	3082 m	3091 w (B)	3080 (2)	3089 (4)	3072	-
	2	Ring stretch[c]	1632	(4, 7)	1640 s	1640 w (A/B)	1640 (0.3)	-	1554	-
	3	Ring stretch (C-F)	1443	(7, 2)	1446 s	1450 s (B)	1445 (0.2)	-	1381	1380
	4	C-F stretch	1401	(0.2, 37)	1405 m	1414 w (B)	1401 (7)	1404 (7)	1361	1358
	5	C-F stretch (ring)	1223	(30, 0.8)	1228 s	1233 s (B)	1226 (0.3)	-	1104	1100
	6	Ring breathing	746	(2, 100)	742 s	742 m (B)	742 (100)	740 (100)	690	709
	7	Ring bending (in-plane)	684	(2, 5)	693 s	692 m (B)	692 (5)	690 (6)	672	689
	8	Ring bending (in-plane)	505	(0.3, 42)	506 m	505 w (B)	505 (53)	503 (39)	451	453
	9	C-F wag (in-plane)	355	(0.3, 0.5)	360 m	358 w (B)	359 (1)	357 (1)	347	347
	10	C-F wag (in-plane)	278	(0.1, 2)	283 m	280 w (B)	282 (3)	280 sh (2)	265	280
A_2	11	Ring twisting	699	(0, 0.1)	-	-	692 (5)	-	383	373
	12	C-F wag (out-of-plane)	454	(0, 17)	-	-	451 (25)	451 (10)	305	302[b]
	13	C-F wag (out-of-plane)	115	(0, 0.004)	-	-	-	-	98	84
B_1	14	C-H wag	897	(4, 2)	895 s	900 s (C)	900 (0.6)	-	406	400
	15	Ring twisting	736	(2, 4)	719 s	723 m (C)	718 (3)	-	335	328
	16	Ring bending (out-of-plane)	485	(0.06, 0.9)	477 w	475 w (C)	477 (0.6)	-	108[a]	110
	17	C-F wag (out-of-plane)	296	(0.2, 9)	303 m	297 w (C)	302 (10)	301 (4)	303	302[b]
	18	C-F wag (out-of-plane)	201	(0.4, 0.1)	211 m	201 w (C)	210 (0.7)	-	198[a]	165
B_2	19	Ring stretch[c]	1634	(0.7, 36)	1640 s	1640 w (A/B)	1640 (0.3)	-	1770	-
	20	Ring stretch (C-F)	1495	(100, 4)	1483 s	1500 s (A)	1482 (0.1)	-	1518	-
	21	Ring stretch	1302	(9, 9)	1274 s	1270 m (A)	1274 (0.7)	-	1385	-
	22	C-H wag	1188	(8.4, 0.02)	1189 s	1191 m (A)	1188 (0.1)	-	1151	-
	23	C-F stretch (ring)	1145	(2.5, 13)	1139 m	1149 m (A)	1139 (1)	1145 (1)	1137	-
	24	C-F stretch	901	(18, 0.9)	896 s	900 s (A)	900 (0.6)	894 (1)	825	809
	25	C-F wag (in-plane)	656	(0.3, 7)	659 m	659 w (A)	658 (2)	-	617	611
	26	Ring bend (in-plane)	448	(0.007, 16)	452 w	-	451 (25)	444 (9)	408	420
	27	C-F wag (in-plane)	299	(0.02, 0.01)	-	297 w (A)	-	299 (4)	293	290

[a] Coupled vibrations
[b] Assigned twice
[c] υ_2 and υ_{19} overlap in the spectra; υ_2 is in Fermi resonance with $\upsilon_{14} + \upsilon_{15}$ and this gives a band near 1611 cm^{-1} in the liquid and vapor infrared and Raman spectra
d Relative intensities for (IR and Raman)
e s: strong m:medium w:weak

Table 8 Ultraviolet absorption spectra (cm^{-1}) and assignments for 2,3,5,6-tetrafluoropyridine

Observed	Peak intensity	Assignment	Inferred
-784	w		
-763	w		
-738	m		
-675	m		
-573	w		
-504	mw		
-480	mw		
-458	w		
-438	w		
-395	m	15_1^1	328-723 = -395
-359	w		
-297	mw		
-280	ms	10_1^0	0-280 = -280
-219	w		
-211	w		
-198	w		
-178	m		
-122	ms		
-112	ms		
-101	mw		
-87	ms	18_2^2	325-412 = -87

Table 8 (Continued)

Observed	Peak intensity	Assignment	Inferred
-38	m	18_1^1	165-201 = -36
-21	s	13_1^1	84-105 = -21
45	ms	$10_1^0 18_2^0$	325-280 = 45
67	ms	$10_1^0 9_0^1$	346-280 = 66
75	m		
101	m		
145	m		
167	ms	13_0^2	84x2 = 168
172	m		
176	m		
193	m		
200	m		
214	ms	16_0^2	110x2 = 220
222	w		
234	w		
244	m		
260	s	$10_0^1 13_1^1$	280+84-105 = 261
275	s	$16_0^1 18_0^1$	110+165 = 275
280	s	10_0^1	280-0 = 280
310	mw		

Table 8 (Continued)

Observed	Peak intensity	Assignment	Inferred
325	s	18_0^2	165x2 = 330
346	s	9_0^1	346-0 = 346
355	mw		
391	m		
411	m	$16_0^1 17_0^1$	302+110 = 412
414	w		
423	m		
428	m		
435	m	$15_0^1 16_0^1$	328+110 = 438
446	s		
453	s	8_0^1	453-0 = 453
522	m		
535	m		
546	mw		
556	mw		
563	s	10_0^2 $14_0^1 18_0^1$	280x2 = 560 400+165 = 565
580	m	27_0^2	290x2 = 580
603	m	12_0^2	302x2 = 604
625	s	$9_0^1 10_0^1$	346+280 = 626
633	m	$15_0^1 17_0^1$	328+302 = 630

Table 8 (Continued)

Observed	Peak intensity	Assignment	Inferred
646	m		
650	mw		
655	m	15_0^2	328x2 = 656
667	mw		
689	ms	7_0^1	689-0 = 689
692	m	9_0^2	346x2 = 692
709	s	6_0^1	710-0 = 710
726	ms	$14_0^1 15_0^1$	400+328 = 728
733	ms	$8_0^1 10_0^1$	453+280 = 733
746	ms	11_0^2	373x2 = 746
754	m		
768	w		
779	w		
788	w		
799	m	14_0^2 $8_0^1 9_0^1$	400x2 = 800 453+346 = 799
841	m	26_0^2	420x2 = 840
862	m		
880	m		
901	m	$25_0^1 27_0^1$	611+290 = 901
906	m	8_0^2	453x2 = 906

Table 8 (Continued)

Observed	Peak intensity	Assignment	Inferred
927	mw		
949	mw		
957	mw		
969	m	$7_0^1 10_0^1$	689+280 = 969
991	s	$6_0^1 10_0^1$	710+280 = 990
1029	m	$25_0^1 26_0^1$	611+420 = 1031
1037	m	$7_0^1 9_0^1$	689+346 = 1035
1051	m		
1058	m	$6_0^1 10_0^1$	710+346 = 1056
1071	m		
1081	m		
1128	m		
1143	m	$7_0^1 8_0^1$	689+453 = 1142
1162	ms	$6_0^1 8_0^1$	710+453 = 1163
1204	mw		
1231	mw	25_0^2 $24_0^1 26_0^1$	611x2 = 1222 809+420 = 1229
1247	Mw		
1255	mw		
1274	mw		
1278	m		

Table 8 (Continued)

Observed	Peak intensity	Assignment	Inferred
1285	m		
1293	m		
1331	m		
1364	m		
1401	m		
1422	m	6_0^2 $24_0^1 25_0^1$	710x2 = 1420 809+611 = 1420
1446	m	$5_0^1 9_0^1$	1100+346 = 1446
1511	w		
1619	m	24_0^2	809x2 = 1618
1705	m	$4_0^1 9_0^1$	1358+346 = 1704
1726	m	$3_0^1 9_0^1$	1380+346 = 1726
1877	mw		
1895	mw		
1987	mw		
2091	mw		
2134	m		
2153	m		
2367	mw		
2415	m		

Table 8 (Continued)

Observed	Peak intensity	Assignment	Inferred
2699	w		
2796	w		
2824	mw		
3106	mw		

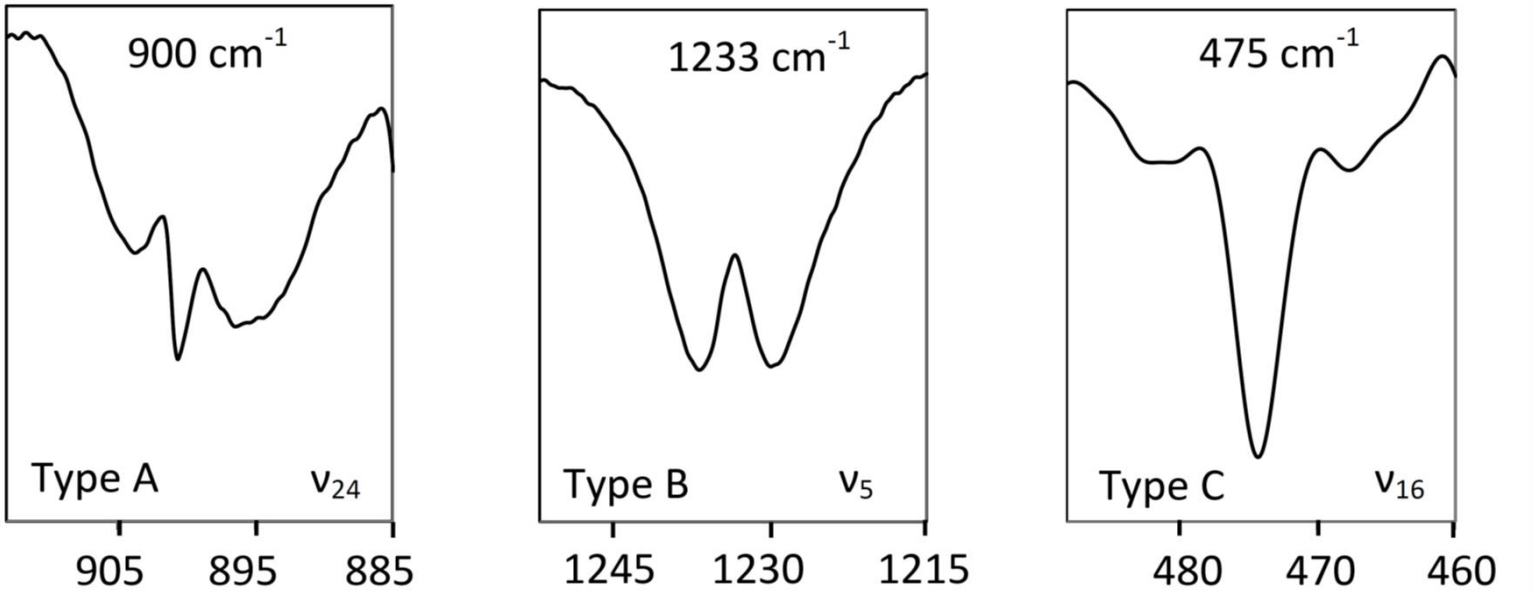

Figure 15 Examples of band types in the infrared spectrum of 2,3,5,6-tetrafluoropyridine

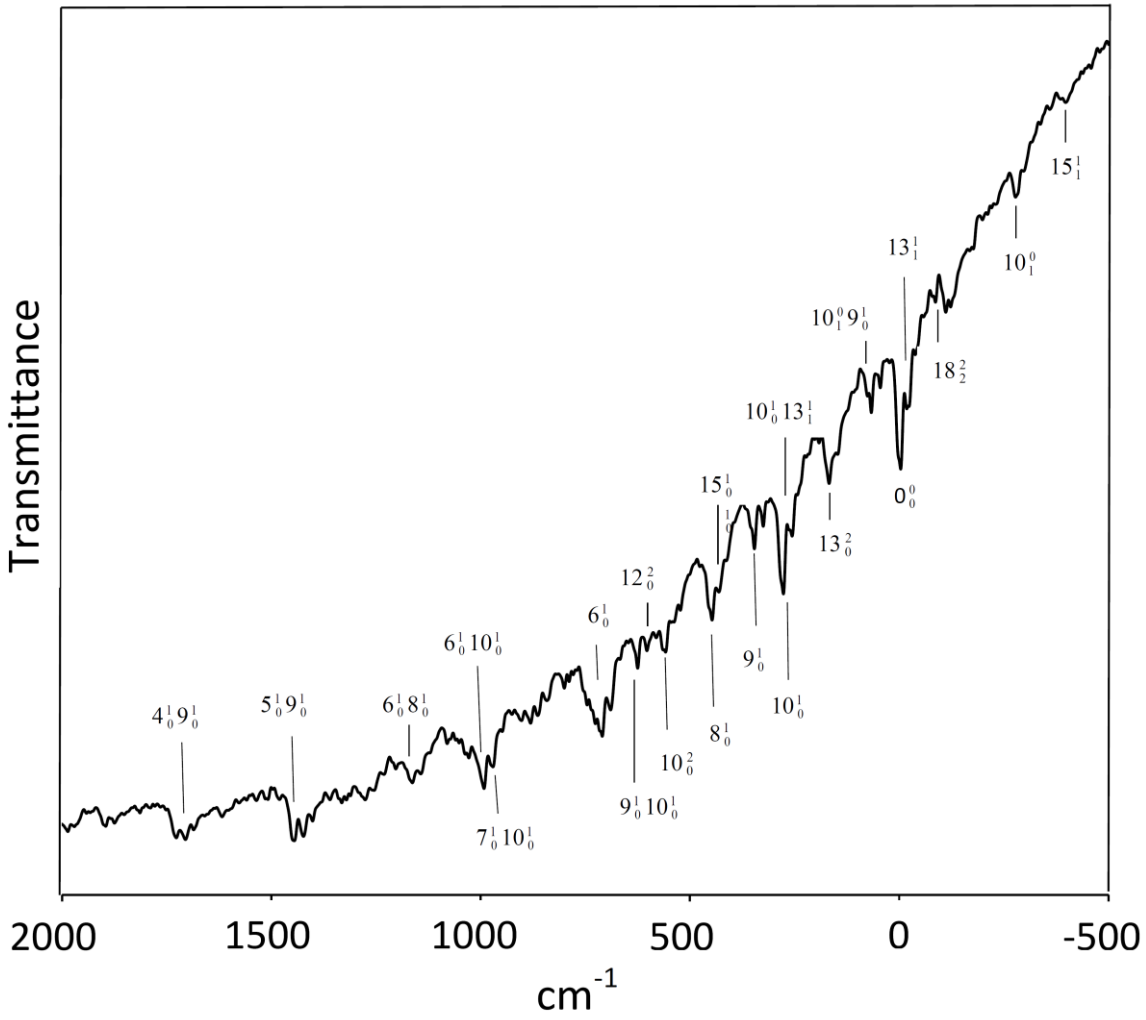

Figure 16 Ultraviolet absorption spectra of 2,3,5,6-Tetrafluoropyridine relative to the band origin

observed. In fact, the out-of-plane ring bending frequency even drops below the out-of-plane C-F wag due to the increased antibonding character in the excited state.

Conclusions

2,3,5,6-Tetrafluoropyridine has a rigid planar structure in its electronic ground state and the structure becomes more floppy in the excited state with a small barrier to planarity of 30 cm^{-1}. The infrared, Raman and ultraviolet absorption spectra were recorded and the vibrational frequencies were assigned for both ground and excited states with the aid of theoretical calculations.

CHAPTER VI

VIBRATIONAL SPECTRA, STRUCTURE, AND THEORETICAL CALCULATIONS OF 2-CHLORO- AND 3-CHLOROPYRIDINE AND 2-BROMO- AND 3-BROMOPYRIDINE IN THEIR ELECTRONIC GROUND STATE*

Introduction

The studies on vibrational analysis of pyridine, 2-fluoropyridine (2FPy) and 3-fluoropyridine (3FPy) in their electronic ground and excited states had been recently reported in Laane's research group.[18-20] The spectra, structures and vibrational levels of 2,6-Difluoropyridine and 2,3,5,6-tetrafluoropyridine in their ground and excited electronic states were also presented in the previous chapters. From all the fluoropyridine studies it was found that the substitution of a fluorine atom on the pyridine ring results in significant π boding interactions within the ring. Hence, the effect of chlorine and bromine atoms substitutions on the pyridine ring is of great interest. The †infrared and Raman spectra with partial assignments for the chloro- and bromopyridine molecules in their electronic ground states had been reported by Green and coworkers,[96] but no structural information was reported. In the present paper the infrared and Raman

* Reprinted with permission from "Vibrational Spectra, Structure, and Theoretical Calculations of 2-Chloro- and 3-Chloropyridine and 2-Bromo- and 3-Bromopyridine" by Boopalachandran, P.; Sheu, H. and Laane, J. *J. Mol. Sruc.* **2012**, 1023, 61. Copyright [2012] by Elsevier.

spectra were recorded and the vibrational frequencies of 2-chloropyridine (2ClPy), 3-chloropyridine (3ClPy), 2-bromopyridine (2BrPy), and 3-bromopyridine (3BrPy) molecules were assigned. Density functional theory (DFT) was used to calculate the vibrational frequencies of the twenty-seven fundamental vibrations for each of the molecules molecule, and *ab initio* computations provided the molecular structures.

Results and Discussion

The bond distances and angles of 2ClPy, 3ClPy, 2BrPy, and 3BrPy are shown in Figure 17 and they are compared to the structures of pyridine (py), 2FPy, and 3FPy. The ring bond distances and C-X bond distances are compared in table 9. The substitution of a halogen atom on pyridine ring has only minor effect on the ring bond distances and angles. The notable exceptions are when the electronegative halogen atom is substituted on the carbon 2 position. The N-C bond distance for pyridine is 1.340 Å but drops to 1.313 Å for 2FPy and 1.325 Å for both 2ClPy and 2BrPy. The remaining bond distances are changed by less than 0.004 Å for each of these molecules.

The liquid-phase and calculated infrared and Raman spectra of 2ClPy are shown in Figures 18 and 19. The spectra for 3ClPy are shown in Figures 20 and 21. The observed and calculated spectra of 2BrPy and 3BrPy are shown in Figures 22 to 25. The observed and calculated vibrational frequencies for all four molecules are summarized in Tables 10 to 13. Partial assignments for these molecules previously made by Green and coworkers[95] are also listed in the same tables. The frequencies are well predicted by B3LYP level of theory calculation.[19, 74-78, 97] The average difference between calculated

Table 9 Ring bond distances (Å) and carbon-halogen bond distances (Å) of halopyridines and pyridine[98]

Bond distances	Pyridine	2FPy	3FPy	2ClPy	3ClPy	2BrPy	3BrPy
N(1) - C(2)	1.340	1.313	1.338	1.325	1.337	1.325	1.337
C(2) - C(3)	1.392	1.391	1.389	1.394	1.394	1.394	1.394
C(3) - C(4)	1.391	1.387	1.384	1.389	1.390	1.389	1.390
C(4) - C(5)	1.391	1.394	1.391	1.393	1.391	1.393	1.391
C(5) - C(6)	1.392	1.388	1.392	1.390	1.392	1.390	1.392
C(6) - N(1)	1.340	1.344	1.340	1.342	1.340	1.343	1.340
C - X	-	1.338	1.340	1.737	1.729	1.890	1.877

Table 10 Observed and calculated vibrational frequencies (cm^{-1}) and intensities for 2-chloropyridine[98]

Cs	ν	Approximate Description	Infrared		Raman			Calculated[a] ν	Calculated[a] Intensity	GKP[b]
A'	1	C-H stretch	3074 sh	mw	3074	10	P	3096	(2, 81)	3080
(i.p.)	2	C-H stretch	3074 sh	mw	3074	10	P	3085	(15, 100)	3080
	3	C-H stretch	3054	mw	3058	12	P	3065	(9, 52)	3057
	4	C-H stretch	3054	mw	3058	12	P	3049	(16, 61)	3057
	5	Ring stretch	1579	vs	1578	4	P	1588	(61, 42)	1573
	6	Ring stretch	1568	vs	1567	4	PP	1585	(99, 63)	1565
	7	Ring stretch	1453	vs	1453	4	PP	1461	(77, 14)	1452
	8	Ring stretch	1420	vs	1420	0.4	PP	1427	(100, 2)	1417
	9	C-H wag	1286	m	1286	2	PP	1295	(3, 9)	1282
	10	Ring stretch	1237	w	1237	2	P	1274	(3, 11)	1253
	11	C-H wag	1148	ms	1148	4	P	1155	(4, 8)	1146
	12	C-H wag[c]	1118	vs	1118	6	P	1121	(123, 23)	1104
	13	C-H wag	1083	m	1083	6	P	1088	(49, 19)	1079
	14	Ring stretch[c]	1044	m	1044	61	P	1047	(17, 94)	1041
	15	Ring bend	990	m	990	100	P	990	(10, 100)	991
	16	C-Cl stretch[d]	725	s	724	26	P	726	(57, 23)	701
	17	Ring bend	618	m	618	8	P	619	(3, 18)	615
	18	Ring bend[d]	407	m	407	0.1	PP	413	(14, 37)	404[e]
	19	C-Cl wag	312	mw	312	4	PP	307	(2, 4)	315[e]
A''	20	C-H wag	980	w	980	2	D?	992	(0.01, 0.4)	960
(o.p.)	21	C-H wag	960	m	960	2	D?	965	(0.4, 0.2)	934
	22	C-H wag	882	w	882	0.2	D	880	(0.03, 0.3)	882
	23	C-H wag	765	vs	768 br	0.3	D?	765	(84, 0.04)	761
	24	Ring twist	-		-			735	(4, 0.4)	722
	25	Ring bend	481	m	481	0.4	D	484	(6, 0.04)	457
	26	Ring bend	407	mw	408	0.1	D	412	(7, 0.8)	404
	27	C-Cl wag	187	w	-			172	(1, 4)	178

Abbreviations: s, strong; m, medium; w, weak; v, very; sh, shoulder; i.p., in-plane; o.p., out-of-plane; P, polarized; PP, partially polarized, D, depolarized

[a] B3LYP/6-311++g(d,p); frequencies scaled with a scaling factor of 0.985 for frequencies less than 1800 cm^{-1} and 0.964 for frequencies greater than 1800 cm^{-1}. The calculated relative intensities are shown as (IR, Raman).

[b] Reference 95

[c] The CH wag and ring stretch are strongly coupled

[d] The C-Cl stretch and ring bend are strongly coupled

[e] Bands have been reassigned

Table 11 Observed and calculated vibrational frequencies (cm^{-1}) and intensities for 3-chloropyridine[98]

Cs	ν	Approximate Description	Infrared		Raman			Calculated[a]		GKP[b]
								ν	Intensity	
A'	1	C-H stretch	3075	mw	3076	1	PP	3087	(9, 150)	3079
(i.p.)	2	C-H stretch	3075	mw	3076	1	PP	3071	(24, 124)	3079
	3	C-H stretch	3053 sh	mw	3054	12	P	3056	(18, 73)	3052
	4	C-H stretch	3045	m	3044 sh	5	P	3045	(35, 100)	3052
	5	Ring stretch	1572	m	1572	5	P	1584	(29, 8)	1573
	6	Ring stretch	1565	m	1565	4	PP	1579	(12, 18)	1569
	7	Ring stretch	1467	vs	1467	0.6	P	1470	(82, 2)	1469
	8	Ring stretch	1416	vs	1416	1	P	1425	(100, 3)	1417
	9	C-H wag	1320	mw	1320	0.3	P	1329	(9, 1)	1319
	10	Ring stretch	1226	vw	1226	0.8	PP	1255	(1, 3)	1227
	11	C-H wag	1189	mw	1190	2	PP	1201	(9, 5)	1190
	12	C-H wag	1107	s	1106	7	P	1119	(29, 0.4)	1107
	13	C-H wag	1094	m	1093	7	P	1098	(162, 12)	1096
	14	Ring stretch	1036	vw	1036	100	P	1041	(6, 45)	1040
	15	Ring bend	1016	vs	1015	2	P	1013	(106, 5)	1016
	16	C-Cl stretch[c]	730	m	729	27	P	727	(50, 7)	730
	17	Ring bend	615	m	615	4	P	617	(15, 4)	615
	18	Ring bend[c]	426	w	426	21	P	415	(24, 9)	428
	19	C-Cl wag	292	vw	293	4	PP	288	(3, 1)	294
A''	20	C-H wag	-		983	0.1		977	(0.2, 0.1)	980
(o.p.)	21	C-H wag	944	w	944	0.1	D	941	(2, 0.01)	943
	22	C-H wag	915	w	914	0.1	D?	917	(3, 0.07)	915
	23	C-H wag	795	s	796	0.3	D	793	(91, 0.1)	795
	24	Ring twist	701	s	702	0.3	D	704	(82, 0.2)	700
	25	Ring bend	461	vw	461	0.7	D?	465	(0.9, 0.3)	460
	26	Ring bend	402	w	404 br	0.3	D	405	(9, 0.1)	404
	27	C-Cl wag	197	w	-			183	(0.06, 1.2)	199

Abbreviations: s, strong; m, medium; w, weak; v, very; sh, shoulder; i.p., in-plane; o.p., out-of-plane; P, polarized; PP, partially polarized, D, depolarized

[a] B3LYP/6-311++g(d,p); frequencies scaled with a scaling factor of 0.985 for frequencies less than 1800 cm^{-1} and 0.964 for frequencies greater than 1800 cm^{-1}. The calculated relative intensities are shown as (IR, Raman)

[b] Reference 95

[c] The C-Cl stretch and ring bend are strongly coupled

Table 12 Observed and calculated vibrational frequencies (cm^{-1}) and intensities for 2-bromopyridine[98]

Cs	ν	Approximate Description	Infrared		Raman			Calculated[a] ν	Calculated[a] Intensity	GKP[b]
A'	1	C-H stretch	3070 sh	mw	3071	11	P	3098	(2, 166)	3069
(i.p.)	2	C-H stretch	3070 sh	mw	3071	11	P	3084	(15, 188)	3069
	3	C-H stretch	3052	m	3053	11	P	3063	(10, 91)	3056
	4	C-H stretch	3052	m	3053	11	P	3050	(17, 100)	3056
	5	Ring stretch	1572	vvs	1572	4	P	1584	(51, 11)	1573
	6	Ring stretch	1561	vvs	1561	3	PP	1580	(123, 17)	1565
	7	Ring stretch	1449	vvs	1449	4	P	1458	(90, 7)	1452
	8	Ring stretch	1414	vvs	1414	0.3	PP	1423	(100, 1)	1417
	9	C-H wag	1283	mw	1284	1	P	1294	(2, 3)	1282
	10	Ring stretch	1239?	w	-	-		1269	(7, 3)	1253
	11	C-H wag	1148	m	1148	2	P	1155	(4, 3)	1146
	12	C-H wag[c]	1106	vvs	1106	3	P	1108	(67, 2)	1104
	13	C-H wag	1077	vvs	1077	3	P	1079	(87, 3)	1079
	14	Ring stretch[c]	1042	m	1042	55	P	1044	(28, 27)	1041
	15	Ring bend	987	m	987	100	P	987	(10, 24)	991
	16	C-Br stretch[d]	700	vs	700	31	P	702	(52, 5)	701
	17	Ring bend	614	m	613	6	P	615	(3, 5)	615
	18	Ring bend[d]	312	w	313	46	P	304	(9, 10)	315
	19	C-Br wag	261	vw	262	3	P	256	(3, 1)	265
A''	20	C-H wag	-		-	-		991	(0, 0.15)	960
(o.p.)	21	C-H wag	960	w	959	0.2	D	964	(0.4, 0.1)	934
	22	C-H wag	882	w	883	0.2	D	883	(0.04, 0.1)	882
	23	C-H wag	759	vvs	761 br	0.1	D	762	(83, 0.01)	761
	24	Ring twist	727	w	726	0.3	D	731	(2, 0.1)	722
	25	Ring bend	467	m	468	0.01	D?	472	(6, 0.01)	457
	26	Ring bend	404	w		-		409	(7, 0.2)	404
	27	C-Br wag	174	w		-		154	(2, 2)	178

Abbreviations: s, strong; m, medium; w, weak; v, very; sh, shoulder; i.p., in-plane; o.p., out-of-plane; P, polarized; PP, partially polarized, D, depolarized

[a] B3LYP/6-311++g(d,p); frequencies scaled with a scaling factor of 0.985 for frequencies less than 1800 cm^{-1} and 0.964 for frequencies greater than 1800 cm^{-1}. The calculated relative intensities are shown as (IR, Raman)

[b] Reference 95

[c] The CH wag and ring stretch are strongly coupled

[d] The C-Br stretch and ring bend are strongly coupled

Table 13 Observed and calculated vibrational frequencies (cm^{-1}) and intensities for 3-bromopyridine[98]

Cs	ν	Approximate Description	Infrared		Raman			Calculated[a] ν	Calculated[a] Intensity	GKP[b]
A'	1	C-H stretch	3071 sh	mw	3071	2	P	3088	(10, 136)	3082
(i.p.)	2	C-H stretch	3071 sh	mw	3071	2	P	3071	(27, 144)	3082
	3	C-H stretch	3050 sh	mw	3051	11	P	3058	(17, 59)	3052
	4	C-H stretch	3050 sh	m	3051	11	P	3045	(40, 107)	3052
	5	Ring stretch	1571	ms	1571	3	P	1581	(37, 9)	1573
	6	Ring stretch	1557	m	1557	5	PP	1573	(14, 17)	1559
	7	Ring stretch	1463	vs	1463	0.6	PP	1467	(80, 2)	1467
	8	Ring stretch	1413	vs	1413	1	P	1422	(100, 4)	1415
	9	C-H wag	1319	w	1320	0.2	PP	1330	(14, 1)	1320
	10	Ring stretch	1219	w	1220	0.8	PP	1252	(1, 3)	1221
	11	C-H wag	1190	mw	1190	2	PP	1202	(10, 5)	1189
	12	C-H wag	1095	m	1094	0.01		1119	(20, 2)	1094
	13	C-H wag	1086	m	1086	9	P	1084	(117, 7)	1087
	14	Ring stretch	1034	w	1034	100	P	1038	(3, 54)	1024
	15	Ring bend	1007	vs	1007	0.5	P	1007	(173, 6)	1008
	16	C-Br stretch[c]	704 sh	ms	704	26	P	703	(50, 6)	705
	17	Ring bend	613	m	612	4	P	614	(17, 3)	614
	18	Ring bend[c]	319	vw	319	60	P	312	(10, 9)	319
	19	C-Br wag	246?	vvw	247	3	PP	242	(2, 1)	246
A''	20	C-H wag	978 sh	vw	978	0.01	D	978	(0.2, 0.1)	978
(o.p.)	21	C-H wag	944	w	944	0.01	D	942	(1, 0.01)	944
	22	C-H wag	916	w	915	0.3	D	919	(2, 0.2)	915
	23	C-H wag	792	vs	793	0.01	D	790	(103, 0.1)	792
	24	Ring twist	700	vs	-			701	(83, 0.2)	699
	25	Ring bend	448	vw	449	0.5	D?	450	(1, 0.1)	447
	26	Ring bend	399	w	399	0.2	D?	401	(10, 0.03)	401
	27	C-Br wag	174	w	-			163	(0.1, 2)	182

Abbreviations: s, strong; m, medium; w, weak; v, very; sh, shoulder; i.p., in-plane; o.p., out-of-plane; P, polarized; PP, partially polarized, D, depolarized

[a] B3LYP/6-311++g(d,p); frequencies scaled with a scaling factor of 0.985 for frequencies less than 1800 cm^{-1} and 0.964 for frequencies greater than 1800 cm^{-1}. The calculated relative intensities are shown as (IR, Raman)

[b] Reference 95

[c] The C-Br stretch and ring bend are strongly coupled

Table 14 Vibrational frequencies (cm^{-1}) of the ring modes and C-X stretching vibrations of the halopyridines compared to pyridine[98]

ν[a]	Approximate Description	Pyridine	2FPy	3FPy	2ClPy	3ClPy	2BrPy	3BrPy
5	Ring stretch	1584	1605	1594	1579	1572	1572	1571
6	Ring stretch	1576	1593	1588	1568	1565	1561	1557
7	Ring stretch	1483	1478	1480	1453	1467	1449	1463
8	Ring stretch	1443	1439	1426	1420	1416	1414	1413
10	Ring stretch	1227	1286	1249	1251	1226	1253[b]	1244
11	C-X stretch[c]	-	1266	1227	725	730	700	704
15	Ring stretch	1031	997	1022	1044	1036	1042	1025
16	Ring bend[c] (i.p.)	991	842	816	990	1016	987	1007
17	Ring bend (i.p.)	654	620	613	618	615	614	613
18	Ring bend[c] (i.p.)	601	554	533	407	426	312	319
24	Ring bend (o.p.)	700	733	701	722[b]	701	727	700
25	Ring bend (o.p.)	403	518	507	481	461	467	448
26	Ring bend (o.p.)	375	414	412	407	402	404	399

Abbreviations: i.p., in-plane; o.p., out-of-plane

[a] Mode number for 2FPy and 3FPy

[b] From Refrence 95

[c] The C-X stretching vibration is strongly coupled to a ring bending (ν_{16} for 2FPy and 3FPy and ν_{18} for 2ClPy, 3ClPy, 2BrPy and 3BrPy)

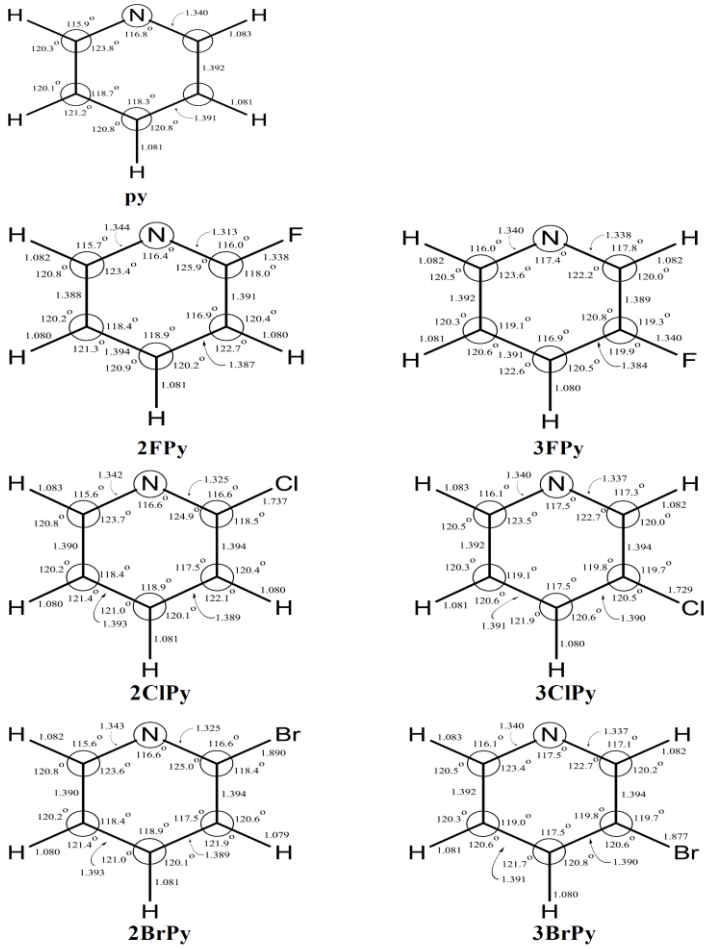

Figure 17 Calculated structures of pyridine (py), 2-fluoropyridine (2FPy), 3-fluoropyridine (3FPy), 2-chloropyridine (2ClPy), 3-chloropyridine (3ClPy), 2-bromopyridine (2BrPy), and 3-bromopyridine (3BrPy) using MP2/cc-pVTZ level of theory[98]

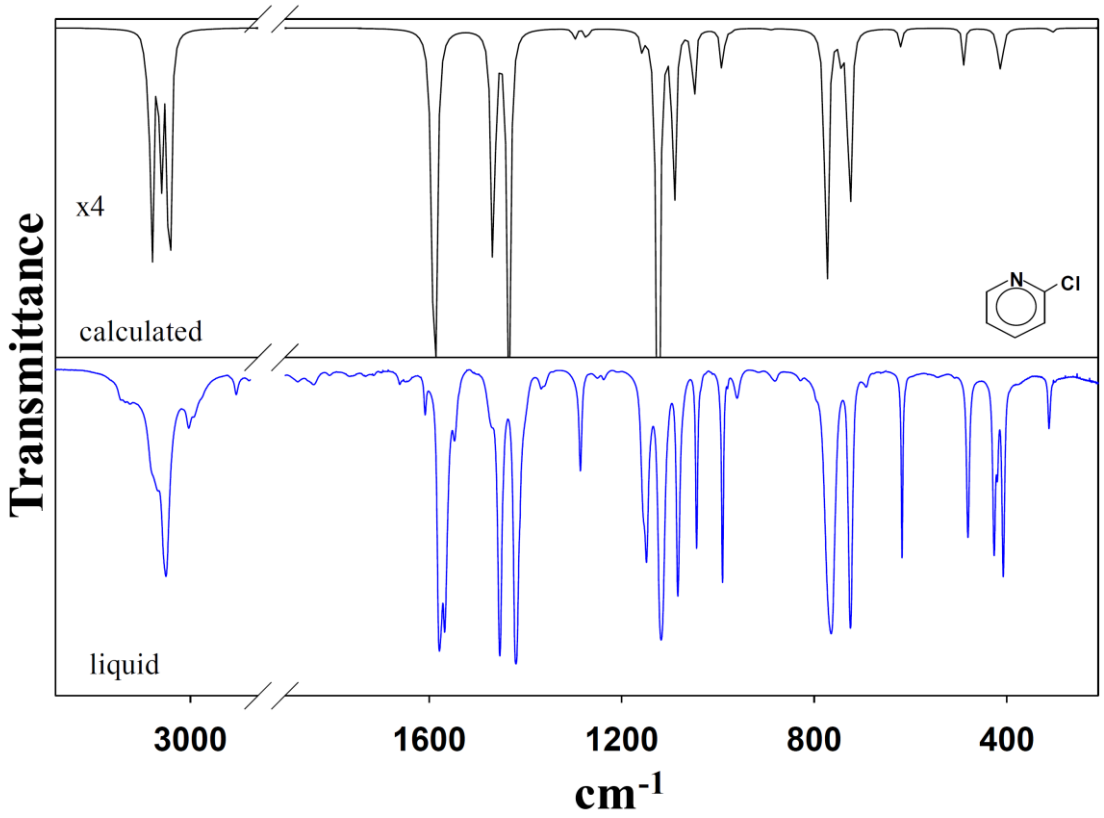

Figure 18 Liquid-phase and calculated infrared spectra of 2-chloropyridine[98]

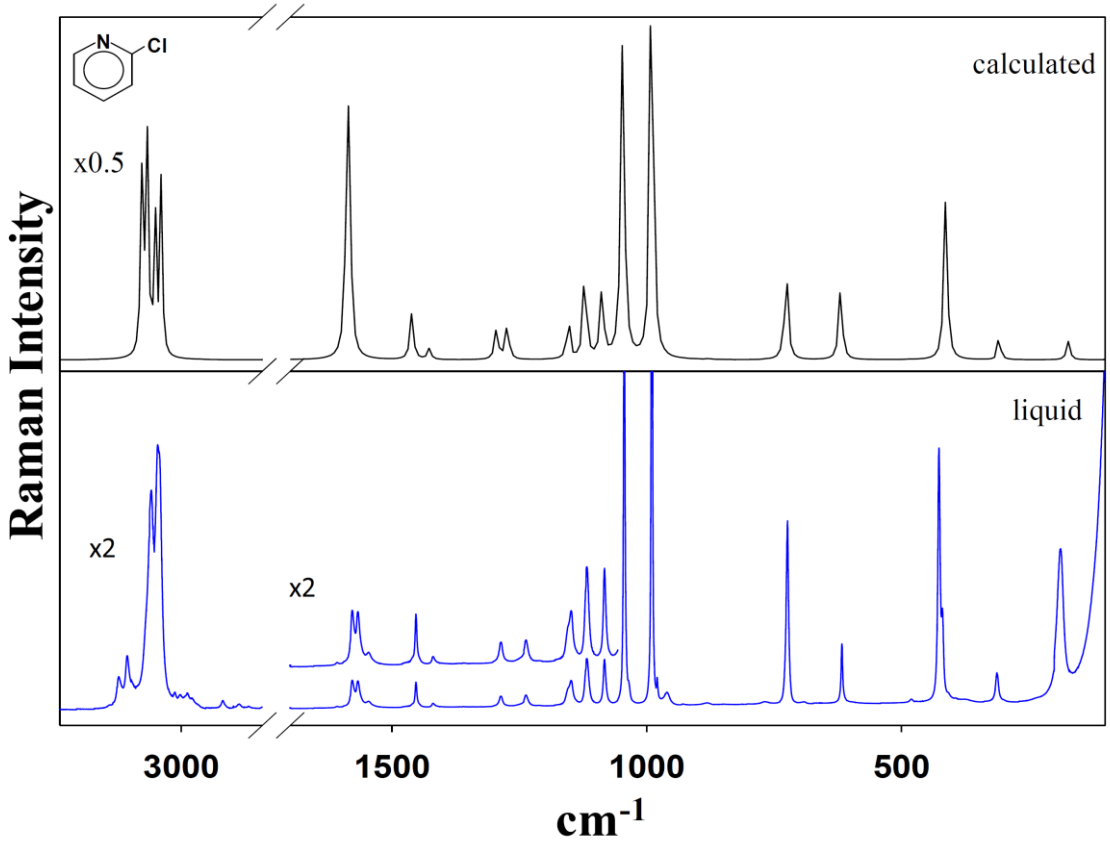

Figure 19 Liquid-phase and calculated Raman spectra of 2-chloropyridine[98]

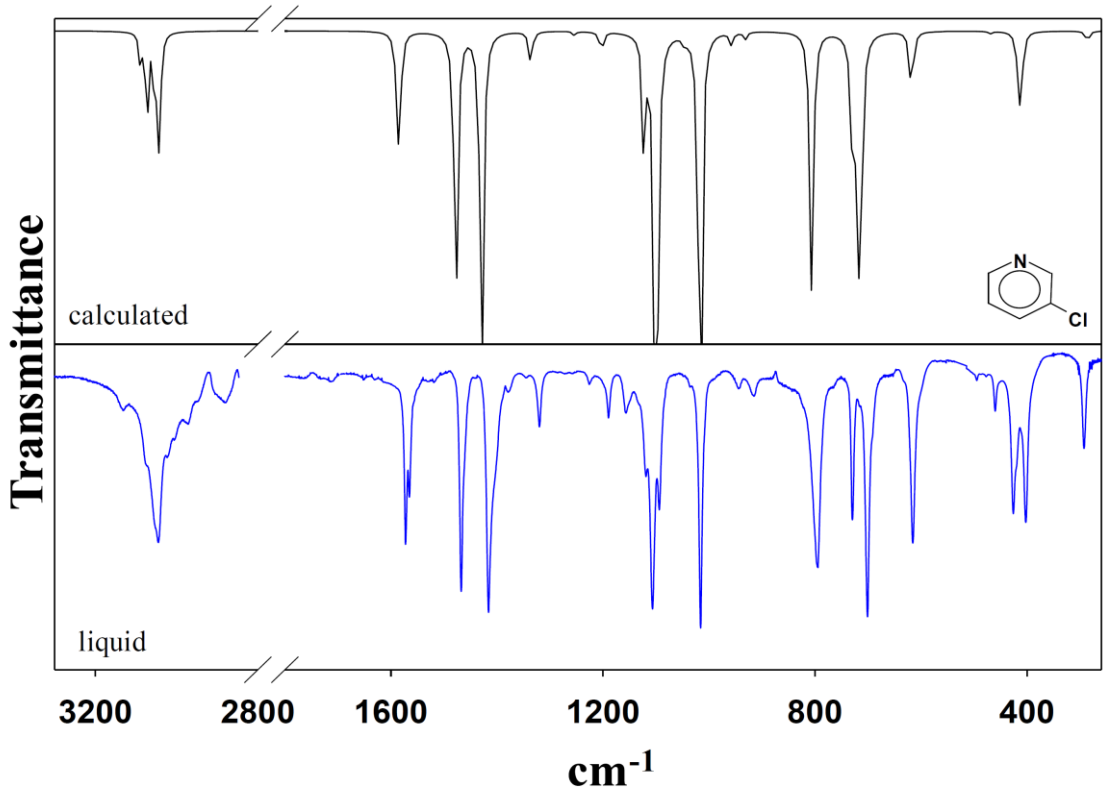

Figure 20 Liquid-phase and calculated infrared spectra of 3-chloropyridine[98]

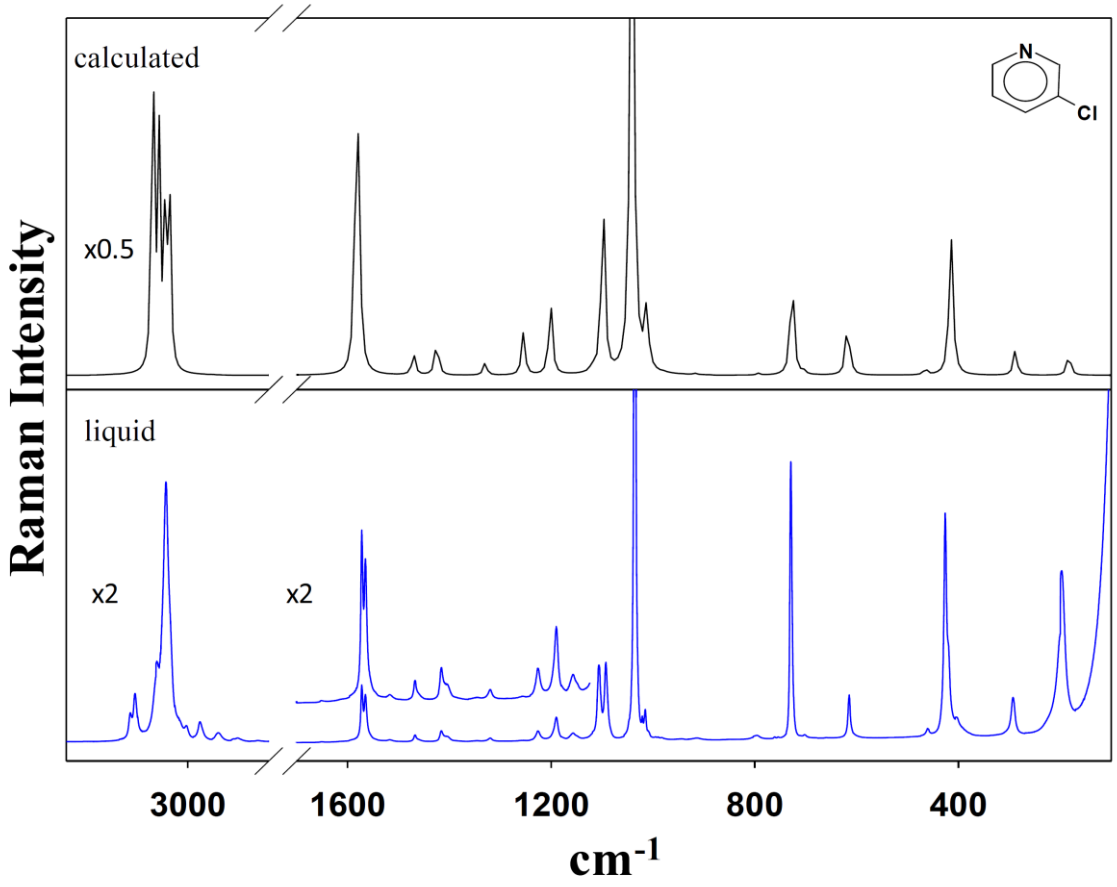

Figure 21 Liquid-phase and calculated Raman spectra of 3-chloropyridine[98]

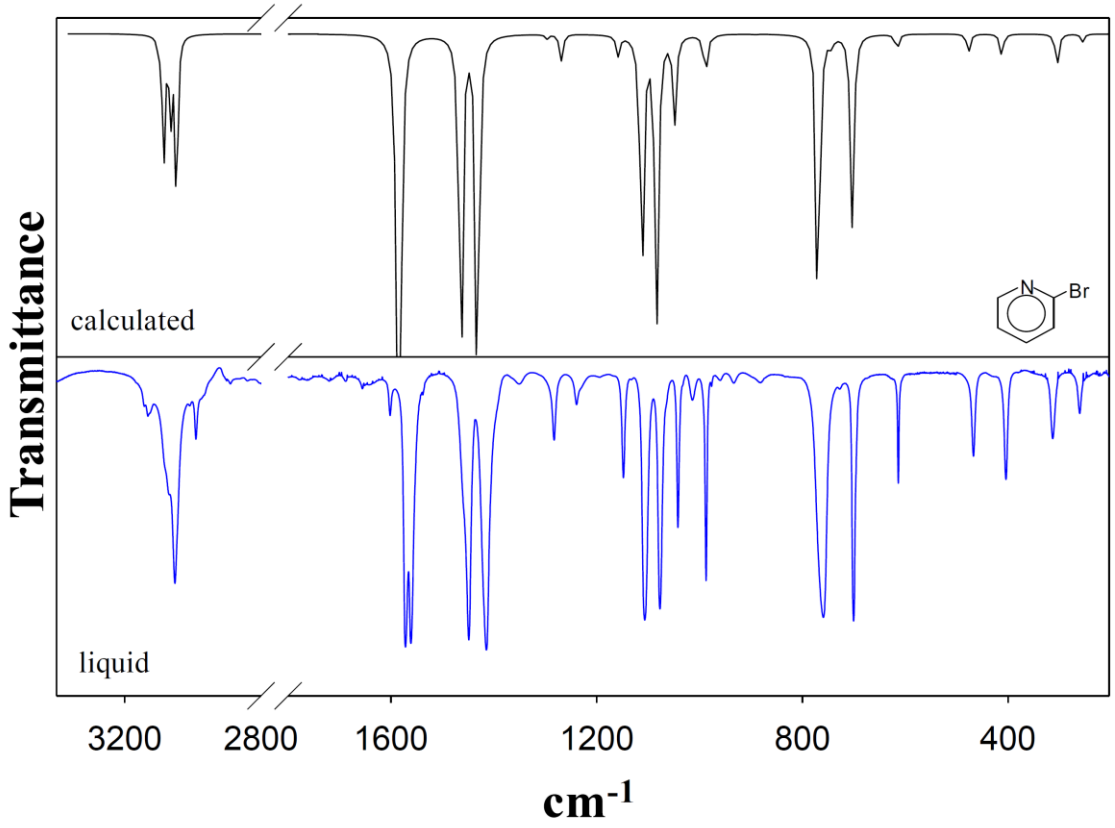

Figure 22 Liquid-phase and calculated infrared spectra of 2-bromopyridine[98]

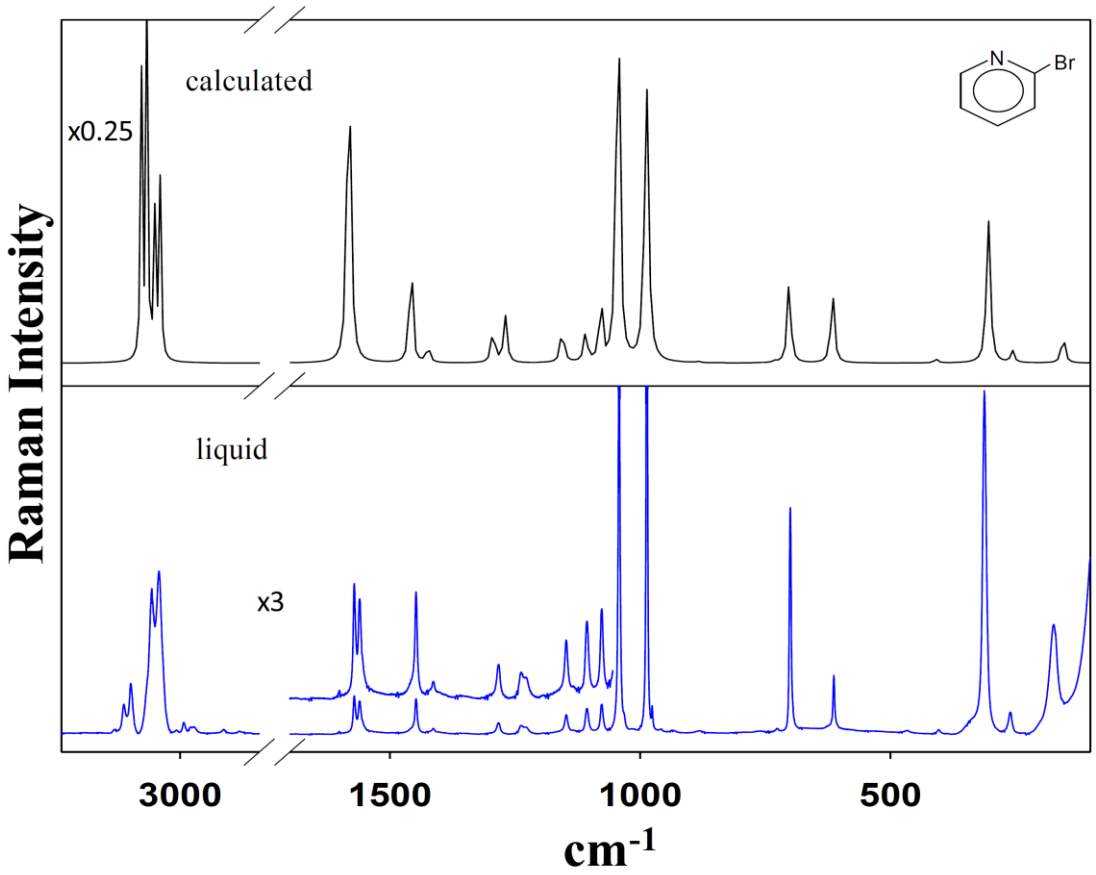

Figure 23 Liquid-phase and calculated Raman spectra of 2-bromopyridine[98]

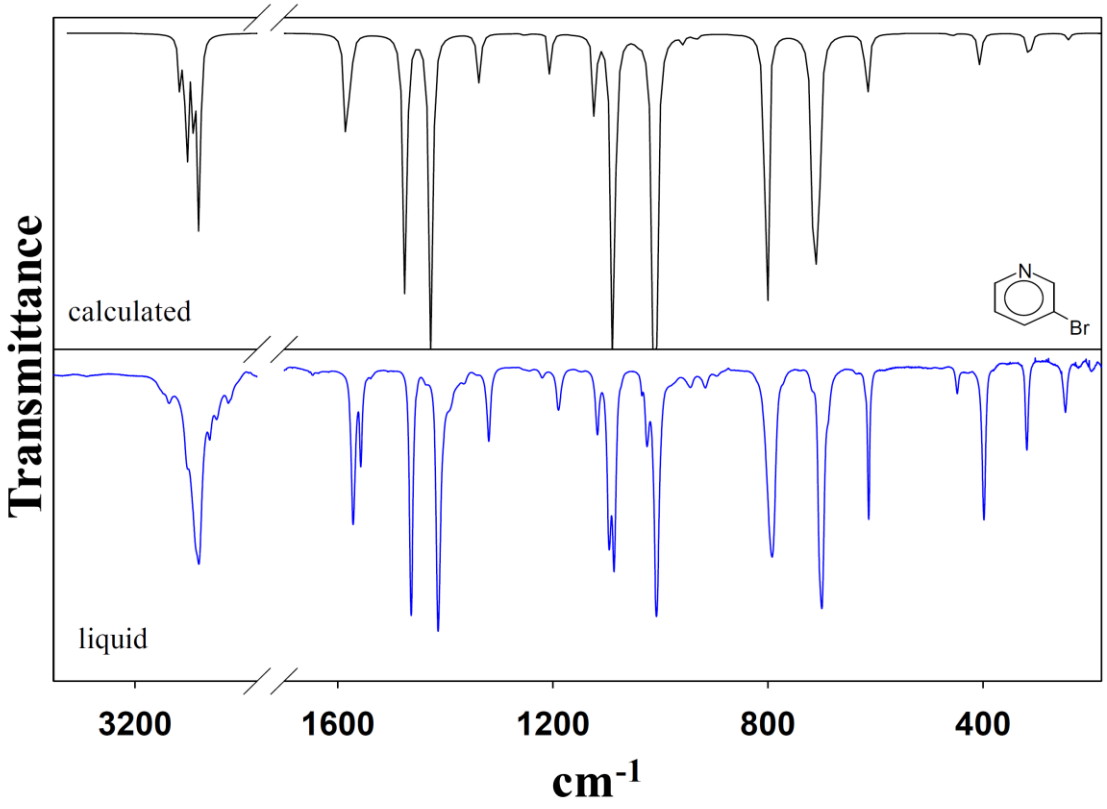

Figure 24 Liquid-phase and calculated infrared spectra of 3-bromopyridine[98]

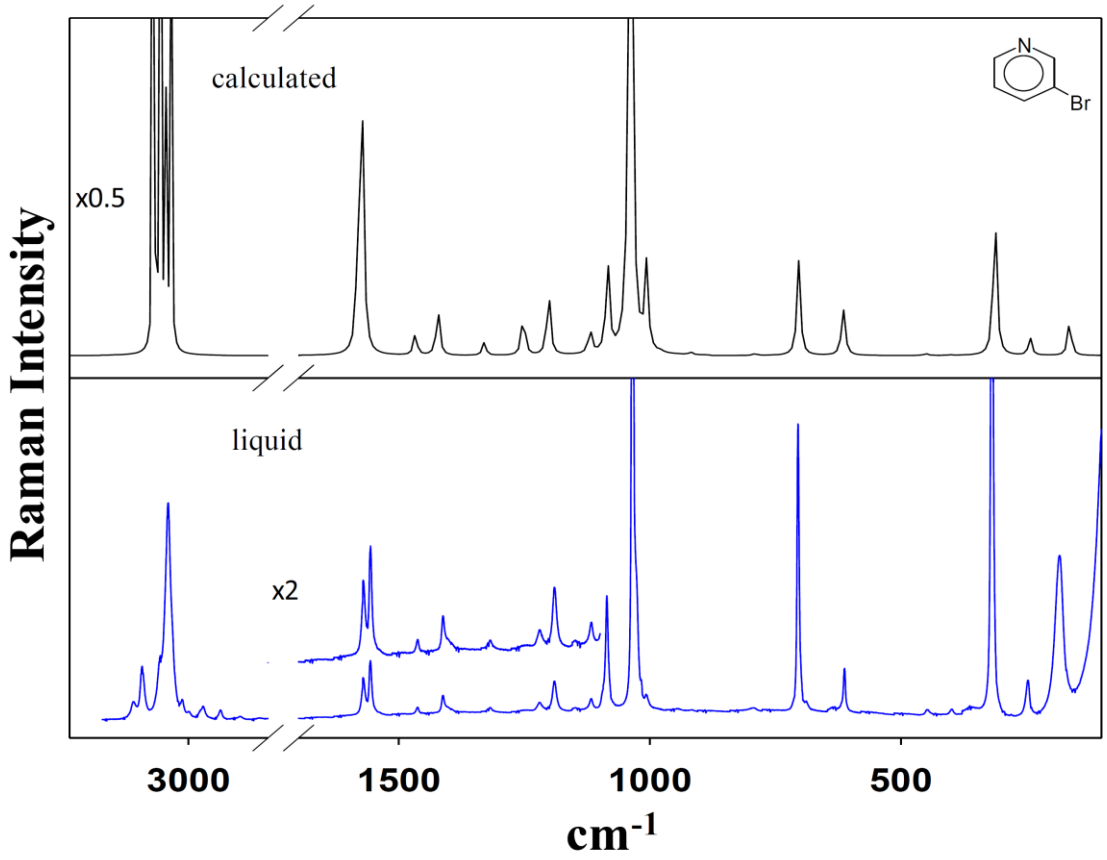

Figure 25 Liquid-phase and calculated Raman spectra of 3-bromopyridine[98]

and experimental wavenumbers was less than 8 cm^{-1}. The vibrational frequencies of the ring modes for all four molecules are compared in Table 14. The ring stretching frequencies of the pyridine ring are very little affected by the halogen substitution. This is consistent with the calculated bond distances, which vary little from molecule to molecule and reflect the fact that the individual bond strengths are nearly the same in all four molecules. However, the C-X stretching frequencies drop from C-F, to C-Cl, to C-Br as shown in Table 14. This can be attributed to both the mass effects and the weakening of the bond. Also, the ring bending modes are more affected by the substitution. This is especially true for the lower frequency vibrations which interact more with the C-X wagging motions.

Conclusions

The calculated structures for the chloro and bromo pyridines are consistent with previously studied fluoropyridines. All vibrational frequencies in the electronic ground state are clearly assigned by the observed infrared and Raman spectra along with density functional theory (DFT) and *ab initio* calculations. The data for the electronic ground states can be prepared for the analysis of electronic excited states.

CHAPTER VII

THE TRANS EFFECT IN HALOBISMUTHATES AND HALOANTIMONATES. MOLECULAR STRUCTURES AND VIBRATIONS FROM THEORETICAL CALCULATIONS*

Introduction

A variety of interesting structures which contain both external and bridging M-X bonds (X = I, Br, Cl) are included in the halobismuthate and haloantimonate anions. The structures of MX_6^{-3}, $M_2X_9^{-3}$, $M_2X_{10}^{-4}$, $(MX_5^{-2})_n$, and $(MX_4^{-1})_n$ anions are shown in Figure 26. The latter two have infinite chain structures. The far-infrared and low-frequency Raman spectra of several bromo- and iodo-bismuthates of formula BiX_6^{-3}, $Bi_2X_9^{-3}$, BiX_4^- and BiX_5^{-2} were reported in Laane's research laboratory in 1980.[47] Except for the BiX_6^{-3} species, both bridging and non-bridging (external) Bi-X bonds are possessed by each of these ions. The Bi-X stretching frequencies for the bridging bonds are the lowest †reflecting the weakest bonds were observed. The trend that the external Bi-X stretching frequencies for bonds across from Bi-X bridging bonds were higher than those across from other external Bi-X bonds were also noticed. The phenomenon that the weaker bridging bonds across from external Bi-X bonds allows the latter to become stronger was

---

* Reprinted with permission from "Trans Effect in Halobismuthates and Haloantimonates Revisited. Molecular Structures and Vibrations from Theoretical Calculations" by Sheu, H. and Laane, J. *Inorg. chem.* **2013**, 52(8), 4244. Copyright [2013] by American Chemical Society.

attributed to the *trans* effect. The spectroscopic data was consistent with the crystal structures reported for the iodo and bromo anions[99-119] in that the shortest Bi-X bonds were found when the halogen atom was across from a bridging bond, and the longest bonds were found for the bridging bonds.

The low-frequency infrared and Raman data for several bromo- and iodo-antimonates were also reported in our laboratory in 1980.[48] SbX_6^{-3}, $Sb_2X_9^{-3}$, SbX_5^{-2}, and SbX_4^{-1} anions associated with several different cations such as n-propyl-ammonium and 4-picolinium were included. The bridging bonds were the weakest, and the strongest external bonds were those *trans* to the bridging bonds as observed for the halobismuthates. The reported crystal structures[22,120-128] again showed the same trend as was observed for the halobismuthates.

Since the publication of research results in the Laane's group described above, a number of crystal structure determinations of chlorobismuthates[23-40] and chloroantimonates[22,41-46] have also been published. In addition, new spectroscopic data has also been reported for the chloro-, bromo-, and iodo-bismuthates[129-136] and antimonates.[137-140]

In the present study the calculation of the structures of these anions along with their vibrational frequencies using *ab initio* (MP2/cc-pVTZ-PP) and DFT (B3LYP/ cc-pVTZ-PP) computations are done. The goal was to confirm and support our previous analysis of the vibrational spectra, which had led us to postulate the *trans* effect. We also wanted to provide an additional perspective to better understand the structural features of these interesting anions, which possess several types of M-X bonds.

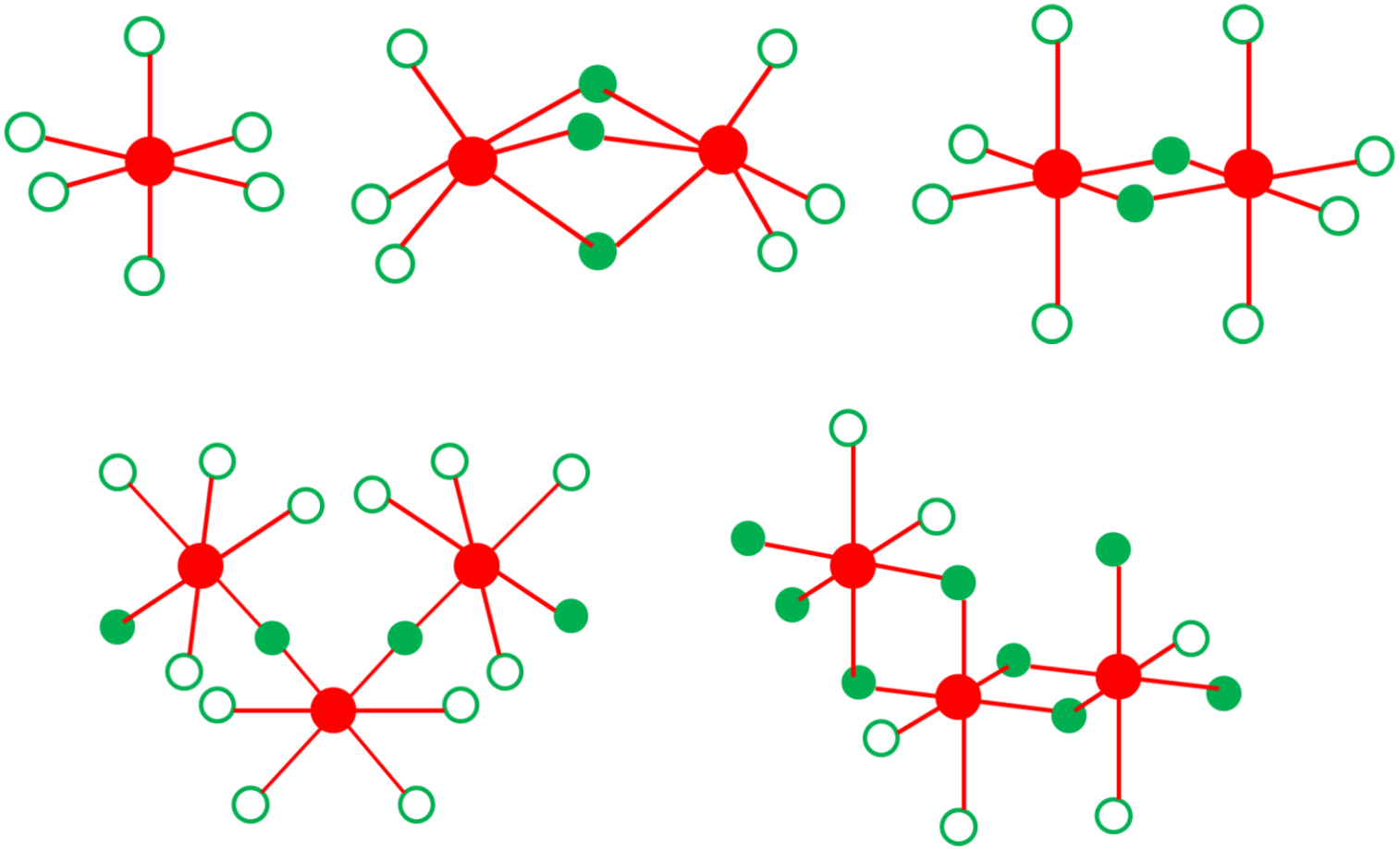

Figure 26 Structures of MX_6^{-3}, $M_2X_9^{-3}$, $M_2X_{10}^{-4}$, $(MX_5^{-2})_n$, and $(MX_4^{-1})_n$ for M = Bi or Sb and X = I, Br, or Cl. The smaller open circles represent external halogen atoms and the smaller black circles represent bridging atoms. The $(MX_5^{-2})_n$ and $(MX_4^{-1})_n$ are infinite chains[141]

Moreover, since the effect of neighboring cations is neglected by the computations, the best representation of the non-interacting anions is provided.

Results and Discussion

The calculated bond distances for the BiX_6^{-3}, $Bi_2X_9^{-3}$, $Bi_2X_{10}^{-4}$, $(BiX_5^{-2})_n$, and $(BiX_4^{-1})_n$ anions for X = I, Br, and Cl are shown in Table 15. The experimental bond distances from a number of crystal structure determinations for different cations are also shown in the same table. For BiX_6^{-3} anions, the experimental bond distances are somewhat dependent on which cation is present but typically agree within ±0.03 Å for each anion. The computed value is that for a free anion without the presence of the cation. Nonetheless, the agreement between calculated and experimental values is good with the former values typically about 0.03 to 0.06 Å larger.

For $Bi_2X_9^{-3}$ anions, two types of Bi-X bonds are present, namely external bonds across from bridging bonds and bridging bonds across from external bonds. The bridging bonds are calculated to be from 0.15 to 0.22 Å longer than the external bonds. The actual bond distances for the bridging bonds are longer by 0.18 to 0.37 Å determined by the crystal structures. However, the calculations are in quite good agreement when the neglected effect of the cation is considered.

For the $Bi_2X_{10}^{-2}$ and BiX_5^{-1} anions, each ion has two types of external halogen atoms: those across from other external atoms and those across from bridging atoms. Each halobismuthate anion also has bridging atoms across from external atoms. The previously postulated *trans* effect[47] are supported by both calculations and experimental

Table 15 Observed and calculated bond distances (Å) of BiX_6^{3-}, $Bi_2X_9^{3-}$, $Bi_2X_{10}^{4-}$, BiX_5^{2-} and BiX_4^- complexes[141]

Anion	Type	trans halogen	Calculated	Observed	Ref.
BiI_6^{3-}	External	External	3.119	3.087	97
				3.065	98
				3.092	99
$BiBr_6^{3-}$	External	External	2.905	2.853	100
				2.857	101
				2.843	102
				2.840	103
$BiCl_6^{3-}$	External	External	2.770	2.731	23
				2.738	24
				2.703	25
				2.717	26
				2.710	27
				2.705	28
				2.719	29
				2.702	30
				2.660	31
				2.715	32
$Bi_2I_9^{3-}$	External	Bridging	3.005	2.920	104
				2.976	105
				2.973	106
	Bridging	External	3.159	3.244	104
				3.228	105
				3.227	106
$Bi_2Br_9^{3-}$	External	Bridging	2.781	2.713	107
				2.749	108
				2.713	109
	Bridging	External	2.972	3.036	107
				3.050	108
				2.979	109
$Bi_2Cl_9^{3-}$	External	Bridging	2.635	2.590	33
				2.558	34

Table 15 (Continued)[141]

Anion	Type	trans halogen	Calculated	Observed	Ref.
$Bi_2Cl_9^{3-}$	Bridging	External	2.858	2.827	33
				2.926	34
$Bi_2I_{10}^{4-}$	External	Bridging	2.987	2.933	110
	External	External	3.046	3.083	110
	Bridging	External	3.130	3.258	110
BiI_5^{2-}	External	Bridging	2.987 [a]	2.949	111
	External	External	3.046 [a]	3.069	111
	Bridging	External	3.130 [a]	3.278	111
$Bi_2Br_{10}^{4-}$	External	Bridging	2.788	2.730	112
				2.730	113
				2.786	114
	External	External	2.835	2.837	112
				2.850	113
				2.808	114
	Bridging	External	2.979	3.050	112
				3.060	113
				3.021	114
$BiBr_5^{2-}$	External	Bridging	2.788 [a]	2.684	115
	External	External	2.835 [a]	2.851	115
	Bridging	External	2.979 [a]	3.071	115
$Bi_2Cl_{10}^{4-}$	External	Bridging	2.608	2.607	35
				2.601	36
				2.580	37
				2.568	30
				2.556	38

Table 15 (Continued)[141]

Anion	Type	trans halogen	Calculated	Observed	Ref.
$Bi_2Cl_{10}^{4-}$	External	External	2.693	2.686	35
				2.712	36
				2.700	37
				2.667	30
				2.697	38
	Bridging	External	2.887	2.862	35
				2.855	36
				2.725	37
				2.970	30
				2.915	38
$BiCl_5^{2-}$	External	Bridging	2.608 [a]	2.546	39
	External	External	2.693 [a]	2.696	39
	Bridging	External	2.887 [a]	2.836	39
BiI_4^-	External	Bridging	2.987 [a]	2.930	116
	Bridging	External	3.130 [a]	3.203	116
$BiBr_4^-$	External	Bridging	2.788 [a]	2.640	117
	Bridging	External	2.979 [a]	3.038	117
$BiCl_4^-$	External	Bridging	2.608 [a]	2.526	40
	Bridging	External	2.887 [a]	2.841	40

[a] Calculated values are from the $Bi_2X_{10}^{-4}$ computations

data. The strongest and shortest bonds are those across from bridging atoms. External bonds across from other external atoms are somewhat longer while the bridging bonds are the longest. This supports the view that external atoms "fight harder" for electron density than bridging atoms so that the bonds across from them cannot be as strong as those across from bridging atoms. For the $Bi_2Cl_{10}^{-4}$ anions the experimental and calculated distances agree very well for all three types of bonds. For the iodide and bromide ions the calculated external bond distances across from other external atoms agree very well with those from crystal structure determinations, but the external bonds across from bridging atoms are calculated to be slightly higher than observed while the bridging bond distances are calculated to be a little lower than observed. The experimentally determined Bi-X bond distances for the BiX_4^{-1} complexes and compares these to the same types of bonds as in our $Bi_2X_{10}^{-4}$ model are also displayed in table 15. All of the external Bi-X bonds are *trans* to bridging halogens and are therefore among the shortest bonds.

The data for the SbX_6^{-3}, $Sb_2X_9^{-3}$, $Sb_2X_{10}^{-4}$, $(SbX_5^{-2})_n$, and $(SbX_4^{-1})_n$ anions are presented in Table 16 and a close agreement between the calculated and experimental bond distances is revealed. As expected for the SbX_6^{-3} anions, the Sb-X distances are less than those for the corresponding bismuth halides given that antimony is higher in the periodic table than bismuth. The $Sb_2X_9^{-3}$ anions are also similar to the bismuth anions. The bridging bonds are longer than the external bonds, and the calculated values are higher than experimental (by 0.07 to 0.10 Å) for the external bonds but lower (by

Table 16 Observed and calculated bond distances (Å) of SbX_6^{3-}, $Sb_2X_9^{3-}$, $Sb_2X_{10}^{4-}$, SbX_5^{2-}, and SbX_4^{-} complexes[141]

Anion	Type	trans halogen	Calculated	Observed	Ref.
SbI_6^{3-}	External	External	3.068	N/A	
$SbBr_6^{3-}$	External	External	2.857	2.826 2.809	118 119
$SbCl_6^{3-}$	External	External	2.720	2.705 2.675 2.643	41 42 43
$Sb_2I_9^{3-}$	External	Bridging	2.950	2.881 2.870 2.862	120 121 122
	Bridging	External	3.105	3.252 3.198 3.199	120 121 122
$Sb_2Br_9^{3-}$	External	Bridging	2.717	2.639 2.630 2.625	107 123 124
	Bridging	External	2.939	3.034 3.072 3.043	107 123 124
$Sb_2Cl_9^{3-}$	External	Bridging	2.557	2.455	44
	Bridging	External	2.848	2.911	44
$Sb_2I_{10}^{4-}$	External	Bridging	2.921	N/A	
	External	External	2.994	N/A	
	Bridging	External	3.091	N/A	
SbI_5^{-}	External	Bridging	2.921 [a]	2.876	125
	External	External	2.994 [a]	3.012	125
	Bridging	External	3.091 [a]	3.190	125

Table 16 (Continued)[141]

Anion	Type	trans halogen	Calculated	Observed	Ref.
$Sb_2Br_{10}^{4-}$	External	Bridging	2.717	N/A	
	External	External	2.785	N/A	
	Bridging	External	2.960	N/A	
$SbBr_5^-$	External	Bridging	2.717 [a]	2.681	126
	External	External	2.785 [a]	2.796	126
	Bridging	External	2.960 [a]	3.014	126
$Sb_2Cl_{10}^{4-}$	External	Bridging	2.482	2.396	45
	External	External	2.631	2.650	45
	Bridging	External	2.981	3.013	45
$SbCl_5^-$	External	Bridging	2.482 [a]	2.452	46
	External	External	2.631 [a]	2.734	46
	Bridging	External	2.981 [a]	2.916	46
SbI_4^-	External	Bridging	2.921 [a]	N/A	
	Bridging	External	3.091 [a]	N/A	
$SbBr_4^-$	External	Bridging	2.717 [a]	2.567	22
	Bridging	External	2.960 [a]	2.816	22
$SbCl_4^-$	External	Bridging	2.482 [a]	2.394	22
	Bridging	External	2.981 [a]	2.659	22

about 0.10 Å) for the bridging bonds. The difference between computed and experimental bond distances can be attributed to the effect of the cations.

The calculations for the $Sb_2X_{10}^{-2}$ anions are also shown in Table 16 and they are compared to $Sb_2Cl_{10}^{-4}$ and to SbX_5^{-1} experimental data for X = I, Br, and Cl. No crystal structures have been reported for the $Sb_2X_{10}^{-2}$ species for X = I or Br. The concept of the *trans* effect is supported by the available data and the calculations again, as the external bonds across from bridging bonds are shorter than those across from other external halogen atoms. The experimentally determined Sb-X bond distances for the SbX_4^{-1} complexes are also shown in the Table 16 and they are compared to the same types of bonds in our $Sb_2X_{10}^{-4}$ model.

The bond distance data for the bismuthates and antimonates are summarized in Table 17 and the magnitude of the *trans* effect are clearly displayed. In all cases the shortest bonds are for the external M-X bonds across from the bridging halogen atoms. For the bismuthates the external Bi-X bonds across from other external bonds are calculated to be 0.085 to 0.110 Å longer than those across from bridging bonds. From crystal structure determinations, these are 0.082 to 0.131 Å longer. The difference arises from the fact that the calculations correspond to values for the free ions not interacting with the neighboring cations. The external Sb-X bonds across from other external atoms are calculated to be longer by 0.095 Å for Sb-I bonds, by 0.104 Å for Sb-Br bonds, and 0.156 Å for Sb-Cl bonds than those across from bridging bonds. From the crystal structure determinations the same Sb-Br bonds are 0.179 Å longer and the Sb-Cl bonds are 0.265 Å longer.

Table 17 Average M-X bond distances (Å) for different types of bonds[141]

M — X	Type	trans halogen	Average bond distances	
			Calculated	Observed
Bi — I	External	Bridging	2.996±0.009	2.951±0.031
	External	External	3.083±0.037	3.082±0.017
	Bridging	External	3.145±0.015	3.239±0.039
Bi — Br	External	Bridging	2.785±0.004	2.759±0.046
	External	External	2.870±0.035	2.841±0.033
	Bridging	External	2.976±0.004	3.043±0.064
Bi — Cl	External	Bridging	2.622±0.014	2.580±0.034
	External	External	2.732±0.039	2.674±0.057
	Bridging	External	2.873±0.015	2.876±0.151
Sb — I	External	Bridging	2.936±0.015	2.871±0.010
	External	External	3.031±0.037	3.012±0.000
	Bridging	External	3.098±0.007	3.216±0.036
Sb — Br	External	Bridging	2.717±0.000	2.631±0.008
	External	External	2.821±0.036	2.810±0.016
	Bridging	External	2.950±0.011	3.050±0.036
Sb — Cl	External	Bridging	2.520±0.038	2.426±0.032
	External	External	2.676±0.045	2.681±0.053
	Bridging	External	2.915±0.067	2.962±0.051

In addition to the calculations of bond distances for the bismuth and antimony ions, their vibrational frequencies using DFT computations are also calculated and the summary of the vibrational results are presented in Table 18. The crystalline materials have well-defined bond-stretching frequencies,[47-48] but the low-frequency bending modes and lattice modes are difficult to distinguish from each other. Hence, since the computations do not take into account any intermolecular or interionic interactions, only the calculated frequencies for the stretching modes are compared to the experimental ones, since these are least affected by the interactions.

In the Laane group's previous work,[47-48] the experimental far-infrared and low-frequency Raman spectra of these anions were analyzed in detail and the spectra were assigned on the basis of octahedral symmetry for the MX_6^{-3} species, C_{2v} for MX_5^{-2}, C_{2v} for MX_4^-, and D_{3h} for $M_2X_9^{-3}$. Each of these has several M-X stretching modes which extend over a range of frequencies. These can be classified as υ_{EE}, where the external M-X bond stretches across from another external bond, as υ_{EB}, where the external bond stretches across from a bridging bond, or as υ_B, for the stretching of a bridging bond. The lower frequency bending modes and the lattice modes of the crystalline structures are extensively interacted and therefore the computation of these frequencies is not particularly meaningful. The stretching modes are partially coupled with the bending modes as shown in Tables 19 to 37. Our calculations for the molecular vibrations were carried out for independent "gas-phase" species, which have no interactions with the cations or the lattice modes of the solid. Hence, the comparison of calculated M-X stretching frequencies to those experimentally observed is focused. The details of the

Table 18 Observed and calculated vibrational frequencies for M-X stretching modes[141]

M — X	Type	trans halogen	Frequency range (cm^{-1})			
			Calculated		Observed	
			Range	Sym. stretch	Range	Sym. stretch
Bi — I	External	Bridging	112-136	126	110-138	N/A
	External	External	85-107	107	105-139	N/A
	Bridging	External	75-113	99	80-99	N/A
Bi — Br	External	Bridging	149-177	171	156-198	169
	External	External	115-148	143	123-164	142
	Bridging	External	88-145	131	99-150	106
Bi — Cl	External	Bridging	226-272	272	238-294	279
	External	External	164-227	222	169-255	244
	Bridging	External	113-200	161	129-246	157
Sb — I	External	Bridging	117-160	140	134-181	154
	External	External	84-127	110	100-135	100
	Bridging	External	78-114	99	85-129	[95]
Sb — Br	External	Bridging	157-196	188	164-215	205
	External	External	109-161	144	129-178	147
	Bridging	External	84-146	126	110-155	[130]
Sb — Cl	External	Bridging	229-316	316	279-323	N/A
	External	External	164-256	211	174-282	N/A
	Bridging	External	77-192	178	N/A	N/A

vibrational calculations are presented in Tables 19 to 37 and the results are compared to previous experimental data. Many of the previous spectroscopic results come from our previous work, but infrared and Raman data from other laboratories are also included. The quality of some of the latter is variable. The experimental and calculated vibrational frequency and intensity data for MX_6^{-3} anions for M = Bi and for X = I, Br, and Cl are presented in Tables 19 to 21 while M = Sb are displayed in Tables 22 to 24. The results for $Bi_2X_9^{-3}$ anions are reported in Tables 25 to 27 and $Sb_2X_9^{-3}$ anions are shown in Tables 28 to 30. Finally, the data for the $M_2X_{10}^{-4}$ and MX_5^{-2} species for M = Bi and Sb are presented in tables 31 to 37. The results are summarized in Table 18 where the range of calculated and observed frequencies for the υ_{EE}, υ_{EB}, and υ_B M-X stretching modes are given for M = Bi and Sb and where X = I, Br, and I. Each anion has several vibrations of one type which span a broad frequency range and have different symmetry species. Thus the frequency ranges can be seen to be large. However, it is clear from both the calculated and observed data that each bismuthate and each antimonite anion has $\upsilon_{EB} > \upsilon_{EE} > \upsilon_B$ as expected from the *trans* effect. To assist in further recognizing this trend in Table 18, specific calculated and observed frequencies for the symmetric υ_{EB}, υ_{EE}, and υ_B vibrations of the $M_2X_{10}^{-4}$ anions are also presented.

Some observations are made about the specific data in Tables 19 to 37. It should again be emphasized that the computations are for independent free-standing anions and the experimental vibration spectra are those from species where the cation has a significant effect. For example, The A_{1g}, E_g, and T_{1u} Bi-I stretching frequencies for

Table 19 Stretching frequencies (cm^{-1}) of BiI_6^{3-} complexes[141]

Sym		Description	Calculated [a]	PED [b]	Observed [c]			
					n-$C_3H_7NH_3$ [d]		$Cr(en)_3$ [d]	
					IR	Raman	IR	Raman
A_{1g}	ν_1	Sym. stretch	104 (0, 10)	$\nu_{EE}(100)$	-	119 (7)	-	139 (10)
E_g	ν_2	Stretching	85 (0, 2)	$\nu_{EE}(100)$	-	105 (10)	-	128 (5)
T_{1u}	ν_4	Stretching	106 (10, 0)	$\nu_{EE}(69)\delta(31)$	110 s	-	135 s	-
				Reference	47		47	

[a] Relative infrared and Raman intensities given in parentheses
[b] Potential energy distribution (applicable to all tables):
ν_{EE} : M-X stretching frequencies for external bond across from an external bond
ν_{EB} : M-X stretching frequencies for external bond across from a bridging bond
ν_B : M-X stretching frequencies for bridging bond
δ: bending and torsional motions
[c] s-strong, m-medium, w-weak, vs-very strong, br-broad, sh-shoulder
[d] cation

Table 20 Stretching frequencies (cm^{-1}) of $BiBr_6^{3-}$ complexes[141]

Sym		Description	Calculated [a]	PED	Observed [b]							
					CH_3NH_3[c]		$C_6H_5CH_2NH_3$[c]		n-$C_3H_7NH_3$ [c]		$C_3H_5NH_3$ [c]	
					IR	Raman	IR	Raman	IR	Raman	IR	Raman
A_{1g}	ν_1	Sym. stretch	144 (0, 10)	$\nu_{EE}(100)$	152 sh	154 (10)	158 s	157 (10)	-	157 (10)	150 sh	158(10)
E_g	ν_2	Stretching	115 (0, 2)	$\nu_{EE}(100)$	-	135 (1)	-	129 (1)	-	138 (3)	-	142 (2)
T_{1u}	ν_4	Stretching	131 (10, 0)	$\nu_{EE}(68)\delta(32)$	126 s	-	124 vs	-	123 vs	-	130 s	-
				Reference	47		47		47		47	

[a] Relative infrared and Raman intensities given in parentheses
[b] s-strong, m-medium, w-weak, vs-very strong, br-broad, sh-shoulder; relative Raman intensities in parentheses
[c] cation

Table 21 Stretching frequencies (cm^{-1}) of $BiCl_6^{3-}$ complexes[141]

Sym		Description	Calculated [a]	PED	Observed	
					$(C_5H_5NH)_3$[b]	
					IR	Raman
A_{1g}	ν_1	Sym. stretch	227 (0, 10)	$\nu_{EE}(100)$	255	252
E_g	ν_2	Stretching	176 (0, 2)	$\nu_{EE}(100)$	-	212
T_{1u}	ν_4	Stretching	169 (10, 0)	$\nu_{EE}(70)\delta(30)$	169	-
				Reference	134	

[a] Relative infrared and Raman intensities given in parentheses
[b] cation

Table 22 Stretching frequencies (cm^{-1}) of SbI_6^{3-} complexes[141]

Sym	Description	Calculated [a]	PED
A_{1g}	ν_1 Sym. stretch	104 (0, 10)	$\nu_{EE}(100)$
E_g	ν_2 Stretching	84 (0, 3)	$\nu_{EE}(100)$
T_{1u}	ν_4 Stretching	127 (10, 0)	$\nu_{EE}(63)\delta(37)$

[a] Relative infrared and Raman intensities given in parentheses; no observed data has been reported.

Table 23 Stretching frequencies (cm^{-1}) of $SbBr_6^{3-}$ complexes[141]

Sym	Description	Calculated [a]	PED	Observed [b]				
				$(n\text{-}C_3H_7)_2NH_2$ [c]		$(C_2H_5)_2NH_2$ [c]		$(CH_3)_2NH_2$ [c]
				IR	Raman	IR	Raman	IR
A_{1g}	ν_1 Sym. stretch	142 (0, 10)	$\nu_{EE}(100)$	-	150 (10)	-	178 s, br	-
E_g	ν_2 Stretching	109 (0, 2)	$\nu_{EE}(100)$	-	129 (7)	-	-	-
T_{1u}	ν_4 Stretching	147 (10, 0)	$\nu_{EE}(64)\delta(36)$	135 s	-	178 s, br	-	150 s, br
			Reference	48		135		136

[a] Relative infrared and Raman intensities given in parentheses
[b] s-strong, m-medium, w-weak, vs-very strong, br-broad, sh-shoulder; relative Raman intensities in parentheses
[c] cation

Table 24 Stretching frequencies (cm^{-1}) of $SbCl_6^{3-}$ complexes[141]

Sym		Description	Calculated [a]	PED	Observed [b]	
					$(CH_3S)_3$ [c]	$(CH_3Se)_3$ [c]
					Raman	Raman
A_{1g}	ν_1	Sym. stretch	224 (0, 10)	$\nu_{EE}(100)$	282 m, br	278 m
E_g	ν_2	Stretching	164 (0, 3)	$\nu_{EE}(100)$	183 mw	174 m
T_{1u}	ν_4	Stretching	178 (10, 0)	$\nu_{EE}(64)\delta(36)$	-	-
				Reference	137	137

[a] Relative infrared and Raman intensities given in parentheses
[b] s-strong, m-medium, w-weak, vs-very strong, br-broad, sh-shoulder; relative Raman intensities in parentheses
[c] cation

Table 25 Stretching frequencies (cm^{-1}) of $Bi_2I_9^{3-}$ complexes[141]

Sym		Description	Calculated [a]	PED	Observed [b]					
					$(CH_3)_2NH_2$[c]		piperidinium[c]		4-picolinium[c]	
					IR	Raman	IR	Raman	IR	Raman
A_1'	ν_1	BiI_3 Sym. stretch	136(0, 10)	$\nu_{EB}(43)\nu_B(28)\delta(29)$	-	138 (10)	-	135 (10)	-	134 (10)
E'	ν_6	BiI_3 Sym. stretch	135 (5, 0)	$\nu_{EB}(44)\nu_B(28)\delta(28)$	128 s	-	129 s	-	134 sh	-
A_2"	ν_{12}	BiI_3 Antisym. stretch	121(10, 0)	$\nu_{EB}(49)\nu_B(24)\delta(27)$	110 sh	-	114 sh	124 w	123 s	123 (1)
E"	ν_{15}	BiI_3 Antisym. stretch	116(0, 5)	$\nu_{EB}(54)\nu_B(14)\delta(32)$	-	112 (3)	-	112 (2)	113 sh	116 (4)
A_1'	ν_2	Sym. stretch (i.p.)	113 (0, 10)	$\nu_B(55)\nu_{EB}(11)\delta(34)$	-	-	99 (2)	99 (2)	-	92 (1)
E'	ν_7	Sym. stretch (i.p.)	100 (0, 2)	$\nu_B(44)\nu_{EB}(24)\delta(32)$	-	-	-	-	-	-
A_2"	ν_{13}	Antisym. stretch (i.p.)	103 (2, 0)	$\nu_B(55)\nu_{EB}(2)\delta(43)$	83 m	-	85 m	-	80 ms	-
E"	ν_{16}	Antisym. stretch (i.p.)	75 (0, 0)	$\nu_B(65)\nu_{EB}(8)\delta(27)$	-	-	-	-	-	-
				Reference	47		47		47	

[a] Relative infrared and Raman intensities given in parentheses

[b] s-strong, m-medium, w-weak, vs-very strong, br-broad, sh-shoulder; relative Raman intensities in parentheses

[c] cation

Table 26 Stretching frequencies (cm^{-1}) of $Bi_2Br_9^{3-}$ complexes[141]

Sym	Description		Calculated [a]	PED	Observed [b]			
					Et_3NH [c]		i-Bu_2NH_2 [c]	
					IR	Raman	IR	Raman
A_1'	ν_1	$BiBr_3$ Sym. stretch	177 (0, 10)	$\nu_{EB}(58)\nu_B(12)\delta(30)$	-	182 (10)	-	180 (10)
E'	ν_6	$BiBr_3$ Sym. stretch	168 (9, 0)	$\nu_{EB}(43)\nu_B(22)\delta(35)$	-	-	-	-
A_2"	ν_{12}	$BiBr_3$ Antisym. stretch	161 (8, 0)	$\nu_{EB}(77)\nu_B(3)\delta(20)$	163 vs	163 w, sh	161 vs	-
E"	ν_{15}	$BiBr_3$ Antisym. stretch	152 (0, 3)	$\nu_{EB}(66)\nu_B(3)\delta(31)$	-	158 (3)	-	165 (3)
A_1'	ν_2	Sym. stretch (i.p.)	145 (0, 3)	ν_B (63)$\nu_{EB}(6)\delta(31)$	-	145 (1)	-	-
E'	ν_7	Sym. stretch (i.p.)	131 (0, 1)	ν_B (45)$\nu_{EB}(18)\delta(37)$	-	123 (1)	-	122 w
A_2"	ν_{13}	Antisym. stretch (i.p.)	130 (10, 0)	$\nu_B(48)\nu_{EB}(12)\delta(40)$	99 vs	-	103 vs	-
E"	ν_{16}	Antisym. stretch (i.p.)	88 (0, 0)	$\nu_B(61)\nu_{EB}(12)\delta(27)$	-	-	-	-
				Reference	47		47	

[a] Relative infrared and Raman intensities given in parentheses
[b] s-strong, m-medium, w-weak, vs-very strong, br-broad, sh-shoulder
[c] cation

Table 27 Stretching frequencies (cm^{-1}) of $Bi_2Cl_9^{3-}$ complexes[141]

Sym	Description		Calculated [a]	PED	Observed [b]		
					$(CH_3)_4P$ [c]	$(CH_3)_2NH_2$ [c]	
					Raman	IR	Raman
A_1'	ν_1	$BiCl_3$ Sym. stretch	268 (0, 10)	$\nu_{EB}(59)\nu_B(12)\delta(29)$	278 s	-	288 vs
E'	ν_6	$BiCl_3$ Sym. stretch	235 (6, 0)	$\nu_{EB}(59)\nu_B(14)\delta(27)$	-	247 s	-
A_2"	ν_{12}	$BiCl_3$ Antisym. stretch	251 (3, 0)	$\nu_{EB}(60)\nu_B(18)\delta(22)$	-	281 m	-
E"	ν_{15}	$BiCl_3$ Antisym. stretch	226 (0, 2)	$\nu_{EB}(67)\nu_B(8)\delta(25)$	235 s	-	238 s
A_1'	ν_2	Sym. stretch (i.p.)	200 (0, 1)	$\nu_B(50)\nu_{EB}(15)\delta(35)$	-	-	-
E'	ν_7	Sym. stretch (i.p.)	194 (1, 1)	$\nu_B(49)\nu_{EB}(5)\delta(46)$	172 m	-	-
A_2"	ν_{13}	Antisym. stretch (i.p.)	175 (10, 0)	$\nu_B(45)\nu_{EB}(18)\delta(37)$	-	165 s	-
E"	ν_{16}	Antisym. stretch (i.p.)	113 (0, 0)	$\nu_B(57)\nu_{EB}(15)\delta(28)$	-	-	-
				Reference	127	128	

[a] Relative infrared and Raman intensities given in parentheses
[b] s-strong, m-medium, w-weak, vs-very strong, br-broad, sh-shoulder; relative Raman intensities in parentheses
[c] cation

Table 28 Stretching frequencies (cm^{-1}) of $Sb_2I_9^{3-}$ complexes[141]

Sym	Description		Calculated [a]	PED	Observed [b]					
					CH_3NH_3 [c]		4-Picolinium [c]		$CH_3O(CH_2)_3NH_3$ [c]	
					IR [c]	Raman	IR [c]	Raman	IR [c]	Raman
A_1'	ν_1	SbI_3 Sym. stretch	160 (0, 7)	$\nu_{EB}(32)\nu_B(29)\delta(39)$	-	170 (10)	-	160 (10)	-	181 (6)
E'	ν_6	SbI_3 Sym. stretch	158 (4, 0)	$\nu_{EB}(33)\nu_B(29)\delta(38)$	160 s	-	161 s	-	150 s	-
A_2"	ν_{12}	SbI_3 Antisym. stretch	136 (10, 0)	$\nu_{EB}(32)\nu_B(30)\delta(38)$	145 sh	-	148 m	-	-	-
E"	ν_{15}	SbI_3 Antisym. stretch	123 (0, 5)	$\nu_{EB}(44)\nu_B(19)\delta(37)$	-	-	-	151 (19)	-	161 (10)
A_1'	ν_2	Sym. stretch (i.p.)	114 (0, 10)	$\nu_B(50)\nu_{EB}(21)\delta(29)$	-	125 (12)	-	129 (4)	-	129 (8)
E'	ν_7	Sym. stretch (i.p.)	100 (0, 2)	$\nu_B(39)\nu_{EB}(25)\delta(36)$	-	110 (20)	-	114(7)	-	-
A_2"	ν_{13}	Antisym. stretch (i.p.)	106 (0, 0)	$\nu_B(42)\nu_{EB}(23)\delta(35)$	-	-	-	-	-	-
E"	ν_{16}	Antisym. stretch (i.p.)	78 (0, 0)	$\nu_B(68)\delta(32)$	-	-	-	-	-	-
				Reference	48		48		48	

[a] Relative infrared and Raman intensities given in parentheses
[b] s-strong, m-medium, w-weak, vs-very strong, br-broad, sh-shoulder; relative Raman intensities in parentheses
[c] cation

Table 29 Stretching frequencies (cm^{-1}) of $Sb_2Br_9^{3-}$ complexes[141]

Sym	Description		Calculated [a]	PED	Observed [b]					
					$N(C_2H_5)_4$ [c]		methylammonium [c]		CH_3NH_3 [c]	
					IR [c]	Raman [c]	IR [c]	Raman [c]	IR [c]	Raman [c]
A_1'	ν_1	$SbBr_3$ Sym. stretch	196 (0, 10)	ν_{EB} (40)ν_B(22)δ38)	-	201 s, br	-	176 s, br	-	215 (9)
E'	ν_6	$SbBr_3$ Sym. stretch	190 (6, 0)	ν_{EB}(36)ν_B(27)δ(37)	199 s	-	201 s, br	-	185 s	-
A_2"	ν_{12}	$SbBr_3$ Antisym. stretch	169 (10, 0)	ν_{EB}(47)ν_B(19)δ(34)	184 sh	-	185 s, br	-	-	-
E"	ν_{15}	$SbBr_3$ Antisym. stretch	160 (0, 5)	ν_{EB}(51)ν_B(13)δ(36)	-	-	-	-	-	192 (10)
A_1'	ν_2	Sym. stretch (i.p.)	146 (0, 5)	ν_B(60)ν_{EB}(5)δ(35)	-	155 s, br	-	115 s, br	-	123 (3)
E'	ν_7	Sym. stretch (i.p.)	129 (0, 2)	ν_B(42)ν_{EB}(22)δ(36)	-	-	-	-	-	-
A_2"	ν_{13}	Antisym. stretch (i.p.)	137 (3, 0)	ν_B(51)δ(49)	152 sh	-	-	-	155 w	-
E"	ν_{16}	Antisym. stretch (i.p.)	84 (0, 0)	ν_B(60)ν_{EB}(7)δ(33)	-	-	-	-	-	-
				Reference	135		135		48	

[a] Relative infrared and Raman intensities given in parentheses
[b] s-strong, m-medium, w-weak, vs-very strong, br-broad, sh-shoulder; relative Raman intensities in parentheses
[c] cation

Table 30 Stretching frequencies (cm^{-1}) of $Sb_2Cl_9^{3-}$ complexes[141]

Sym	Description		Calculated [a]	PED	Observed [b]			
					CH_3NH_3 [c]		$(CH_3)_2NH_2$ [c]	
					IR	Raman	IR	Raman
A_1'	ν_1	$SbCl_3$ Sym. stretch	281 (0, 10)	ν_{EB} (65)δ(35)	-	323 vs	-	322 vs
E'	ν_6	$SbCl_3$ Sym. stretch	248 (7, 0.3)	ν_{EB}(47)ν_B(20)δ(33)	279 m	-	270 m	-
A_2"	ν_{12}	$SbCl_3$ Antisym. stretch	253 (6, 0)	ν_{EB}(71)ν_B(8)δ(21)	263 s	-	-	-
E"	ν_{15}	$SbCl_3$ Antisym. stretch	229 (0, 3)	ν_{EB}(68)δ(32)	-	278 s	-	275 s
A_1'	ν_2	Sym. stretch (i.p.)	192 (0, 1)	ν_B(53)ν_{EB}(11)δ(36)	-	-	-	-
E'	ν_7	Sym. stretch (i.p.)	189 (0.4, 1)	ν_B(46)ν_{EB}(12)δ(42)	-	-	-	-
A_2"	ν_{13}	Antisym. stretch (i.p.)	175 (10, 0)	ν_B(44)ν_{EB}(15)δ(41)	168 s	-	183	-
E"	ν_{16}	Antisym. stretch (i.p.)	101 (0, 0.3)	ν_B(42)ν_{EB}(28)δ(30)	-	-	-	-
				Reference	138		138	

[a] Relative infrared and Raman intensities given in parentheses
[b] s-strong, m-medium, w-weak, vs-very strong, sh-shoulder
[c] cation

Table 31 Calculated stretching frequencies (cm^{-1}) of $Bi_2I_{10}^{4-}$ complexes[141]

Sym	Description		Calculated [a]	PED
A_g	ν_1	BiI_2 Sym. stretch	126 (0, 10)	$\nu_{EB}(51)\nu_{EE}(13)\nu_B(13)\delta(23)$
B_{3u}	ν_{26}	BiI_2 Sym. stretch	120 (2, 0)	$\nu_{EB}(52)\nu_{EE}(22)\nu_B(10)\delta(16)$
B_{2g}	ν_{10}	BiI_2 Antisym. stretch	112 (0, 3)	$\nu_{EB}(72)\nu_B(4)\delta(24)$
B_{1u}	ν_{18}	BiI_2 Antisym. stretch	118 (7, 0)	$\nu_{EB}(49)\nu_B(24)\delta(27)$
A_g	ν_2	BiI_2 Sym. stretch	107 (0, 2)	$\nu_{EE}(38)\nu_B(28)\nu_{EB}(19)\delta(15)$
B_{3u}	ν_{27}	BiI_2 Sym. stretch	105 (1, 0)	$\nu_{EE}(48)\nu_{EB}(30)\nu_B(9)\delta(13)$
B_{1g}	ν_7	BiI_2 Antisym. stretch	97 (0, 0)	$\nu_{EE}(72)\delta(28)$
B_{2u}	ν_{22}	BiI_2 Antisym. stretch	99 (10, 0)	$\nu_{EE}(72)\delta(28)$
A_g	ν_3	BiI_2 Sym. stretch	99 (0, 2)	$\nu_B(50)\nu_{EE}(21)\delta(29)$
B_{3u}	ν_{28}	BiI_2 Sym. stretch	91 (7, 0)	$\nu_B(46)\nu_{EB}(20)\nu_{EE}(6)\delta(28)$
B_{2g}	ν_{11}	BiI_2 Antisym. stretch	87 (0, 1)	$\nu_B(63)\nu_{EB}(21)\delta(16)$
B_{1u}	ν_{19}	BiI_2 Antisym. stretch	100 (1, 0)	$\nu_B(58)\nu_{EB}(8)\delta(34)$

[a] Relative infrared and Raman intensities given in parentheses; no experimental data has been reported.

Table 32 Stretching frequencies (cm^{-1}) of $Bi_2Br_{10}^{4-}$ complexes[141]

Sym	Description		Calculated [a]	PED	Observed [b]		
					$C_2H_5N_4S$ [c]	$C_3N_2H_5$ [c]	
					IR	IR	Raman
A_g	ν_1	$BiBr_2$ Sym. stretch	171 (0, 10)	$\nu_{EB}(44)\nu_{EE}(19)\nu_B(12)\delta(25)$	-	-	164 vs
B_{3u}	ν_{26}	$BiBr_2$ Sym. stretch	162 (1, 0)	$\nu_{EB}(43)\nu_{EE}(21)\nu_B(19)\delta(17)$	-	185 vw	-
B_{2g}	ν_{10}	$BiBr_2$ Antisym. stretch	149 (0, 2)	$\nu_{EB}(65)\nu_B(2)\delta(33)$	-	-	-
B_{1u}	ν_{18}	$BiBr_2$ Antisym. stretch	159 (6, 0)	$\nu_{EB}(45)\nu_B(20)\delta(35)$	180	198 vs	-
A_g	ν_2	$BiBr_2$ Sym. stretch	143 (0, 2)	$\nu_{EE}(33)\nu_{EB}(20)\ \nu_B(27)\delta(20)$	-	-	-
B_{3u}	ν_{27}	$BiBr_2$ Sym. stretch	134 (3, 0)	$\nu_{EE}(39)\nu_{EB}(29)\ \nu_B(14)\delta(18)$	-	-	-
B_{1g}	ν_7	$BiBr_2$ Antisym. stretch	139 (0, 0)	$\nu_{EE}(72)\delta(28)$	-	-	-
B_{2u}	ν_{22}	$BiBr_2$ Antisym. stretch	148 (10, 0)	$\nu_{EE}(72)\delta(28)$	164	-	-
A_g	ν_3	$BiBr_2$ Sym. stretch	131 (0, 1)	$\nu_B(40)\nu_{EE}(20)\nu_{EB}(8)\delta(32)$	-	-	106 m
B_{3u}	ν_{28}	$BiBr_2$ Sym. stretch	119 (9, 0)	$\nu_B(41)\nu_{EB}(16)\nu_{EE}(13)\delta(30)$	150	143 vs	-
B_{2g}	ν_{11}	$BiBr_2$ Antisym. stretch	104 (0, 1)	$\nu_B(65)\nu_{EB}(19)\delta(16)$	-	-	-
B_{1u}	ν_{19}	$BiBr_2$ Antisym. stretch	125 (0.2, 0)	$\nu_B(45)\nu_{EB}(11)\delta(44)$	-	114 vw	-
				Reference	129	130	

[a] Relative infrared and Raman intensities given in parentheses
[b] s-strong, m-medium, w-weak, vs-very strong, br-broad, sh-shoulder; relative Raman intensities in parentheses
[c] cation

Table 33 Stretching frequencies (cm^{-1}) of $BiBr_5^{2-}$ complexes[141]

Sym	Description	Calculated [a]	PED	Observed [b]			
				4-picolinium[c]		pyridinium[c]	
				IR	Raman	IR	Raman
A_g ν_1	$BiBr_2$ Sym. stretch	171 (0, 10)	$\nu_{EB}(44)\nu_{EE}(19)\nu_B(12)\delta(25)$	-	169 (10)	-	180 (10)
B_{3u} ν_{26}	$BiBr_2$ Sym. stretch	162 (1, 0)	$\nu_{EB}(43)\nu_{EE}(21)\nu_B(19)\delta(17)$				
B_{2g} ν_{10}	$BiBr_2$ Antisym. stretch	149 (0, 2)	$\nu_{EB}(65)\nu_B(2)\delta(33)$	159 ms	156 (5)	157 s	166 (1)
B_{1u} ν_{18}	$BiBr_2$ Antisym. stretch	159 (6, 0)	$\nu_{EB}(45)\nu_B(20)\delta(35)$				
A_g ν_2	$BiBr_2$ Sym. stretch	143 (0, 2)	$\nu_{EE}(33)\nu_{EB}(20)\nu_B(27)\delta(20)$	-	142 (1)	-	-
B_{3u} ν_{27}	$BiBr_2$ Sym. stretch	134 (3, 0)	$\nu_{EE}(39)\nu_{EB}(29)\nu_B(14)\delta(18)$				
B_{1g} ν_7	$BiBr_2$ Antisym. stretch	139 (0, 0)	$\nu_{EE}(72)\delta(28)$	-	-	-	-
B_{2u} ν_{22}	$BiBr_2$ Antisym. stretch	148 (10, 0)	$\nu_{EE}(72)\delta(28)$				
A_g ν_3	$BiBr_2$ Sym. stretch	131 (0, 1)	$\nu_B(40)\nu_{EE}(20)\nu_{EB}(8)\delta(32)$	-	-	108 vs	-
B_{3u} ν_{28}	$BiBr_2$ Sym. stretch	119 (9, 0)	$\nu_B(41)\nu_{EB}(16)\nu_{EE}(13)\delta(30)$				
B_{2g} ν_{11}	$BiBr_2$ Antisym. stretch	104 (0, 1)	$\nu_B(65)\nu_{EB}(19)\delta(16)$	122 s, br	-	-	-
B_{1u} ν_{19}	$BiBr_2$ Antisym. stretch	125 (0.2, 0)	$\nu_B(45)\nu_{EB}(11)\delta(44)$				
			Reference	47		47	

[a] Relative infrared and Raman intensities given in parentheses; calculated for $Bi_2Br_{10}^{4-}$

[b] s-strong, m-medium, w-weak, vs-very strong, br-broad, sh-shoulder; relative Raman intensities in parentheses

[c] cation

Table 34 Stretching frequencies (cm^{-1}) of $BiCl_5^{2-}$ complexes[141]

Sym	Description	Calculated [a]	PED	Observed [b]		
				$bpyH_2$ [c]	$C_{12}H_{12}N$ [c]	$C_{12}H_{18}N$ [c]
				Raman	Raman	Raman
A_g ν_1	$BiCl_2$ Sym. stretch	272 (0, 10)	$\nu_{EB}(46)\nu_{EE}(28)\nu_B(5)\delta(21)$	248	285	279
B_{3u} ν_{26}	$BiCl_2$ Sym. stretch	259 (2, 0)	$\nu_{EB}(46)\nu_{EE}(20)\nu_B(19)\delta(15)$			
B_{2g} ν_{10}	$BiCl_2$ Antisym. stretch	233 (0, 2)	$\nu_{EB}(64)\nu_B(15)\delta(21)$	-	-	-
B_{1u} ν_{18}	$BiCl_2$ Antisym. stretch	230 (5, 0)	$\nu_{EB}(69)\nu_B(9)\delta(22)$			
A_g ν_2	$BiCl_2$ Sym. stretch	222 (0, 2)	$\nu_{EE}(52)\nu_{EB}(34)\delta(14)$	208	244	246
B_{3u} ν_{27}	$BiCl_2$ Sym. stretch	203 (1, 0)	$\nu_{EE}(55)\nu_{EB}(29)\nu_B(6)\delta(10)$			
B_{1g} ν_7	$BiCl_2$ Antisym. stretch	164 (0, 0)	$\nu_{EE}(72)\delta(28)$	-	197	-
B_{2u} ν_{22}	$BiCl_2$ Antisym. stretch	185 (10, 0)	$\nu_{EE}(71)\delta(29)$			
A_g ν_3	$BiCl_2$ Sym. stretch	161 (0, 1)	$\nu_B(46)\nu_{EE}(40)\nu_{EB}(12)\delta(2)$	-	157	-
B_{3u} ν_{28}	$BiCl_2$ Sym. stretch	153 (7, 0)	$\nu_B(60)\nu_{EB}(20)\delta(20)$			
B_{2g} ν_{11}	$BiCl_2$ Antisym. stretch	133 (0, 2)	$\nu_B(48)\nu_{EE}(9)\nu_{EB}(18)\delta(25)$	-	147	-
B_{1u} ν_{19}	$BiCl_2$ Antisym. stretch	155 (2, 0)	$\nu_B(28)\delta(72)$			
			Reference	131	132	133

[a] Relative infrared and Raman intensities given in parentheses; calculated for $Bi_2Cl_{10}^{4-}$

[b] s-strong, m-medium, w-weak, vs-very strong, br-broad, sh-shoulder; relative Raman intensities in parentheses

[c] cation

Table 35 Stretching frequencies (cm^{-1}) of SbI_5^{2-} complexes[141]

Sym		Description	Calculated [a]	PED	Observed [b]					
					$C_2H_5NH_3$ [c]		$C_5H_{11}NH_3$ [c]		$H_3N(CH_2)_6NH_3$ [c]	
					IR [c]	Raman	IR [c]	Raman	IR [c]	Raman
A_g	ν_1	SbI_2 Sym. stretch	140 (0, 10)	ν_{EB}(40)ν_B(24)ν_{EE}(4)δ(32)	-	160 (10)	170 sh	169 (10)	160 sh	154
B_{3u}	ν_{26}	SbI_2 Sym. stretch	120 (2, 0)	ν_{EB}(56)ν_{EE}(20)ν_B(2)δ(22)						
B_{2g}	ν_{10}	SbI_2 Antisym. stretch	117 (0, 5)	ν_{EB}(56)ν_B(14)δ(30)	145	155 (5)	135 m	134 (1)	-	-
B_{1u}	ν_{18}	SbI_2 Antisym. stretch	132 (7, 0)	ν_{EB}(39)ν_B(28)δ(33)						
A_g	ν_2	SbI_2 Sym. stretch	110 (0, 3)	ν_{EE}(38)ν_B(36) ν_{EB}(4)δ(22)	-	100 (2)	-	100 (2)	-	100 (1)
B_{3u}	ν_{27}	SbI_2 Sym. stretch	105 (3, 0)	ν_{EE}(31)ν_{EB}(28)ν_B(21)δ(20)						
B_{1g}	ν_7	SbI_2 Antisym. stretch	108 (0, 0)	ν_{EE}(60)δ(40)	-	-	-	-	135 s	-
B_{2u}	ν_{22}	SbI_2 Antisym. stretch	107 (10, 0)	ν_{EE}(65)δ(35)						
A_g	ν_3	SbI_2 Sym. stretch	99 (0, 1)	ν_B(40)ν_{EE}(26)ν_{EB}(11)δ(23)	-	-	-	-	-	-
B_{3u}	ν_{28}	SbI_2 Sym. stretch	96 (5, 0)	ν_B(40)ν_{EB}(16)ν_{EE}(12)δ(32)						
B_{2g}	ν_{11}	SbI_2 Antisym. stretch	87 (0, 1)	ν_B(59)ν_{EB}(18)δ(23)	85 sh	-	90 m	-	-	-
B_{1u}	ν_{19}	SbI_2 Antisym. stretch	100 (0, 0)	ν_B(49)ν_{EB}(22)δ(29)						
				Reference	48		48		48	

[a] Relative infrared and Raman intensities given in parentheses; calculated for $Sb_2Cl_{10}^{4-}$

[b] s-strong, m-medium, w-weak, vs-very strong, br-broad, sh-shoulder; relative Raman intensities in parentheses

[c] cation

Table 36 Stretching frequencies (cm^{-1}) of $SbBr_5^{2-}$ complexes[141]

Sym	Description		Calculated [a]	PED	Observed [b]			
					$C_6H_5CH_2NH_2$ [c]		$C_4H_9NH_3$ [c]	
					IR [c]	Raman	IR [c]	Raman
A_g	ν_1	$SbBr_2$ Sym. stretch	188 (0, 10)	$\nu_{EB}(38)\nu_B(18)\nu_{EE}(11)\delta(33)$	210 m	213 (10)	-	205 (10)
B_{3u}	ν_{26}	$SbBr_2$ Sym. stretch	163 (4, 0)	$\nu_{EB}(53)\nu_{EE}(19)\delta(28)$				
B_{2g}	ν_{10}	$SbBr_2$ Antisym. stretch	157 (0, 4)	$\nu_{EB}(60)\ \nu_B(9)\ \delta(31)$	187 m	164 (2)	175 s	190 (8)
B_{1u}	ν_{18}	$SbBr_2$ Antisym. stretch	180 (6, 0)	$\nu_{EB}(41)\ \nu_B(26)\ \delta(33)$				
A_g	ν_2	$SbBr_2$ Sym. stretch	144 (0, 3)	$\nu_{EE}(35)\nu_B(26)\nu_{EB}(11)\delta(28)$	-	148 (2)	-	147 (3)
B_{3u}	ν_{27}	$SbBr_2$ Sym. stretch	136 (5, 0)	$\nu_{EE}(26)\nu_B(26)\nu_{EB}(22)\delta(26)$				
B_{1g}	ν_7	$SbBr_2$ Antisym. stretch	152 (0, 0)	$\nu_{EE}(65)\delta(35)$	150 sh	-	-	-
B_{2u}	ν_{22}	$SbBr_2$ Antisym. stretch	161 (10, 0)	$\nu_{EE}(65)\delta(35)$				
A_g	ν_3	$SbBr_2$ Sym. stretch	126 (0, 2)	$\nu_B(37)\nu_{EE}(18)\nu_{EB}(10)\delta(35)$	-	-	-	-
B_{3u}	ν_{28}	$SbBr_2$ Sym. stretch	113 (5, 0)	$\nu_B(42)\nu_{EE}(19)\nu_{EB}(6)\delta(33)$				
B_{2g}	ν_{11}	$SbBr_2$ Antisym. stretch	91 (0, 1)	$\nu_B(56)\nu_{EB}(11)\delta(33)$	115 s	-	110 s	-
B_{1u}	ν_{19}	$SbBr_2$ Antisym. stretch	117 (0, 0)	$\nu_B(46)\nu_{EB}(23)\delta(31)$				
				Reference	48		48	

[a] Relative infrared and Raman intensities given in parentheses; calculated for $Sb_2Br_{10}^{4-}$

[b] s-strong, m-medium, w-weak, vs-very strong, br-broad, sh-shoulder; relative Raman intensities in parentheses

[c] cation

Table 37 Stretching frequencies (cm^{-1}) of $Sb_2Cl_{10}^{4-}$ complexes[141]

Sym	Description		Calculated [a]	PED
A_g	ν_1	$SbCl_2$ Sym. stretch	316 (0, 10)	$\nu_{EB}(32)\nu_{EE}(22)\nu_B(11)\delta(35)$
B_{3u}	ν_{26}	$SbCl_2$ Sym. stretch	274 (4, 0)	$\nu_{EB}(60)\nu_{EE}(16)\nu_B(4)\delta(20)$
B_{2g}	ν_{10}	$SbCl_2$ Antisym. stretch	252 (0, 7)	$\nu_{EB}(75)\delta(25)$
B_{1u}	ν_{18}	$SbCl_2$ Antisym. stretch	257 (5, 0)	$\nu_{EB}(65)\nu_B(12)\delta(23)$
A_g	ν_2	$SbCl_2$ Sym. stretch [b]	258 (5, 0)	$\nu_{EB}(43)\nu_{EE}(13)\ \nu_B(21)\delta(23)$
			211 (0, 2)	$\nu_{EE}(34)\nu_{EB}(14)\nu_B(14)\delta(38)$
B_{3u}	ν_{27}	$SbCl_2$ Sym. stretch	183 (1, 0)	$\nu_{EE}(50)\nu_{EB}(20)\nu_B(18)\delta(12)$
B_{1g}	ν_7	$SbCl_2$ Antisym. stretch	161 (0, 0)	$\nu_{EE}(63)\delta(37)$
B_{2u}	ν_{22}	$SbCl_2$ Antisym. stretch	182 (10, 0)	$\nu_{EE}(68)\delta(32)$
A_g	ν_3	$SbCl_2$ Sym. stretch [b]	178 (0, 3)	$\nu_B(39)\nu_{EE}(20)\nu_{EB}(4)\delta(37)$
B_{3u}	ν_{28}	$SbCl_2$ Sym. stretch [b]	123 (4, 0)	$\nu_B(38)\delta(62)$
B_{2g}	ν_{11}	$SbCl_2$ Antisym. stretch	77 (0, 1)	$\nu_B(50)\nu_{EB}(6)\delta(44)$
B_{1u}	ν_{19}	$SbCl_2$ Antisym. stretch	181 (1, 0)	$\nu_B(67)\delta(33)$

[a] Relative infrared and Raman intensities given in parentheses
[b] Strongly coupled with bending motions

BiI_6^{-3} are 119, 105, and 110 cm^{-1}, respectively, when the cation is n-$C_3H_7NH_3^+$ but increase to 139, 128, and 135 cm^{-1} when the cation is $Cr(en)_3^{+3}$. The computed values are 104, 85, 106 cm^{-1}, respectively, and agree much better with the n-$C_3H_7NH_3^+$ system. As is evident in Table 19-37, the calculated frequencies for the "gas-phase" anions tend to be about 10% lower than the experimental values. However, the effect of replacing one cation by another can affect the frequencies considerable more than that.

The calculated potential energy distributions (PEDS) for each M-X stretching vibration for each anion are also presented in Tables 19 to 37. These confirm that the highest frequencies are mostly υ_{EB} with smaller contributions from the υ_{EE} and υ_B stretchings. All of the bending modes together typically contribute less than 30%. The next highest group of frequencies is that for the υ_{EE} modes. These again have smaller contributions from the other two types of stretchings and the bending modes. The υ_B stretching modes are the most coupled to the bending modes as they are the lowest in frequency and not much separated from the bendings.

In addition to the primary observations described above, a few unusual features are found from the vibrational calculations and these can be seen by a more detailed inspection of Tables 19 to 37. For example, for $Sb_2Cl_{10}^{-4}$ there is a very strong coupling between the A_g υ_{EB} stretching and an A_g bending motion giving rise to vibrational frequencies of 258 and 211 cm^{-1}. This makes it seem at first glance that there is an extra stretching vibration. Other couplings in the other metallates can also be noticed.

The most important feature to reiterate about the vibrational calculations and observed spectra is that the *trans*-effect is well supported by the data in Tables 18 to 37.

The M-X stretching frequencies for external M-X bonds across from bridging bonds tend to be about 20% higher than those across from other external bonds. This is true for the halobismuthates and haloantimonates.

Conclusions

The *trans*-effect postulated in the Laane group's original work[47-48] was based on the fact that higher vibrational frequencies were observed for the M-X stretching modes for bonds across from bridging atoms. The concept was supported by the limited amount of crystal structure data at that time. Over the past thirty years much more crystallographic data has now become available, the *trans* effect is still clearly supported by all of the experimental structural and vibrational studies of the halobismuthates and haloantimonates. Examination of the experimental data clearly shows that the choice of cation can have a significant effect on which structure results, on what the bond distances are, and what the vibrational frequencies are.

CHAPTER VIII

INFRARED AND RAMAN VIBRATIONALSPECTRA, THEORETICAL CALCULATIONS, CONFORMATIONS, AND TWO-DIMENSIONAL POTENTIAL ENERGY SURFACE OF 2-CYCLOPENTEN-1-ONE ETHYLENE KETAL

Introduction

The vibrational spectra, conformations, and potential energy surfaces (PES) have been investigated by Laane's research group for several decades.[142-144] Most recently the two-dimensional PES calculation for the two ring-puckering vibrations of 4-silaspiro-3,3-heptane (SSH)[145] was reported in Laane's laboratory. For this molecule the two four-membered rings are identical and each is puckered in its lowest energy conformation. Therefore, the PES for SSH has four equivalent energy minima and gives rise to a most interesting pattern of four-fold degenerate quantum states. In the present study the results for 2-cyclopenten-1-one ethylene ketal (CEK) is reported. The experimental infrared and Raman spectra are presented and are compared to the computed spectra using DFT calculations. The calculated structures and conformational energies for its two low energy conformations is also reported. Later on, the calculated two-dimensional PES in terms of its puckering and twisting coordinates along with the quantum energy states and wavefunctions that result from this PES will be presented. Unlike the case for SSH where all four energy minima have the same energy, CEK has two pairs of energy

minimum at different energies. Therefore, its pattern of resulting quantum states is most instructive to analyze.

Results and Discussion

The calculated structures for the two low energy conformations of CEK is shown in Figure 27. For structure L (at lower energy) the ring-puckering angle for the olefinic ring (ring A) was calculated to be 22.1° and the twisting angle for the dioxo ring (ring B) was calculated to be 24.1°. Structure H (at higher energy) was calculated to be 154 cm^{-1} higher in energy with a puckering angle of 20.1° and a twisting angle of 26.2°. The direction of the twisting relative to the puckering of the second ring is different for the two conformations. The calculated bond distances and angles are also shown in Figure 27 and these can be seen to be very similar for both structures.

The calculated and experimental infrared spectra for liquid CEK are shown in Figure 28, and the Raman spectrum of the liquid is compared to the calculated spectrum in Figure 29. The calculated spectra are shown for both structure L and structure H. The experimental spectra result from the mixed sample, which, based on the calculated conformational energy difference between the two structures, is expected to be about 68% L and 32% H at 25° C. The observed vibrational frequencies and intensities to those calculated are compared in Table 38. For frequencies above 250 cm^{-1} the agreement between the observed and calculated values can be seen to be very good, and the calculated spectra for structures L and H can be seen to be very similar.

Table 38 Observed and Calculated vibrational spectra (cm^{-1}) of CEK

ν	Approximate description	Observed		Calculated[a]	
		Infrared[b]	Raman[c]	Lower well	Upper well
1	Ring bend (B)	-	-	48 (5, 1)	52 (4, 0.1)
2	Ring puckered (A)	-	-	76 (1, 2)	94 (0.4, 1)
3	Ring twist (B)	-	-	201 (0.2, 3)	196 (0.3, 1)
4	Ring twist (A)	267 w	263 (4)	266 (1, 3)	285 (1, 0.4)
5	Skeletal twist	328 w	330 (3)	333 (1, 1)	323 (2, 0.4)
6	Ring angle bend (A)	436 m	432 (100)	427 (1, 19)	432 (2, 3)
7	Skeletal twist	468 m	465 (6)	450 (6, 1)	454 (7, 0.2)
8	Skeletal twist	496 m	496 (8)	492 (11, 7)	508 (8, 2)
9	Ring angle bend (B)	650 w	650 (2)	640 (2, 6)	641 (2, 1)
10	Ring angle bend (A)	-	691 (1)	695 (1, 3)	680 (1, 1)
11	Ring angle bend (B)	-	-	737 (9, 5)	748 (13, 1)
12	Ring stretch (A/B)	758 m	758 (19)	755 (3, 8)	759 (8, 1)
13	Ring stretch (A/B)	786 s	790 (15)	784 (23, 13)	793 (8, 20)
14	C-H out-of-plane wag (A)	-	821 (15)	828 (8, 11)	849 (4, 2)
15	CH_2 rock (A)	-	-	887 (8, 9)	889 (3, 1)
16	CH_2 rock (B)	909 s	916 (60)	906 (16, 17)	910 (31, 2)
17	CH_2 rock (B)	-	-	919 (20, 10)	918 (7, 4)
18	CH_2 rock (A)	947 s	946 (57)	938 (12, 25)	945 (13, 4)
19	C-H out-of-plane wag (A)	-	-	966 (6, 6)	959 (6, 1)
20	Ring stretch (A)	979 ms	977 (5)	972 (4, 2)	977 (4, 1)
21	Ring stretch (B)	1027 s	1023 (23)	1028 (29, 36)	1026 (23, 6)
22	Ring stretch (B)	1048 s	-	1042 (23, 2)	1045 (23, 1)
23	Ring stretch (B)	-	-	1057 (19, 1)	1062 (18, 0.3)
24	C-H in-plane wag (A)	1080 s	1078 (25)	1087 (100, 31)	1083 (83, 6)
25	Ring stretch (A)	-	-	1130 (24, 1)	1134 (4, 1)
26	Ring stretch (A)	1154 s	-	1149 (86, 3)	1138 (100, 1)
27	CH_2 twist (A)	-	1160 (6)	1168 (17, 5)	1172 (4, 2)
28	Ring stretch (A)	1210 ms	1211 (10)	1184 (89, 21)	1207 (45, 6)
29	CH_2 twist (B)	-	-	1211 (4, 22)	1209 (2, 2)
30	CH_2 twist (A/B)	-	-	1230 (23, 14)	1236 (25, 2)
31	CH_2 twist (A/B)	1264 m	1262 (1)	1238 (4, 10)	1241 (17, 2)

Table 38 (Continued)

ν	Approximate description	Observed		Calculated[a]	
		Infrared[b]	Raman[c]	Lower well	Upper well
32	CH_2 wag (A)	1302 m	1298 (6)	1272 (12, 6)	1282 (4, 1)
33	CH_2 wag (A)	-	-	1309 (2, 10)	1310 (3, 2)
34	CH_2 wag (B)	-	-	1347 (2, 3)	1346 (2, 1)
35	CH_2 wag (B)	-	-	1359 (2, 8)	1355(2, 2)
36	C-H in-plane wag (A)	1364 s	1362 (7)	1370 (47, 13)	1371 (44, 2)
37	CH_2 deformation (A)	1430 m	1428 (18)	1451 (2, 32)	1454 (2, 8)
38	CH_2 deformation (A)	1452 m	1450 (23)	1475 (6, 41)	1472 (6, 6)
39	CH_2 deformation (B)	1477 m	1474 (15)	1492 (2, 38)	1488 (2, 6)
40	CH_2 deformation (B)	-	-	1499 (0.2, 15)	1498 (0.1, 3)
41	Ring stretch (A)	1619 m	1616 (86)	1658 (6, 100)	1617(7, 18)
42	CH_2 stretch (B)	2883 s	2884 (70)	2882 (42, 100)	2903 (36, 64)
43	CH_2 stretch (B)	-	-	2893 (68, 19)	2928 (59, 53)
44	CH_2 stretch (A)	-	-	2914 (30, 84)	2929 (18, 100)
45	CH_2 stretch (A)	2948 ms	2938 (67)	2938 (17, 52)	2960 (9, 42)
46	CH_2 stretch (A)	-	2944 (67)	2959 (16, 60)	2971 (22, 79)
47	CH_2 stretch (B)	2980 s	2980 (43)	2980 (35, 80)	2986 (31, 68)
48	CH_2 stretch (B)	-	-	2986 (28, 60)	3014 (22, 70)
49	CH_2 stretch (A)	-	-	3004 (13, 28)	3016 (14, 35)
50	CH stretch (A)	3059 m	3065 (46)	3061 (11, 59)	3066 (9, 59)
51	CH stretch (A)	-	-	3091 (9, 71)	3093 (8, 76)

[a] Relative infrared and Raman intensities given in parentheses (IR,Raman)

[b] s: strong,m: medium, w: weak

[c] Relative Raman intensities given in parentheses

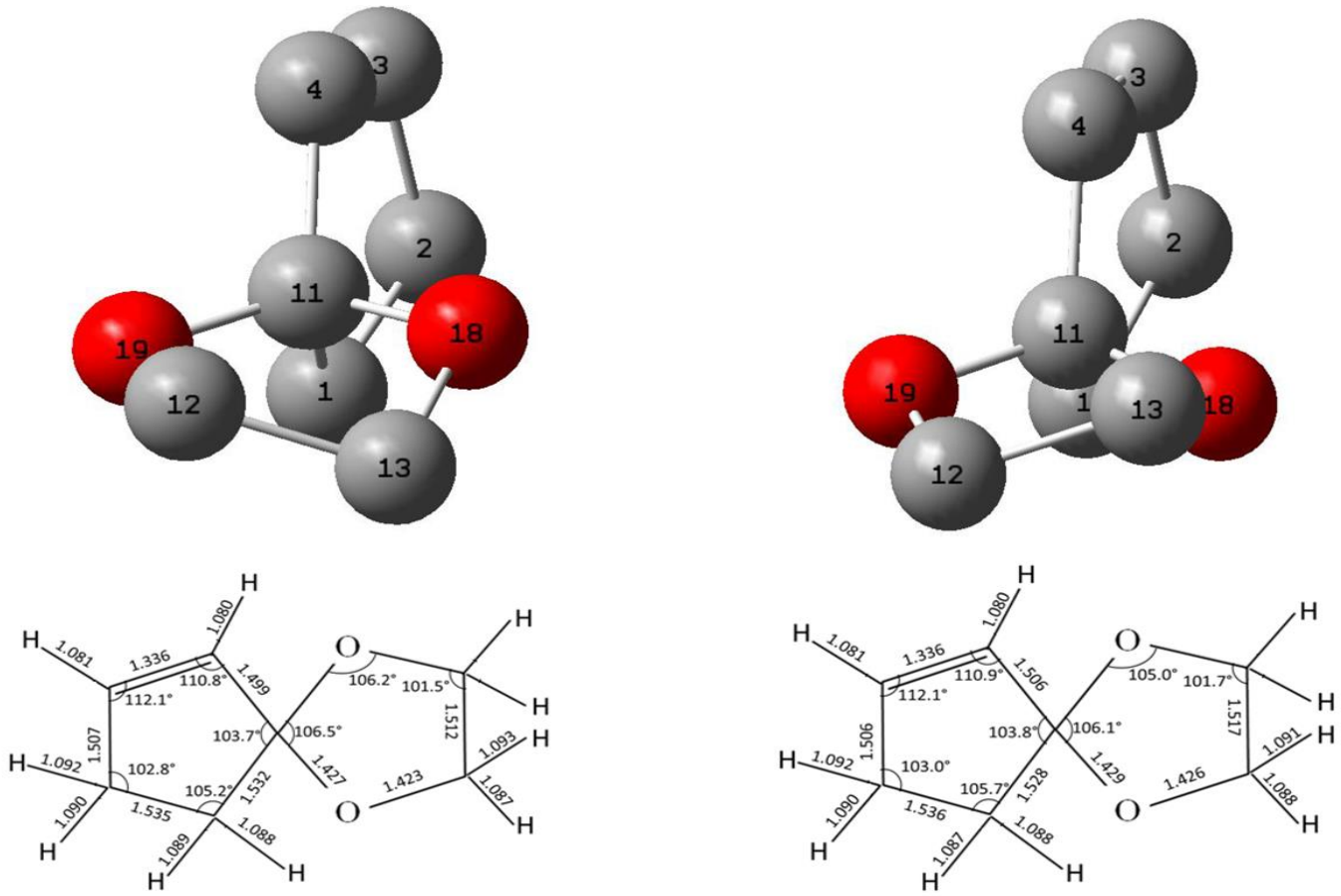

Figure 27 Calculated structures for the two conformations of CEK. Structure L on the left is for the lower energy conformation and structure H is for the conformation which is calculated to be 154 cm^{-1} higher in energy

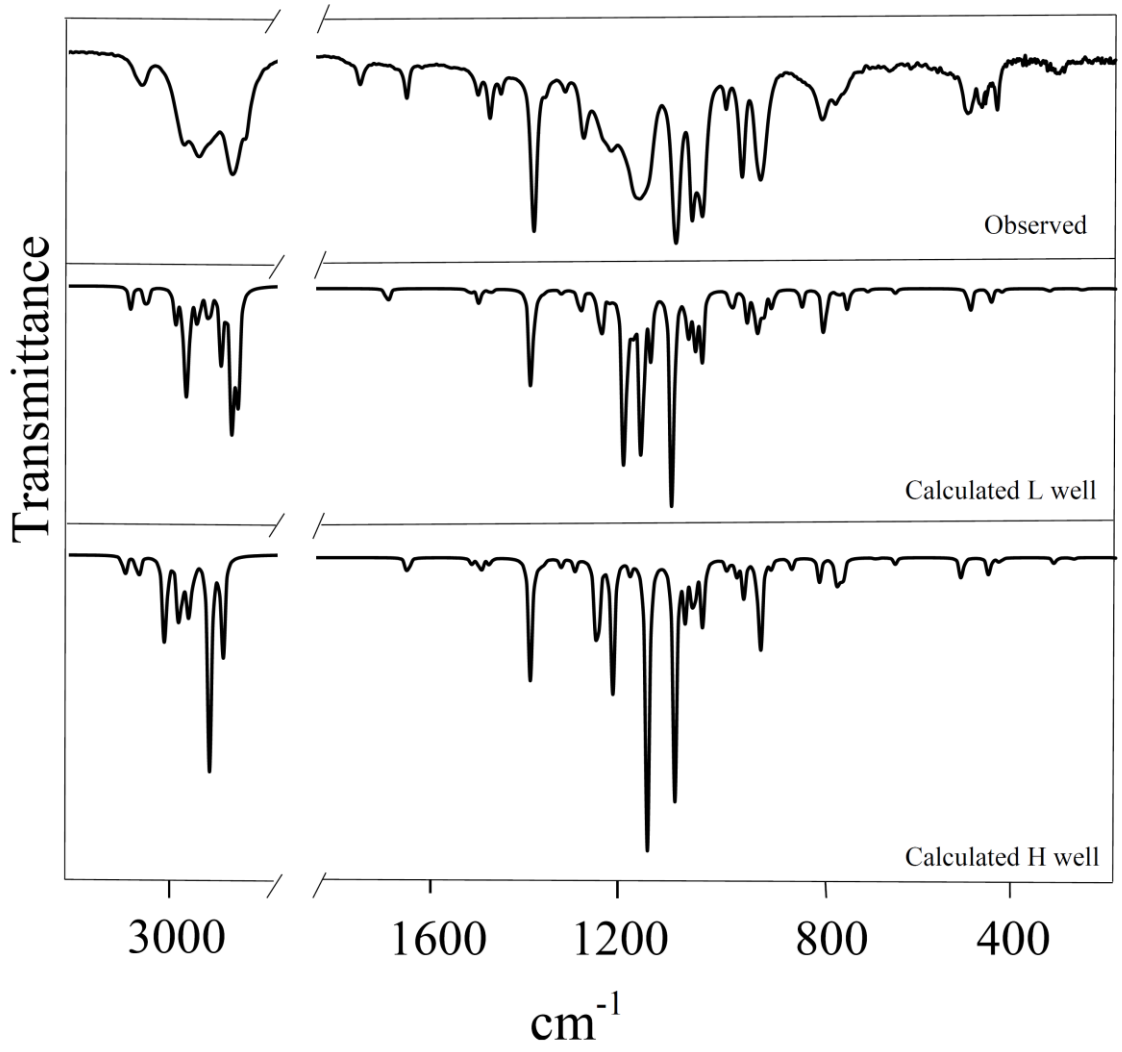

Figure 28 Observed liquid and calculated infrared spectra of CEK

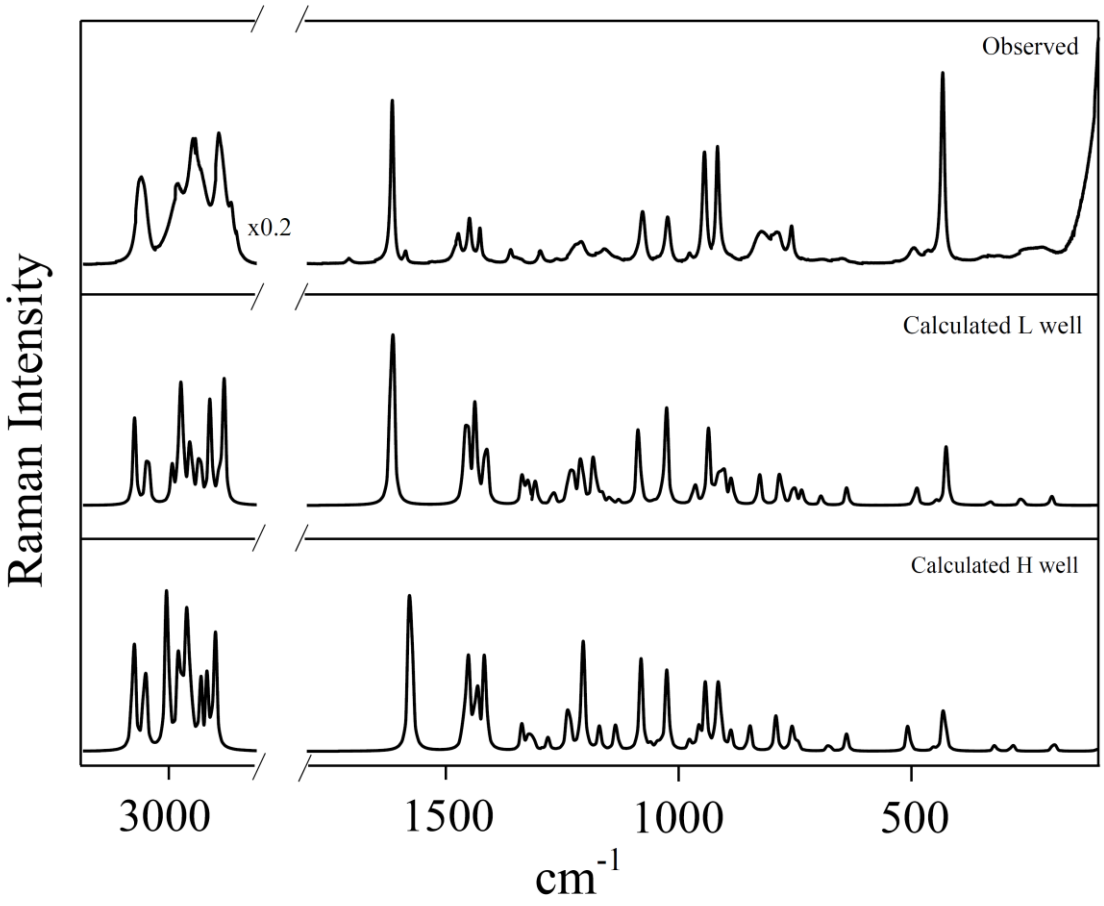

Figure 29 Observed liquid and calculated Raman spectra of CEK

The CEK molecule has four vibrational frequencies below 300 cm^{-1}. These are the out-of-plane ring-bending (ring-puckering) and the twisting about the C=C bond of ring A and the ring-bending and twisting of ring B with the two oxygen atoms. The two conformational minima of the molecule are achieved by optimizing the extent of ring-bending in ring A and the degree of twisting in B. The other two low-frequency vibrations do not play a significant role in establishing the conformations of the molecule. Hence, the main work is on the calculation of the conformational energies of the molecule as a function of the bending of A (x) and the twisting of B (τ). In the following section the results for the calculation of the two-dimensional potential energy surface (PES) in terms of x and τ for CEK will be discussed.

For CEK the out-of-plane ring-bending motion x in ring A (the one with the double bond) is defined as the distance that carbon atom 4 is out of the plane of the other four carbon atoms. This definition is chosen due to the complexity of this molecule. In previous work,[142-144] the ring-puckering coordinate as half the distance between the two ring diagonals was defined, but the choice of that coordinate here would be very cumbersome. Nonetheless, the coordinate here can be related to this traditional puckering coordinate by the geometrical relationships presented elsewhere.[146-148] The twisting coordinate τ for ring B (the one with two oxygen atoms) is defined as the angle between the O-C-O plane and the C-C bond. This is the same definition utilized in previous work.[149-151]

Utilizing the *ab initio* calculations, the conformational energy in cm^{-1} for CEK was computed as a function of x (Å) and τ (radians) for the energy minima, for the central

barrier at $x = \tau = 0$, and for the barriers where either x or τ was fixed at its minimum energy value. In addition, several additional conformational energy values were calculated for additional values of x and τ. The data were then used to calculate a potential energy surface (PES) which closely fits all these data points. This PES was found to be

$$V(x,\tau) = 9970.9\, x^4 - 2650.6\, x^2 + 33385.3\, \tau^4 - 12829.0\, \tau^2 - 183.2\, x^2 \tau^2 - 2008.2\, x\, \tau + 277.0\, x^3\tau + 7585.0\, x\tau^3 + 1494 \quad (1)$$

This is shown in Figure 30. As can be seen, there are two pairs of energy minima for structure L at the two lowest energies and structure H at the two energies 154 cm^{-1} higher. The puckering barrier when the twisting τ is at its minimum value is 264 cm^{-1}, and the twisting barrier when the bending x is at its minimum value is 1318 cm^{-1}. When x and τ are both zero, the central barrier is 1494 cm^{-1}. The ring-puckering and ring-twisting energy levels for this surface have been calculated and these results will be discussed in some detail.

In order to calculate the energy levels for the PES in Eq. (1) it is necessary to have the reduced mass values corresponding to x and τ. Because of the complexity of the molecule, these were not calculated rigorously, but were calculated so that the fundamental bending and twisting frequencies would match those obtained from the DFT calculation. This procedure was found to work well in previous studies.[145, 152-156]

The lowest quantum states correspond to either structure L at the lowest energy or to structure H at the higher energy. They can be labeled according to (v_B,v_T) indicating how many quanta of bending or twisting are excited. They are also labeled sequentially

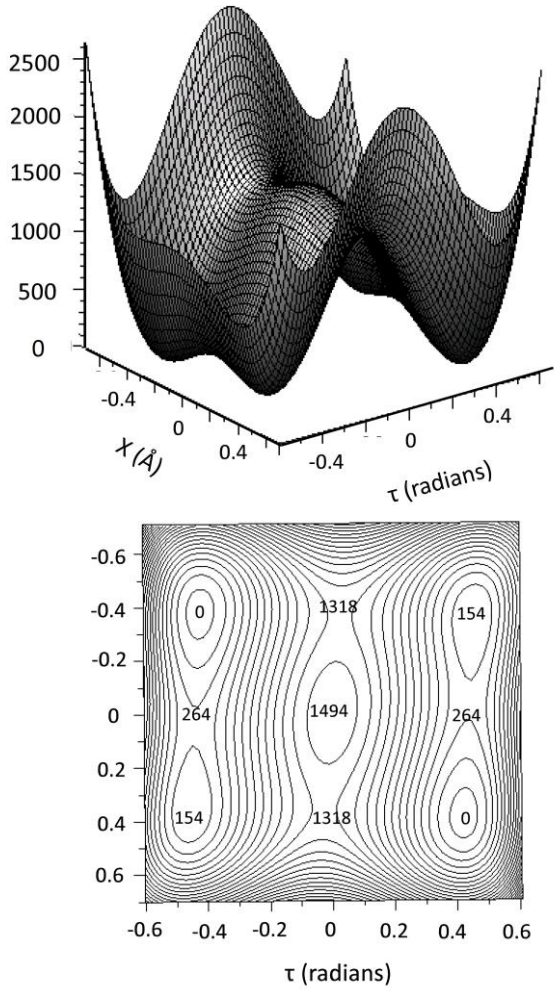

Figure 30 Vibrational potential energy surface for CEK in terms of its ring-bending x and ring-twisting τ coordinates. The conformational energies are shown for the minima and for barriers to interconversion

beginning with 0 for the lowest energy state (0,0). The quantum states calculated for the PES of Eq. (1) and Figure 30 are shown in Figure 31. The lowest quantum states are almost totally localized in either the lower potential energy well for structure L or in the higher well for structure H. Consequently, the L levels on the left side of the figure separated from those in the higher well on the right side of the figure are shown. Levels for $v_B \geq 8$ are shown in the center since these have nearly equal probabilities for either L or H. To understand the origin of these quantum states it is helpful simultaneously to also examine Figure 32, which shows the potential energy curve and energy levels for the ring-bending coordinate when the ring-twisting coordinate τ is at its minimum energy value. Similarly, the potential energy curve along the ring-twisting coordinate when the bending x is at its minimum energy value is shown in Figure 33. For the one-dimensional functions in these figures the energy levels have been adjusted so they do not include the zero-point energy of the other vibration. Thus for Figure 32 only the bending zero-point energy of 38 cm^{-1} is included while the zero-point energy for the twisting in Figure 33 is 103 cm^{-1}. The levels (0,0), (1,0), (2,0) and (4, 0) are almost totally isolated in well L while (3,0) and (5,0) are isolated in the higher well H as shown in Figure 32. Levels ($v_{B,0)}$ for v_B = 6 to 8 tend to favor one well or the other but begin to show significant probability in the second well also. By $v_B \geq 8$ the wavefunctions show substantial probability for both wells. All of the wavefunctions through level 34 (2x35 = 70 functions) are shown in Figure 34 and these support the description given above. The calculated energy values for all of these levels are shown in Table 39. In the figure the levels are identified by their sequence number and the symmetric and antisymmetric

Table 39 Calculated energy levels for the PES of CEK

n	Energy (cm^{-1})
0	0
1	75.6
2	144.9
3	154.8
4	201.1
5	205.1
6	213.6
7	247.5
8	269.1
9	276.4
10	300.9
11	334.7
12	345.3
13	350.5
14	371.8
15	395.1
16	404.5
17	409.9
18	411.3
19	445.4
20	453.1
21	466.9
22	470.1
23	496.9
24	499.0
25	532.8
26	538.6
27	538.7
28	543.0
29	569.9
30	581.3
31	590.8
32	595.9
33	599.5
34	609.5

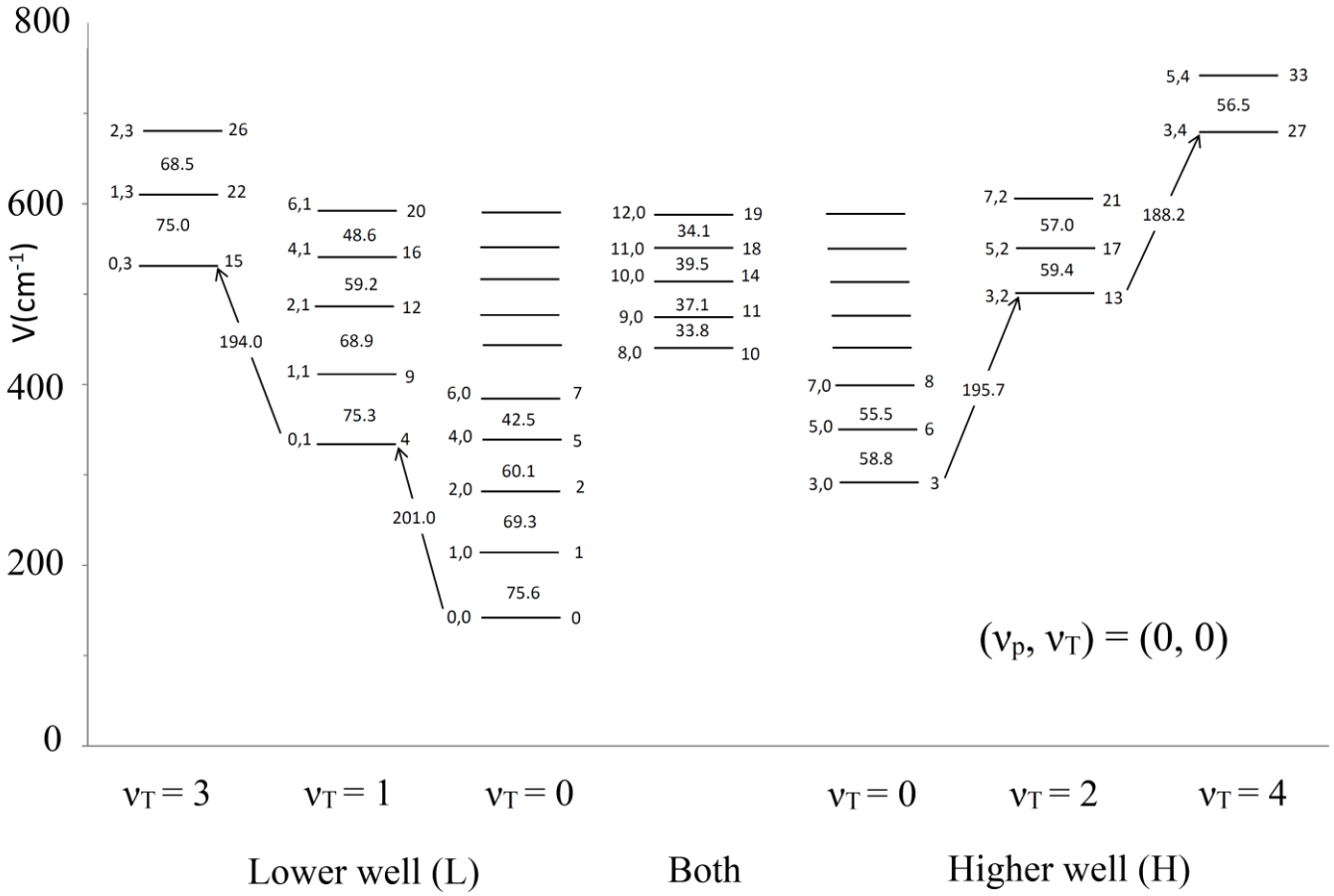

Figure 31 Quantum states (v_B,v_T) for the ring-bending(B) and ring-twisting (T) vibrations of CEK

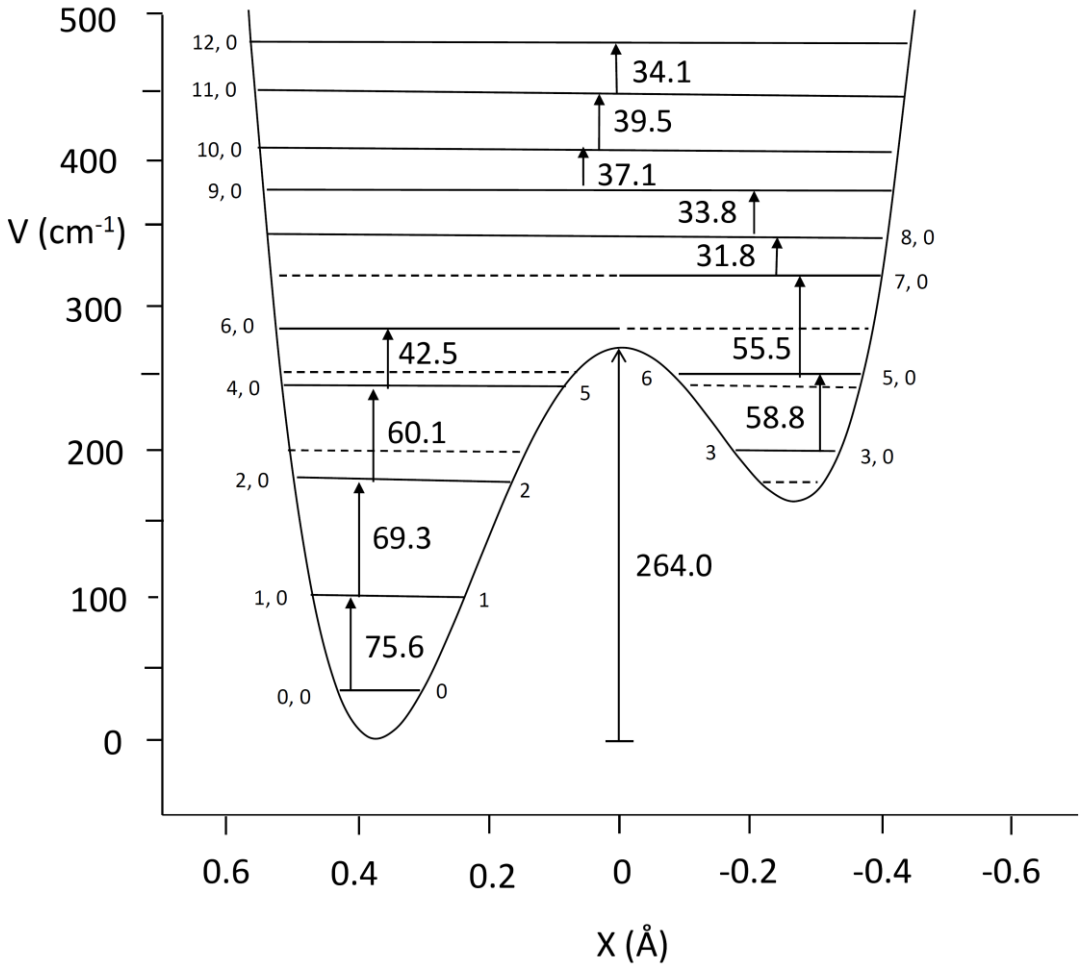

Figure 32 Ring-bending potential energy function in terms of x and energy levels calculated for τ at its minimum energy value

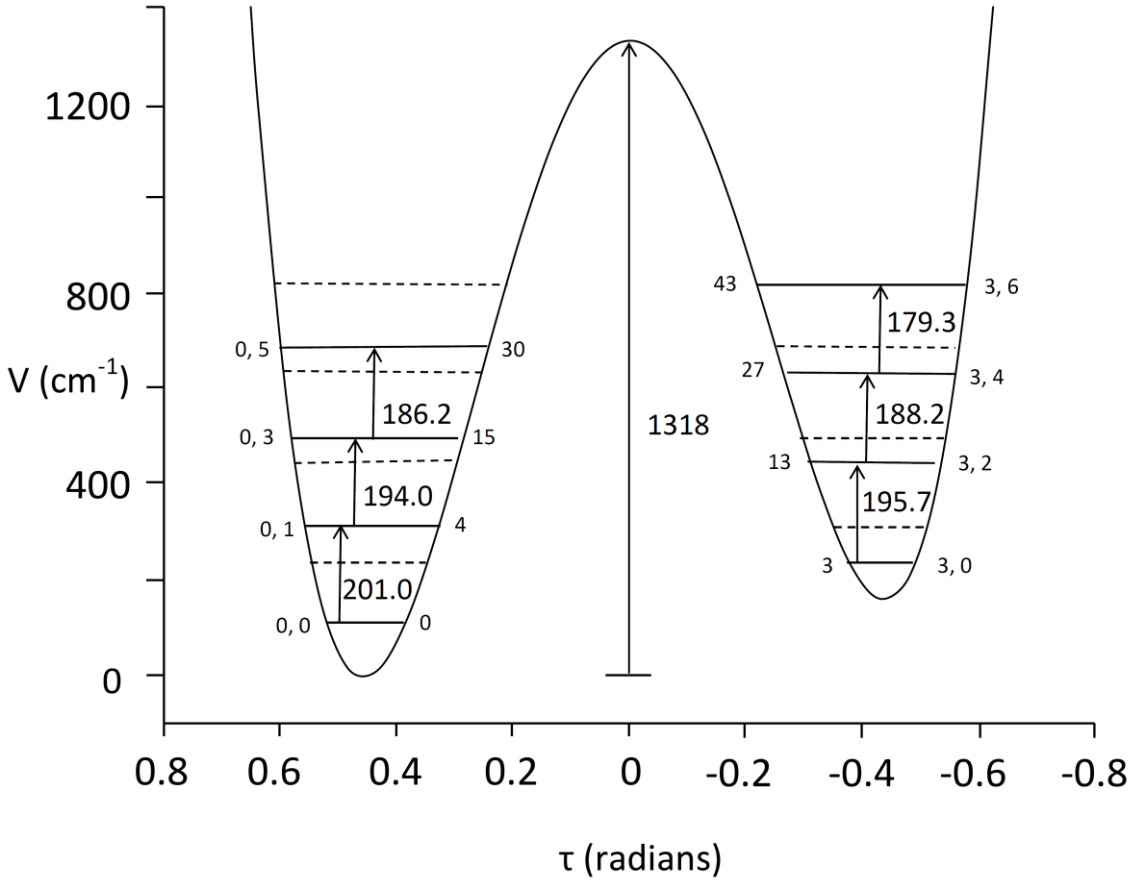

Figure 33 Ring-twisting potential energy function in terms of τ and energy levels calculated for x at its minimum energy value

Figure 34 Calculated wavefunctions for CEK

components are labeled as A and B, respectively. The energy level values are given relative to the lowest state at 0.0 cm^{-1} with the zero point energy excluded. Both the A and B components are shown for levels 0 to 4, but for higher levels only the A component is shown.

In Figure 34 levels 0, 1, 2, and 4 can be seen to correspond to conformation L. Levels 1 and 2 are excited states of the bending as confirmed by the fact that the functions change sign along the x direction. Similarly, level 4 changes sign along τ and thus corresponds to the excited state of the twisting as level (0,1), Level 3 is the lowest energy state for conformation H and this is clearly shown in the figure. Levels 5 and 6 are mostly constrained to conformations L and H, respectively, but both begin to show probabilities for the other potential energy well. Level 9 and 12 are the (1,1) and (2,1) states with both the bending and twisting motions being excited, and this is evident as their wavefunctions show directionality along both x and τ. Level 10 (or 8,0) lies above the puckering barrier to interconversion and shows almost equal probability for structures L and H. In other words, the molecule is essentially puckering freely between L and H while passing through the planar structure of ring A. Level 13 corresponds to H and has directionality along τ indicating that it is the first excited twisting state for this structure. The wavefunctions for several other states are also shown and these confirm the assignments we have given in Figure 31.

Each of the twisting excited states with $v_T \geq 1$ the sequence of puckering levels is fairly similar as shown in Figure 31 although the energy separations differ more between the lower and higher wells. For example, in the higher well the lowest puckering

transition is about 59 cm^{-1} vs. 76 cm^{-1} for the lower well. Because of the high twisting barrier, the lowest eight twisting quantum states are highly localized in one well or the other as shown in Figure 33. Since the ground state of the higher well is labeled as (3,0), each of the twisting levels in Figure 34 is labeled as $(3,v_T)$ indicating no additional excitation of the ring-bending.

Conclusions

The two-dimensional potential energy surface of CEK in terms of the two low-frequency, large-amplitude vibrations have been calculated which govern the conformational energies of this molecule. The PES has two pairs of energy minima which are at two different energies and this creates a most interesting case for the study of its quantum state patterns. The characteristics of these energy levels are elucidated in Figure 31 to 33 and the rather fascinating wavefunctions are displayed in Figure 34. Although the PES for CEK was generated from *ab initio* computations and is only approximate, the energy level patterns and wavefunctions calculated should provide a fairly accurate description for this molecule.

CHAPTER IX

CONCLUSIONS

Spectroscopic studies using infrared and Raman spectroscopy for the electronic ground states and ultraviolet absorption spectroscopy for electronic excited state were carried out. The spectroscopic data were analyzed and vibrational assignments were made for both ground and excited states. Computational methods including *ab initio* and DFT calculations were utilized to predict structures and to guide vibrational assignments.

For the 2,6-difluoropyridine (26DFPy) molecule, the band of origin is at 37,820.2 cm^{-1} and corresponds to a transition to the $S_1(\pi,\pi^*)$ state. The molecule is rigidly planar in its ground state while the $S_2(n,\pi^*)$ state is predicted to be puckered with a barrier to planarity of 256 cm^{-1}. Although the structure is predicted to be planar in the $S_1(\pi,\pi^*)$ state, it becomes much more floppy as the out-of-plane ring bending frequency drops from 460 cm^{-1} to 127 cm^{-1}. The bond distances also increase in the excited states compared to ground state due to the decreased π bonding character. The most notable change in excited state frequencies result from the strong coupling between ring-puckering and C-F out-of-plane wagging motions. This makes the examination of puckering frequencies much more complicated.

2,3,5,6-Tetrafluoropyridine (TFPy) has a planar structure in its S_0 ground state and a puckered structure with a barrier to planarity of 30 cm^{-1} in the $S_1(\pi,\pi^*)$ excited state. The band of origin is at 35,704.4 cm^{-1} which corresponds to a transition to the $S_1(\pi,\pi^*)$

state. As was the case for 2,6-difluoropyridine, a strong coupling between out-of-plane ring bending and out-of-plane C-F wag was also observed.

When the structures of 2-fluoropyridine (2FPy), 3-fluoropyridine (3FPy), 26DFPy and TFPy were compared with that of the pyridine molecule, a decrease in N-C(F) bond distances caused by the substitution of fluorine atom on the carbon atom was observed. In addition, a decrease of the C-F stretching frequencies in the excited state was observed and this can be explained by the bonding participation of the fluorine p orbitals with the ring π system. The ring stretching and bending vibrations for pyridine, 2FPy, 3FPy, 25DFPy and TFPy all drop in frequency in the excited state due to the decreased π bonding character which indicates a more floppy ring structure.

2-Chloro-, 3-chloro-, 2-bromo-, and 3-bromopyridine structures were calculated using density functional theory (DFT) and *ab initio* methods. Infrared and Raman spectra were obtained for their electronic ground states and vibrational frequencies were assigned with the aid of theoretical calculations. Good agreement between calculated and experimental values was observed.

The structures and bond-stretching vibrational frequencies for the halobismuthates and haloantimonates including MX_6^{-3}, $M_2X_9^{-3}$, $M_2X_{10}^{-4}$, $(MX_5^{-2})_n$, and $(MX_4^{-1})_n$ anions (M= Bi or Sb, X= I, Br or Cl) were calculated. Although the computed values are for free anions without the presence of cations, the agreement between calculated and observed values is good. The results confirm that the strongest and shortest bonds are those across from bridging atoms. Bridging bonds are the weakest and longest while the external bonds across from other external atoms are intermediate. This supports the view

that external atoms fight harder for electron density than bridging atoms so that the bonds across from them cannot be as strong as those across from bridging atoms. Therefore, the previously postulated *trans* effect based on far infrared and Raman spectra are verified by theoretical calculations.

The observed and calculated vibrational spectra for the lower and upper well conformations of 2-cyclopenten-1-one ethylene ketal molecule were found to be in good agreement. A two dimensional potential energy surface was calculated for the out-of-plane vibrations, and two pairs of energy minima were found for structure L at the two lowest energies and structure H at energies 154 cm^{-1} higher. The puckering barrier when the twisting τ is at its minimum value is 264 cm^{-1}, and the twisting barrier when the bending x is at its minimum value is 1318 cm^{-1}. When x and τ are both zero, the central barrier is 1494 cm^{-1}. The calculated energy levels for the PES were shown to be in either the lower potential energy well for structure L or in the higher well for structure H. At the 9^{th} level and above nearly equal probabilities were found for wells L or H.

REFERENCE

1. Dijk, C. W.; Sun, M.; Wijngaarden, J. *J. Mol. Spec.* **2012**, 280, 34
2. Stiefvater, O. L. *Zeit. F. Natur.* **1976**, 31A(1), 53
3. Medhi, K. C. *Spectrochim. Acta, Part A* **1986**, 42A(12), 1393
4. Itoh, T. *J. Mol. Spec.* **2012**, 274, 9
5. Vasylyeva, V.; Merz, K. *J. Fluor. Chem.* **2010**, 131, 446
6. Wann, D. A.; Masters, S. L.; Robertson, H. E.; Rankin, D. W. H. *J. Phys. Chem. A* **2007**, 111, 7882
7. Nibu, Y.; Okabe, C.; Shimada, H. *J. Phys. Chem.* A **2003**, 107, 1945
8. Snavely, D.L.; Overly, J. A.; Waiters, V.A. *J. Chem. Phys.* **1995**, 201, 567
9. Doewiswamy, S.; Sharma, S.D. *Chem. Phys. Lett.* **1976**, 37(3)
10. King, G. H.; Murrell, J. N.; Suffolk, R. J. *J. Chem. Soc.* **1972**, 4, 564
11. Medhi *Indian J. Phys.* **1987**, 61B(1), 62
12. Stephen, L. *Spectrochim. Acta, Part A* **1978**, 34A(6), 583
13. Green, J. *Spectrochim. Acta, Part A* **1973**, 29(6), 1177
14. Bailey, R. *Spectrochim. Acta, Part A* **1967**, 23(12), 2997
15. Stammler, H. G.; Vishnevskiy, Y. V.; Sicking, C.; Mitzel, N. W. *CrystEngComm.* **2013**, 15, 3536
16. Vasylyeva, V.; Shishkin, O. V.; Maleev, A. V.; Merz, K. *Cryst. Growth Des.* **2012**, 12, 1032
17. Ang, S. G.; Huang, H. *J. Chem. Soc. Perkin Trans.* **1986**, 11, 1407

18. Boopalachandran, P.; Laane, J. *Chem. Phys. Lett.* **2008**, 462, 178

19. Boopalachandran, P.; Laane, J. *Spectrochim. Acta, Part A* **2011**, 79, 1191

20. Boopalachandran, P.; Kim, S.; Choo, J.; Laane, J. *Chem. Phys. Lett.* **2011**, 514, 214

21. Singh, D.; Vikram,K.; Singh, D. K.; Kiefer W.; Singh, R. K. *J. Raman Spec.* **2008**, 39, 1423

22. Kulicka B., Jakubas R., Bator G., Ciunik Z., and Medycki, W. *J. Phys.: Condens. Matter* **2004**, 16, 8155

23. Jarraya, S.; Salah, A.; Daoud, A. *Acta Crystallogr., Sect. C: Cryst. Struct. Commun.* **1993**, 49, 1594

24. Lazarini, F. *Acta Crystallogr., Sect. C: Cryst. Struct. Commun.* **1987**, 43, 637

25. Herdtweck, E.; Kreusel, U. *Acta Crystallogr., Sect. C: Cryst. Struct. Commun.* **1993**, 49, 318

26. Benetollo, F.; Bombieri, G.; Alonzo, G.; Bertazzi, N.; Casella, G. *J. Chem. Crystallogr.* **1998**, 28, 791

27. Wang, Y.; Xu, L. *J. Mol. Struct.* **2008**, 875, 570

28. Yang, Z.; Chen, G.; Xua, W.; Fan, Z. *Acta Crystallogr. Sect. E: Struct. Rep. Online* **2009**, E65, m887

29. Battaglia, L.; Corradi, A. *Inorg. Chim. Acta* **1986**, 121, 131

30. Benetollo, F.; Bombieri, G.; Del P. A.; Alonzo, G.; Bertazzi, N. *Inorg. Chim. Acta* **2001**, 319, 49

31. Morss, L.; Robinson, W. *Acta Crystallogr., Sect. B: Struct. Sci*. **1972**, B28, 653

32. Ouasri, A.; Jeghnou, H.; Rhandour, A.; Dhamelincourt, M.; Dhamelincourt, P.; Mazzah, A.; Roussel P. *J. Raman Spectrosc.* **2005**, 36, 791

33. Rao, A. S.; Babu, E. S.; Swamy, K. C. K.; Das, S. K. *Polyhedron* **2010**, 29, 1706

34. Gerasimenko, A.; Karaseva, E.; Polishchuk, A. *Acta Crystallogr., Sect. E: Struct. Rep. Online* **2008**, E64, m378

35. Khelifi, M.; Zouari, R.; Salah, A. *Acta Crystallogr. Sect. E: Struct. Rep. Online* **2008**, E64, i80

36. Bigoli, F.; Lanfranchi, M.; Pellinghelli, M. *Inorg. Chim. Acta* **1984**, 90, 215

37. Rhandour, A.; Ouasri, A.; Roussel, P.; Mazzah, A. *J. Mol. Struct.* **2011**, 990, 95

38. Chaabouni, S.; Kamoun, S.; Jaud, J. *J. Chem. Crystallogr.* **1998**, 28, 209

39. Ferjani, H.; Boughzala, H.; Driss, A. *Acta Cryst.* **2012**, E68, m615

40. Wang Y. C. *Acta Cryst.* **2012**, E68, m181

41. Vezzosi, I. *Inorg. Chim. Acta* **1984**, 89, 151

42. Bujak, M.; Osadczuk, P.; Zaleski, J. *Acta Crystallogr. Sect. C: Cryst. Struct. Commun.* **2001**, C57, 388

43. Schroeder, D.; Jacobson, R. *Inorg. Chem.* **1973**, 12, 210

44. Wojtaś, M.; Jakubas, R. *J. Phys.: Condens. Matter* **2004**, 16, 7521

45. Zarychta, B.; Bujak, M.; Zaleski, J. *Z. Naturforsch., B: Chem. Sci.* **2007**, 62, 44

46. Gerasimenko, A. V.; Polishchuk, A. V.; Karaseva, E. T.; Karasev, V. E. *Russian J. Coord. Chem.* **2008**, 34, 647

47. Laane, J.; Jagodzinski, P.W. *Inorg. Chem.* **1980**, 19, 44

48. Laane, J.; Jagodzinski, P. W. *J. Raman Spectrosc.* **1980**, 9, 22

49. Yang, J.; Laane, J. *J. Mol. Struct.* **2006**, 798, 27

50. Laane, J. *J. Phys. Chem. A* **2000**, *104*, 7715

51. Klots, T.; Sakurai, S.; Laane, J. *J. Chem. Phys.* **1998**, 108(9)

52. Bondoc, E.; Klots, T.; Laane, J. *J. Phys. Chem. A* **2000**, 104, 275

53. Bondoc, E.; Laane, J. *J. Mol. Struct.* **1998**, 470, 237

54. Klots, T.; Lee, S.; Laane J. *J. Phys. Chem. A* **1999**, 103, 833

55. Lee, S.; Meinander, N.; Sagear, P.; Nath, D. N.; Laane J. *J. Chem. Phys.* **1998**, 108(21), 8884

56. Rosario, A.; Bitschenauer, R.; Dakkouri, M.; Haller, K.; Laane J. *J. Phys. Chem. A* **1998**, 102, 10261

57. Sakurai, S.; Meinander, N.; Morris, K.; Laane J. *J. Am. Chem. Soc.* **1999**, 121, 5056

58. Bondoc, E.; Sakurai, S.; Morris, K.; Chiang, W.; Laane J. *J. Chem. Phys.* **2000**, 112(15), 6700

59. Villarreal, J. R.; Bauman, L. E.; Laane, J.; Harris, W. C.; Bush, S. F. *J. Chem. Phys.* **1975**, 63(9), 3727

60. Cortez, E.; Verastegui, R.; Villarreal J. R.; Laane, J. *J. Am. Chem. Soc.* **1993**,115, 12132

61. Villarreal, J. R.; Bauman, L. E., and Laane, J. *J. Phys. Chem. A.* **1976**, 80(11)

62. Laane, J. *Inter. Rev. Phys. Chem.* **1999**, 18(2), 301

63. Laane, J.; Bondoc, E.; Sakurai, S.; Morris, K.; Meinander, N.; Choo, J. *J. Am. Chem. Soc.* **2000**, 122, 2628

64. Laane, J. *J. Mol. Struct.* **1985**, 1(26), 99

65. Bauman, L. E.; Klllough, P. M.; Cooke, J. M.; Vlllarreal, J. R. ; Laane, J. *J. Phys. Chem. A.* **1982**, 86(11), 2001

66. Sakurai, S.; Meinander, N.; Laane, J. *J. Chem. Phys.* **1998**, 108(9), 3537

67. Laane, J. *Annu. Rev. Phys. Chern.* **1994**, 45, 179

68. Esther J. O.; Bauman, L. E.; Laane, J. *J. Phys. Chem. A* **2011**, 115, 6531

69. Haller K.; Chiang, W.; Rosario, A.; Laane J. *J. Mol. Struct.* **1996**, 379, 19

70. Frisch, M. J.; Trucks, G. W.; Schlegel, H. B.; Scuseria, G. E.; Robb, M. A.; Cheeseman, J. R.; Scalmani, G.; Barone, V.; Mennucci, B.; Petersson, G. A.; *et al.* Gaussian 09, Revision A.02, Gaussian, Inc., Wallingford CT, **2009**.

71. Schmidt, M. W.; Gordon, M. S. *Annu. Rev. Phys. Chem.* **1998**, 49, 233

72. Schmidt, M. W.; Baldridge, K. K.; Boatz, J. A.; Elbert, S. T.; Gordon, M. S.; Jensen, J. H.; Koseki, S.; Matsunaga, N.; Nguyen, K. A.; Su, S. *et al. J. Comput. Chem.* **1993**, 14, 1347

73. Meinander, N.; Laane, J. *J. Mol. Struct.* **2001**, 569, 1

74. Yang, J.; McCann, K.; Laane, J. *J. Mol. Struct*. **2004**, 695, 339

75. Yang, J.; Choo, J.; Kwon, O.; Laane, J. *Spectrochim. Acta, Part A* **2007**, 68, 1170

76. Autrey, D.; Yang, J.; Laane, J. *J. Mol. Struct*. **2003**, 661, 23

77. Al-Saadi A. A.; Laane, J. *J. Mol. Struct*. **2007**, 830, 46

78. Autrey, D.; Choo, J.; Laane, J. *J. Phys. Chem. A* **2001**, 105, 10230

79. Sheu, H.; Kim, S. and Laane, J. *J. Phys. Chem. A* **2013**, 117(50), 13596

80. Laane, J. *Appl. Spectrosc.* **1970**, 24, 73

81. Laane J. *J. Phys. Chem. A* **2000**, 104A, 7715

82. Al-Saadi, A. A.; Ocola, E. J.; Laane, J. *J. Phys. Chem. A* **2010**, 114, 7453

83. McCann, K.; Wagner, M.; Guerra, A.; Coronado, P.; Villareal, J. R.; Choo, J.; Kim, S.; Laane, J. *J. Chem. Phys.* **2009**, 131, 1

84. Rishard, M. Z. M.; Wagner, M.; Choo, J.; Laane, J. *J. Phys. Chem. A* **2009**, 113, 7753

85. Al-Saadi, A. A.; Laane, J. *Spectrochim. Acta, Part A* **2008**, 71, 326

86. Al-Saadi, A. A.; Laane, J. *Organomet.* **2008**, 27, 3435

87. Rishard, M. Z. M.; Wagner, M.; Yang, J.; Laane, J. *Chem. Phys. Lett.* **2007**, 442, 182

88. Al-Saadi, A. A.; Laane, J. *J. Phys. Chem. A* **2007**, 111, 3302

89. Rishard, M. Z. M.; Irwin, R. M.; Laane, J. *J. Phys. Chem. A* **2007**, 111, 825

90. Al-Saadi, A. A.; Wagner, M.; Laane, J. *J. Phys. Chem. A* **2006**, 110, 12292

91. Yang, J.; Wagner, M.; Laane, J. *J. Phys. Chem. A* **2006**, 110, 9805

92. Yang, J.; Wagner, M.; Okuyama, K.; Morris, K.; Arp, Z.; Choo, J.; Meinander, N.; Laane, J. *J. Chem. Phys.* **2006**, 125, 1

93. Autrey, D.; Haller, K.; Laane, J.; Mlynek, C.; Hopf, H. *J. Phys. Chem. A* **2004**, 108, 403

94. Autrey, D.; Arp, Z.; Choo, J.; Laane, J. *J. Chem. Phys.* **2003**, 119(5), 2557

95. Arp, Z.; Meinander, N.; Choo, J.; Laane, J. *J. Chem. Phys.* **2002**, 116, 6648

96. Green, H. S.; Kynaston, W.; Paisley, H. M. *Spectrochim. Acta, Part A* **1963**, 19, 549

97. Boopalachandran, P.; Craig, N. C.; Laane, J. *J. Phys. Chem. A* **2012**,116, 271

98. Boopalachandran, P.; Sheu, H. and Laane, J. *J. Mol. Sruc.* **2012**, 1023, 61

99. Bi, W.; Louvain, N.; Mercier, N.; Lucb, J.; Sahraoui, B. *CrystEngComm.* **2007**, 9, 298

100. Lindsjö, M.; Fischer, A.; Kloo, L. *Z. Anorg. Allg. Chem.* **2005**, 631, 1497

101. Samet, A.; Ahmed, A.; Mlayah, A.; Boughzala, H.; Hlil, E.; Abid, Y. *J. Mol. Struct.* **2010**, 977, 72

102. Lazarini, F. *Acta Crystallogr. Sect. B: Struct. Sci.* **1978**, 34, 2288

103. Lazarini, F. *Acta Crystallogr. Sect. B: Struct. Sci.* **1980**, 36, 2748

104. McPherson, W. G.; Meyers, E. A. *J. Phys. Chem. A* **1968**, 72, 3117

105. Work, R.; Good, M. *Spectrochim. Acta, Part A* **1973**, 29, 1547

106. Chabot, B.; Parthi, E. *Acta Crystallogr. Sect. B: Struct. Sci*. **1978**, 34, 645

107. Lazarini, F. *Acta Crystallogr. Sect. C: Cryst. Struct. Commun.* **1987**, C43, 875

108. Goforth, A. M.; Peterson L.; Smith, M.D.; Loye, H. C. *J. Solid State Chem*. **2005**, 178, 3529

109. Wojtaś, M.; Jakubas, R.; Ciunik, Z.; Medycki, W. *J. Solid State Chem*. **2004**, 177, 1575

110. Lazarini, F. *Acta Crystallogr. Sect. B: Struct. Sci*. **1977**, 33, 2686

111. Lazarini, F. *Acta Crystallogr. Sect. B: Struct. Sci*. **1977**, 33, 2961

112. Hrizi, C.; Samet, A.; Abid, Y.; Chaabouni, S.; Fliyou, M.; Koumina, A. *J. Mol. Struct.* **2011**, 992, 96

113. Bi, W., Louvain, N., Mercier, N., Luc, J., Rau, I., Kajzar, F., and Sahraoui, B. *Adv. Mater.* **2008**, 20, 1013

114. Lazarini, F.; Leban, I. *Acta Crystallogr. Sect. B: Struct. Sci*. **1980**, 36, 2745

115. Lazarini, F. *Acta Crystallogr., Sect. B: Struct. Sci*. **1980**, 36, 2748

116. Piecha, A.; Kinzhybalo, V.; Jakubas, R.; Baran, J.; Medycki, W. *Solid State Sci.* **2007**, 9, 1036

117. McPherson, W.; Meyers, E *J. Phys. Chem. A* **1968**, 72, 532

118. Geiser, U.; Wang, H. H., Budz, S. M., Lowry, M. J., Williams, J. M., Ren, J., and Whangbo, M. *Inorg. Chem.* **1990**, 29, 1611

119. Robertson, B. K., McPherson, W. G., and Meyers, E. H. *J. Phys. Chem. A* **1967**, 71, 3531

120. Piecha, A.; Gągor, A.; Pietraszko, A.; Jakubas, R. *J. Solid State Chem*. **2010** 183, 3058

121. Płowaś, I.; Białońska, A.; Jakubas, R.; Bator, G.; Zarychta, B.; Baran, J. *J. Chem. Phys.* **2010**, 375, 16

122. Carmalt, C.; Farrugia, L.; Norman, N. *Z. Anorg. Allg. Chem.* **1995**, 621, 47

123. Chabot, B.; Parthi, E. *Acta Crystallogr. Sect. B: Struct. Sci*. **1978**, B34, 645

124. Ho, D.; Riley, W. C.; Jacobson, R. A. *Cryst. Struct. Comm*. **1978**, 7, 111

125. Bujak, M.; Zaleski, J. *Acta Crystallogr. Sect. E: Struct. Rep. Online* **2007**, *63*, m102.

126. Hubbard, C.; Jacobson, R. *Inorg. Chem.* **1972**, 11, 2247

127. Louvain, N. Mercier, and F. Boucher *Inorg. Chem.* **2009**, 48, 879

128. Bukvetskii V., Sedakova T. V., and Mirochnik A. G. *J. Struc. Chem.* **2009**, 50, 322

129. Wojtaś, M.; Jakubas, R.; Baran, J. *Vib. Spectrosc.* **2005**, 39, 23

130. Wojtaś, M.; Bator, G.; Baran, J. *Vib. Spectrosc.* **2003**, 33, 143

131. Benedetti, A.; Fabretti, A.; Malavasi, W. *J. Crystallogr. Spectrosc. Res.* **1992**, 22, 145

132. Piecha, A.; Kinzhybalo, V.; Jakubas, R.; Baran, J.; Medycki, W. *Solid State Sci.* **2007**, 9, 1036

133. Bowmaker, G.; Junk, P.; Lee, A. M.; Skelton, B. W.; White, A. H. *Aust. J. Chem*. **1998**, 51, 293

134. Khili, H.; Chaari, N.; Fliyou, M.; Koumina, A.; Chaabouni, S. *Polyhedron* **2012**, 36, 30

135. Zouari, F.; Salah, A. *Phase Trans.* **2005**, 78, 317

136. Tarasiewicz, J.; Jakubas, R.; Bator, G.; Zaleski, J.; Baran, J. and Medycki, W. J. Mol. Struct. **2009**, 932, 6

137. Allen, G.; McMeeking, R. *Inorg. Chim. Acta* **1977**, 23, 185

138. Bator, G.; Jakubas, R.; Majerz, I.; Malarski, Z. *J. Mol. Struct.* **1992**, 274, 1

139. Laitinen, R.; Steudel, R. *J. Chem. Soc., Dalton Trans*. **1986**, 1, 1095

140. Varma, V., Bhattacharjee, R., Vasan, H. and Raot, C. *Spectrochim. Acta, Part A* **1992**, 48A, 1631

141. Sheu, H. and Laane, J. *Inorg. chem.* **2013**, 52(8), 4244

142. Laane, J. Feature Article- Experimental Determination of Vibrational Potential Energy Surfaces and Molecular Structures in Electronic Excited States. *J. Phys. Chem.* **2000**, 104A, 7715

143. Laane, J. Vibrational Potential Energy Surfaces in Electronic Excited States in *Frontiers of Molecular Spectroscopy*, pp. 63, J. Laane (Ed.), Elsevier Publishing, Amsterdam, The Netherlands, 706 pp. (2009)

144. Yang, J.; Laane, J. Spectroscopic Determination of Vibrational Potential Energy Surfaces in Ground and Excited Electronic States. *J. Elec. Spectrosc. and Related Phenomena* **2007**, 156-158, 45

145. Ocola, E. J.; Medders, C.; Cooke, J. M.; and Laane, J. Vibrational Spectra, Theoretical Calculations, and Structure of 4-Silaspiro(3,3)heptane. *Spectrochim. Acta*, accepted **2014**.

146. Egawa, T.; Shinashi, K.; Ueda, T.; Ocola, E. J.; Chiang, W.-Y.; Laane, J. Vapor-phase Raman spectra, theoretical calculations and the vibrational and structural properties of *cis*- and *trans*-stilbene. *J. Phys. Chem. A* **2014**, 118, 1103

147. Ocola, E. J.; Shin, H. W.; Laane, J. Infrared and Raman Spectra and Theoretical Calculations for Benzocyclobutane in its Electronic Ground State. *Spectrochim. Acta, Part A* **2014,** in press.

148. Boopalachandran, P.; Sheu, H.-L.; Laane, J. Vibrational Spectra, Structure, and Theoretical Calculations of 2-Chloro and 3-Chloropyridine and 2-Bromo and 3-Bromopyridine. *J. Mol. Struct.* **2012**, 1023, 61

149. Laane, J.; Harthcock, M. A.; Killough, P. M.; Bauman, L. E.; Cooke, J. M. Vector Representation of Large Amplitude Vibrations for the Determination of Kinetic Energy Functions. *J. Mol. Spectrosc.* **1982**, 91, 286

150. Harthcock, M. A.; Laane, J. Calculation of Kinetic Energy Terms for the Vibrational Hamiltonian: Application to Large Amplitude Vibrations Using One-, Two-, and Three-Dimensional Models. *J. Mol. Spectrosc.* **1982**, 91, 300

151. Schmude, R. W.; Harthcock, M. A.; Kelly, M. B.; Laane, J. Calculation of Kinetic Energy Functions for the Ring-Puckering of Asymmetric Five-Membered Rings. *J. Mol. Spectrosc.* **1987**, 124, 369

152. Chun, H. J.; Laane, J. Theoretical Calculations, Far-Infrared Spectra and the Potential Energy Surfaces of Four Cyclic Silanes. *Chem. Phys.* **2014**, 431-432, 15

153. Chun, H. J.; Colegrove, L. F.; Laane, J. Vibrational Spectra, Theoretical Calculations, and Structures for 1,3-Disilacyclopent-4-ene and 1,3-Disilacyclopentane and Their Tetrachloro Derivatives. *J. Mol. Struct.* **2013**, 1049, 172

154. Grubbs II, G. S.; Novick, S. E.; Pringle Jr., W. C.; Laane, J.; Ocola, E. J.; and Cooke, S. A. A Bis-trifluoromethyl Effect: Doubled Transitions in the Rotational

Spectra of Hexafluoroisobutene, $(CF_3)_2C=CH_2$. *J. Phys. Chem. A* **2012**, 116, 8169

155. McCann, K.; Wagner, M.; Guerra, A.; Coronado, P.; Villareal, J. R.; Choo, J.; Kim, S.; Laane, J. Spectroscopic Investigations and Potential Energy Surfaces of the Ground and Excited Electronic States of 1,3-Benzodioxan. *J. Chem. Phys.* **2009**, 131, 1

156. Al-Saadi, A. A.; Laane, J. Vibrational Spectra, *Ab Initio* Calculations, and Ring-Puckering Potential Energy Function for γ-Crotonolactone. *J. Phy. Chem. A* **2007**, 111, 3302